SELENOP MODIFIES SPORADIC COLORECTAL CARCINOGENESIS AND WNT SIGNALING ACTIVITY THROUGH LRP5/6 INTERACTIONS

By

Jennifer Marie Pilat

Dissertation

Submitted to the Faculty of the

Graduate School of Vanderbilt University

in partial fulfillment of the requirements

for the degree of

DOCTOR OF PHILOSOPHY

in

Cancer Biology

August 11, 2023

Nashville, Tennessee

Approved:

James R. Goldenring, M.D., Ph.D.

Ken S. Lau, Ph.D.

Ethan Lee, M.D., Ph.D.

Christopher S. Williams, M.D., Ph.D.

Keith T. Wilson, M.D.

ACKNOWLEDGEMENTS

Above all else, my time in graduate school has highlighted the duality of life. This journey has been more challenging, yet more rewarding, than I could have ever anticipated. Thankfully, I was never alone—many individuals in my life supported me in innumerable ways, and for this (and for them) I am truly grateful.

First, I would like to thank my dissertation advisor, Dr. Chris Williams, who has supported me as an individual, first, and as a scientist, second, for the last 7 years. Thank you for your guidance through the more opaque aspects of academia, from preparing for a committee meeting to submitting a manuscript. Thank you for valuing and cultivating honest, open communication in our relationship. Despite the inherent student-mentor power dynamic, you always made me feel comfortable sharing my thoughts on experimental approaches, lab culture, current events, or personal matters that were impacting my work (looking at you, 2020).

Second, I would like to thank all current and former members of the Williams lab. Dr. Sarah Short, you have been a tremendous (albeit unofficial) co-mentor and an exceptional friend. I just know you will lead a fantastic research team of your own. Dr. Yash Choksi, your unique perspective (both scientific and otherwise) has been incredibly helpful. Dr. Rachel Brown, your passion for rigorous science continually inspires and motivates me to conduct tougher experiments for the sake of stronger data. Dr. Josh Thompson, your two-day Western blot crash course has paid dividends on dividends. Chase Jones, your positivity has brightened many a difficult day in the lab. Adrian Othon, Nathaniel Berle, and Choksi lab members Dr. Justin Jacobse, Dr. Matt Buendia, and Aaron Kwag, you all have provided more social support than you know.

I would also like to thank my dissertation committee members: Drs. Jim Goldenring, Ethan Lee, Ken Lau, and Keith Wilson, for all the expertise, feedback, and time they invested in me throughout my Ph.D. Dr. Ethan Lee and his former graduate student Dr. Victoria Ng, as well as Dr. Ken Lau and his

current graduate student Lucy Chen, were particularly instrumental to this study. I would also like to thank Dr. Suguru Kurokawa for sharing all his SELENOP constructs, as well as Dr. Kay Washington for reviewing all my histology.

Last, but certainly not least, I would like to thank my family and friends. To my parents, Diane and Rich Pilat: thank you for your endless support, prayers, love, encouragement, and advice. Since August 18th, 1994, you two have believed in me, even (and especially) when I didn't believe in myself. To my sister, Sarah Pilat: thank you for being my own personal sunshine committee; that is, helping me see the good in the world when everything feels bleak. To my best friend, Steph Marengere: thank you for helping me navigate and weather the challenges of young adulthood. I look forward to many more decades of friendship. To my partner, Jack Henning, thank you for anchoring me to the things that truly matter in this life. Your unparalleled understanding, support, and patience throughout this journey made all the difference.

This work was supported by the NIH (F31CA232272 to J.M.P., F30DK120149 to R.E.B., F30DK111107 to J.J.T., R03DK123489 to J.A.G., R01CA244188 to E.L., R35GM122516 to E.L., R01DK103831 to K.S.L., U54CA274367 to K.S.L., K01DK123495 to S.P.S., R01DK099204 to C.S.W., P30DK058404 to the VUMC DDRC, P50CA236733 to the Vanderbilt-Ingram Cancer Center SPORE in Gastrointestinal Cancer, P30CA068485 and U24DK059637 to the VUMC TPSR, T32GM00734 to the VU Medical Scientist Training Program, R25GM134979 to the VU VERTICES Postbaccalaureate Research Education Program, and T32CA00959228 to the VU Microenvironmental Influences in Cancer Training Program), the Crohn's and Colitis Foundation (623541 to C.S.W. and 662877 to S.P.S.), and the US Department of Veterans Affairs Office of Medical Research (IK2BX004648 to Y.A.C. and I01BX001426 to C.S.W.). J.J. was supported by the Prince Bernhard Cultural Foundation (Cultural Foundation Grant) and the Royal Netherlands Academy of Arts and Sciences (Academy Ter Meulen Grant). We would also like to thank the VUMC TPSR and Western Division of the Cooperative Human Tissue Network for aid with histology and tissue procurement, respectively.

TABLE OF CONTENTS

LIST OF TABLES

LIST OF FIGURES

LIST OF ABBREVIATIONS

β-TRCP: β-transducin repeat-containing E3 ubiquitin protein ligase

μg: microgram

μL: microliter

μM: micromolar

ACF: aberrant crypt foci

AMPK: 5′-adenosine monophosphate-activated protein kinase

AOM: azoxymethane

APC: adenomatous polyposis coli

ASC: adenoma-specific cells

Asp: aspartic acid

ATP: adenosine triphosphate

BMP: bone morphogenetic protein

BRAF: v-raf murine sarcoma viral oncogene homolog B1

BP: β-propeller

Ca^{2+}: calcium

CAC: colitis-associated cancer

CaMKII: Ca^{2+}/calmodulin-dependent protein kinase type II

CBC: crypt base columnar

Cdc42: cell division control protein 42 homolog

CDKN2A: cyclin-dependent kinase inhibitor 2A

ChIP: chromatin immunoprecipitation

CHTN: Cooperative Human Tissue Network

CITED1: CREB-binding protein/p300-interacting transactivator with Asp/Glu-rich C-terminal domain

CK1α: casein kinase 1α

Colonoids: colon organoids

CRC: colorectal cancer

CRISPRa: CRISPR activation

CTNNB1: β-catenin

Cys: cysteine

CytoTRACE: Cellular Trajectory Reconstruction Analysis Using Gene Counts and Expression

Daam1: Dishevelled-associated activator of morphogenesis 1

DAG: diacylglycerol

dCas9: nuclease-deficient Cas9

DIO: iodothyronine deiodinase

DKK1: Dickkopf-1

DLL: delta-like

DMEM: Dulbecco's Modified Eagle Medium

DSS: dextran sodium sulfate

eEFSec: eukaryotic elongation factor, selenocysteine-tRNA specific

EGF: epidermal growth factor

ELISA: enzyme-linked immunosorbent assay

EMT: epithelial-mesenchymal transition

Enteroids: small intestinal organoids

EPA: eicosapentaenoic acid

ER: endoplasmic reticulum

ERAD: endoplasmic reticulum-associated protein degradation

FAP: familial adenomatous polyposis

FBS: fetal bovine serum

FOXO: forkhead box, class O

GALT: gut-associated lymphoid tissue

GFR: growth factor-reduced

Gln: glutamine

Glu: glutamic acid

GPX: glutathione peroxidase

GSH: glutathione

GSK-3β: glycogen synthase kinase 3β

H&E: hematoxylin and eosin

H_2O_2: hydrogen peroxide

H_2O_3PSe: monoselenophosphate

H_2Se: hydrogen selenide

Hep: liver-specific

His: histidine

HNF-4α: hepatic nuclear factor 4α

HSPG: heparan sulfate proteoglycan

IE: intestinal epithelial

IF: immunofluorescence

IFN-γ: interferon-γ

IgG: immunoglobulin G

IL: interleukin

i.p.: intraperitoneal

IP: immunoprecipitation

IP3: inositol trisphosphate

IRB: Institutional Review Board

JNK: c-Jun N-terminal kinase

KD: knockdown

kDa: kilodalton

kg: kilogram

KO: knockout

KRAS: Kirsten rat sarcoma virus

L: length

LDL: low-density lipoprotein

LDLR: low-density lipoprotein receptor

LEF: lymphoid enhancer factor

Leu: leucine

LGR5: leucine-rich repeat-containing G protein-coupled receptor 5

LOF: loss-of-function

LOH: loss-of-heterozygosity

LRIG1: leucine-rich repeats and immunoglobulin-like domains 1

LRP: low-density lipoprotein receptor-related protein

Lys: lysine

M: microfold

MAP3K7: mitogen-activated protein kinase kinase kinase 7

ME-MIRAGE: Mutant Enteroid miRNA and Gene Expression

mg: milligram

Mg^{2+}: magnesium

mL: milliliter

mM: millimolar

MMR: mismatch repair

MSI-H: microsatellite instability-high

MSRB1: methionine sulfoxide reductase B1

MSS: microsatellite stable

MxIF: multiplex immunofluorescence

Mye: myeloid-specific

$NaClO_3$: sodium chlorate

Na_2SeO_3: sodium selenite

NFAT: nuclear factor of activated T cells

ng: nanogram

NGS: normal goat serum

NLK: Nemo-like kinase

$ONOO^-$: peroxynitrite

p53: tumor protein p53

PBS: phosphate-buffered saline

p-BSC: p-methoxybenzylselenocyanate

PCOOH: phosphatidylcholine hydroperoxide

PCP: planar cell polarity

PCR: polymerase chain reaction

PGC-1α: peroxisome proliferator-activated receptor gamma coactivator 1α

PIP2: phosphatidylinositol-4,5-bisphopshate

PKB: protein kinase B

PKC: protein kinase C

PLC: phospholipase C

PTK7: protein tyrosine kinase 7

p-XSC: p-xyleneselenocyanate

Rac: Ras-related C3 botulinum toxin substrate

R-ChIP: reverse chromatin immunoprecipitation

Rho: Ras homologous protein

rhWNT3A: recombinant human WNT3A

rmWNT3A: recombinant mouse WNT3A

RNA-seq: RNA sequencing

ROCK: Rho-associated protein kinase

ROR: receptor tyrosine kinase-like orphan receptor

ROS: reactive oxygen species

RPMI: Roswell Park Memorial Institute

RSPO: R-spondin

RT-qPCR: reverse transcription-quantitative polymerase chain reaction

RYK: receptor-like tyrosine kinase

SCENIC: Single-Cell Regulatory Network Inference and Clustering

SCLY: selenocysteine lyase

scRNA-seq: single-cell RNA sequencing

Se: selenium

Sec: selenocysteine

SECIS: selenocysteine insertion sequence

SECISBP2: selenocysteine insertion sequence binding protein 2

SELENO: selenoprotein

SeP: selenoprotein

SEPHS2: selenophosphate synthetase 2

Ser: serine

SFRP: secreted Frizzled-related protein

siRNA: small interfering RNA

SMAD: mothers against decapentaplegic homolog

SNP: single nucleotide polymorphism

SOST: sclerostin

SOX9: sex-determining region Y-box transcription factor 9

SREBP-1c: sterol regulatory element-binding protein 1c

SSC: serrated-specific cells

STAT3: signal transducer and activator of transcription 3

STF: Super TOPFlash

T3: triiodothyronine

T4: thyroxine

TA: transit-amplifying

TAM: tumor-associated macrophage

TBS: Tris-buffered saline

TBS-T: Tris-buffered saline with Tween-20

tBuOOH: tert-Butyl hydroperoxide

TCF: T cell factor

TCGA: The Cancer Genome Atlas

TEER: transepithelial electrical resistance

TGF-β: transforming growth factor β

Thr: threonine

TIL: tumor-infiltrating lymphocyte

TNF-α: tumor necrosis factor α

TPSR: Translational Pathology Shared Resource

$tRNA^{Sec}$: selenocysteine-specific tRNA

Tumoroids: tumor organoids

TXN: thioredoxin

TXNRD: thioredoxin reductase

U: selenocysteine

UC: ulcerative colitis

UTR: untranslated region

VLDLR: very low-density lipoprotein receptor

VU: Vanderbilt University

VUMC: Vanderbilt University Medical Center

v/v: volume per volume

W: width

WT: wild-type

w/v: weight per volume

CHAPTER 1: INTRODUCTION

The intestinal epithelium

The term “intestine” describes two related, yet distinct organs: the small and large intestine. The small intestine is subdivided into three segments: the duodenum, jejunum, and ileum. The large intestine is subdivided into four segments: the cecum, colon, rectum, and anus. The small intestine predominantly digests food and absorbs macro- and micronutrients, whereas the colon absorbs electrolytes and residual water (1). Macronutrients are carbohydrates, fats, and proteins, while micronutrients are organic and inorganic molecules commonly referred to as vitamins and minerals, respectively. Essential vitamins include vitamin A, B_1, B_2, B_3, B_5, B_6, B_7, B_9, B_{12}, C, D, E, and K. Essential minerals include calcium, chloride, cobalt, copper, fluoride, iodine, iron, magnesium, manganese, phosphorus, potassium, selenium, sodium, sulfur, and zinc. Unlike macronutrients, micronutrients do not directly provide energy; however, they are required in small quantities to support metabolism, immunity, and fertility, among other functions. Additionally, several micronutrients (e.g. selenium) act as antioxidants to protect cells from free radical damage (2).

Both the small intestine and colon are lined by a single layer of columnar cells, collectively referred to as the intestinal epithelium, organized into tubular invaginations called crypts (**Figure 1**). Small intestinal crypts are juxtaposed with villi, finger-like protrusions that maximize surface area available for nutrient and water absorption. At the base of the crypt, stem cells characterized by expression of leucine-rich repeat-containing G protein-coupled receptor 5 (LGR5) are intercalated by specialized secretory cells that support the stem cell niche, called Paneth cells in the small intestine and deep crypt secretory cells in the colon. LGR5-positive crypt base columnar (CBC) cells divide into transit-amplifying (TA) cells, which divide two to five times and differentiate into absorptive and secretory cells as they migrate towards the top of the crypt.

Absorptive colonocytes and enterocytes in the colon and small intestine, respectively, compose 80-90% of all differentiated epithelial cells and function to absorb nutrients and water. Microfold (M) cells sample and transport antigens from the lumen to immune cells found within gut-associated lymphoid tissue (GALT). Secretory cell types include Paneth/deep crypt secretory cells, goblet cells, tuft cells, and enteroendocrine cells. Paneth and deep crypt secretory cells in the small intestine and colon, respectively, secrete antimicrobial proteins as well as epidermal growth factor (EGF) and Notch ligands (delta-like 1, DLL1; delta-like 4, DLL4) to support CBC cell proliferation. Paneth cells, but not deep crypt secretory cells, also secrete WNTs to promote CBC cell self-renewal. Goblet cells secrete mucus to protect and lubricate the epithelial surface. Tuft cells secrete context-dependent immuno- and neuromodulators, while enteroendocrine cells secrete hormones. Most mature intestinal epithelial cells, with the notable exceptions of Paneth/deep crypt secretory cells, continue to migrate upwards over the course of four to seven days until they reach the top of the villi/crypts and undergo anoikis into the lumen (1).

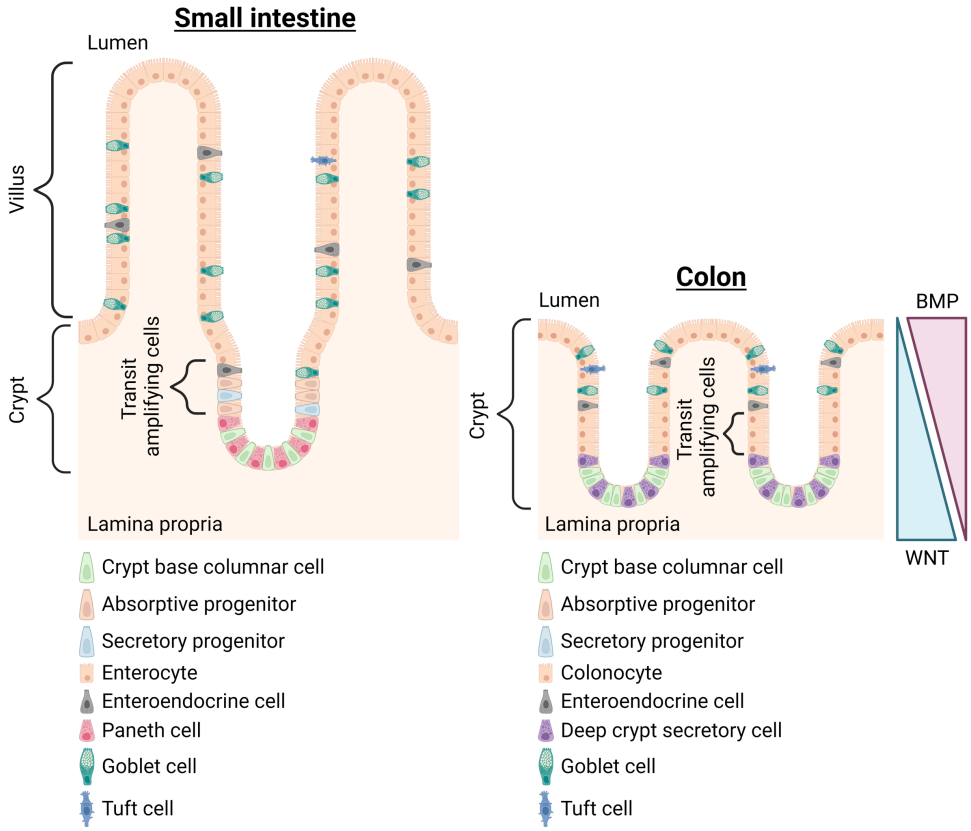

Figure 1. Organization and composition of the intestinal epithelium. BMP: bone morphogenetic protein.

WNT signaling

The highly evolutionarily conserved WNT signaling pathway is crucial for the development, renewal, and regeneration of the intestinal epithelium. WNT signaling can be divided into canonical, or β-catenin-dependent, and noncanonical, or β-catenin-independent, pathways. In canonical WNT signaling, a "destruction complex" primarily composed of glycogen synthase kinase 3β (GSK-3β), casein kinase 1α (CK1α), β-transducin repeat-containing E3 ubiquitin protein ligase (β-TRCP), Axin, and adenomatous polyposis coli (APC) sequesters β-catenin in the cytosol. β-catenin phosphorylation by CK1 and GSK3β triggers ubiquitination by β-TRCP and subsequent degradation by the proteasome (**Figure 2**). When extracellular WNTs bind their co-receptors Frizzled and low-density lipoprotein receptor-related protein 5/6 (LRP5/6), Dishevelled recruits the destruction complex to the plasma membrane. This allows stabilized β-catenin to accumulate and translocate into the nucleus, where it binds T cell factor/lymphoid enhancer factor (TCF/LEF) transcription factors to induce transcription of WNT target genes (**Figure 2**). Importantly, there are numerous known canonical WNT target genes, many of which promote cell survival and proliferation in tissue- and context-specific fashions (3).

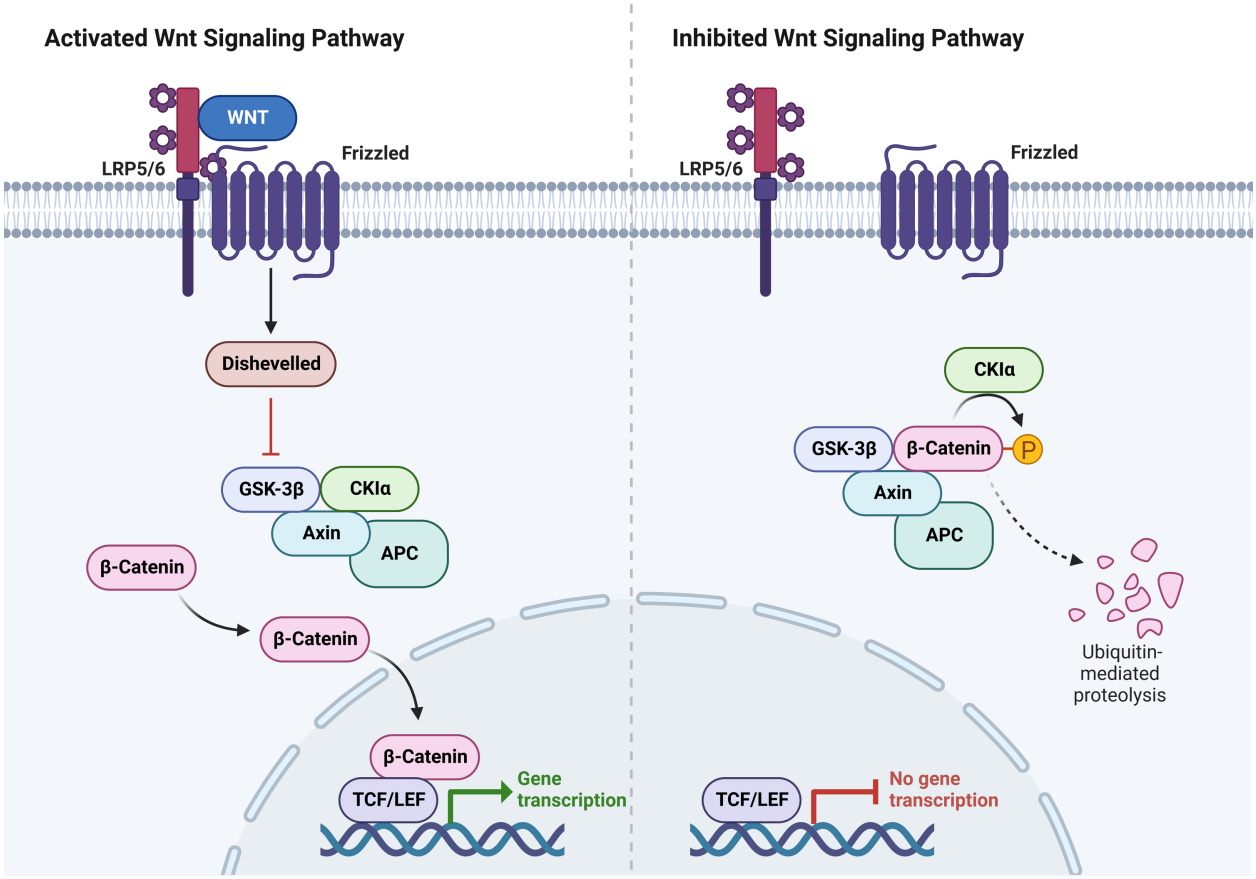

Figure 2. The canonical WNT signaling pathway. Adapted from "Wnt Signaling Pathway Activation and Inhibition," by BioRender.com (2023). Retrieved from https://app.biorender.com/biorender-templates.

Noncanonical WNT signaling encompasses two major pathways: the WNT/planar cell polarity (PCP) signaling pathway and the WNT/Ca^{2+} signaling pathway. In the WNT/PCP signaling pathway, WNTs bind Frizzled and one of several possible pseudokinase co-receptors, including receptor-like tyrosine kinase (RYK), receptor tyrosine kinase-like orphan receptor 1 (ROR1), ROR2, or protein tyrosine kinase 7 (PTK7). This heterotrimerization recruits Dishevelled, which then complexes with Dishevelled-associated activator of morphogenesis 1 (Daam1). Daam1 can interact directly with the actin-binding protein profilin, or activate small GTPases of the Ras homologous protein (Rho) and Ras-related C3 botulinum toxin substrate (Rac) families. Rhos and Racs activate Rho-associated protein kinases (ROCKs) and c-Jun N-terminal kinases (JNKs), respectively. The downstream effectors of both ROCKs and JNKs modulate cytoskeletal rearrangement; however, JNKs also regulate cellular processes such as apoptosis, migration, and proliferation (4).

In the WNT/Ca^{2+} signaling pathway, WNTs bind Frizzled alone, which recruits Dishevelled and G proteins. These G proteins, in turn, activate phospholipase C (PLC); PLC cleaves the membrane phospholipid phosphatidylinositol-4,5-bisphopshate (PIP2) into the second messengers inositol trisphosphate (IP3) and diacylglycerol (DAG). IP3 mobilizes Ca^{2+} from the endoplasmic reticulum (ER), which activates calcineurin and Ca^{2+}/calmodulin-dependent protein kinase type II (CaMKII), whereas DAG recruits and activates protein kinase C (PKC). Calcineurin activates the transcription factor nuclear factor of activated T cells (NFAT), CaMKII activates Nemo-like kinase (NLK) as well as mitogen-activated protein kinase kinase kinase 7 (MAP3K7), and PKC activates cell division control protein 42 homolog (Cdc42). Together, NFAT, NLK, MAP3K7, and Cdc42 modulate cellular proliferation, morphology, migration, endocytosis, differentiation, apoptosis, and adhesion (5).

In summary, canonical WNT signaling involves WNT-induced heterodimerization of Frizzled and LRP5/6, whereas noncanonical WNT signaling entails either WNT-induced heterodimerization of Frizzled and RTK pseudokinases (WNT/PCP) or WNT-induced, Frizzled-mediated activation of G proteins (WNT/Ca^{2+}). Canonical WNT signaling, with the transcription factor β-catenin as its key

downstream effector, robustly regulates transcription of genes implicated in cellular survival, proliferation, and fate. In contrast, noncanonical WNT signaling involves activation of complex signaling cascades that modulate diverse cellular processes. Notably, individual WNTs exhibit broad specificity for their co-receptors, and thus mediate both noncanonical and canonical WNT signaling. Additionally, noncanonical WNT signaling can antagonize canonical WNT signaling, indicative of substantial cross-talk between these pathways (6).

Low-density lipoprotein receptor-related proteins

The LRP family includes seven core members: low-density lipoprotein receptor (LDLR), LRP1, LRP1b, LRP2 (megalin), LRP4 (MEGF7), LRP8 (ApoER2), and very low-density lipoprotein receptor (VLDLR) (**Figure 3**). Although initially identified as endocytic receptors for lipoproteins, now all LRPs but LDLR are understood to play signaling and endocytic roles beyond lipid homeostasis. LDLR, the founding member of the LRP family, mediates low-density lipoprotein (LDL) uptake (7). LRP1 and its lesser studied homolog LRP1b endocytose >100 different ligands, such as cytokines, extracellular matrix proteins, growth factors, heat shock proteins, lipoproteins, necrotic cell debris, proteases, protease inhibitor complexes, and viruses. LRP1 and LRP1b thus modulate innumerable cellular processes (8). LRP2 primarily endocytoses hormones, lipoproteins, and vitamins, and plays related roles in bone, brain, and reproductive development (9). LRP4 has been implicated in the development and maintenance of the neuromuscular junction as well as bone. Interestingly, LRP4 can antagonize canonical WNT signaling, by competing with LRP5/6 for Frizzleds or binding WNT inhibitors such as Dickkopf-1 (DKK1), sclerostin (SOST), and Wise (10). Both LRP8 and VLDLR interact with Reelin, a large, secreted extracellular matrix glycoprotein crucial for proper brain development and function (11). In addition to its role in Reelin signaling, some reports indicate that LRP8 promotes canonical WNT signaling activity, although the mechanism(s) awaits further elucidation (12, 13). Lastly, VLDLR mediates endocytic uptake of very low-density lipoproteins, and thus contributes to cholesterol homeostasis (7).

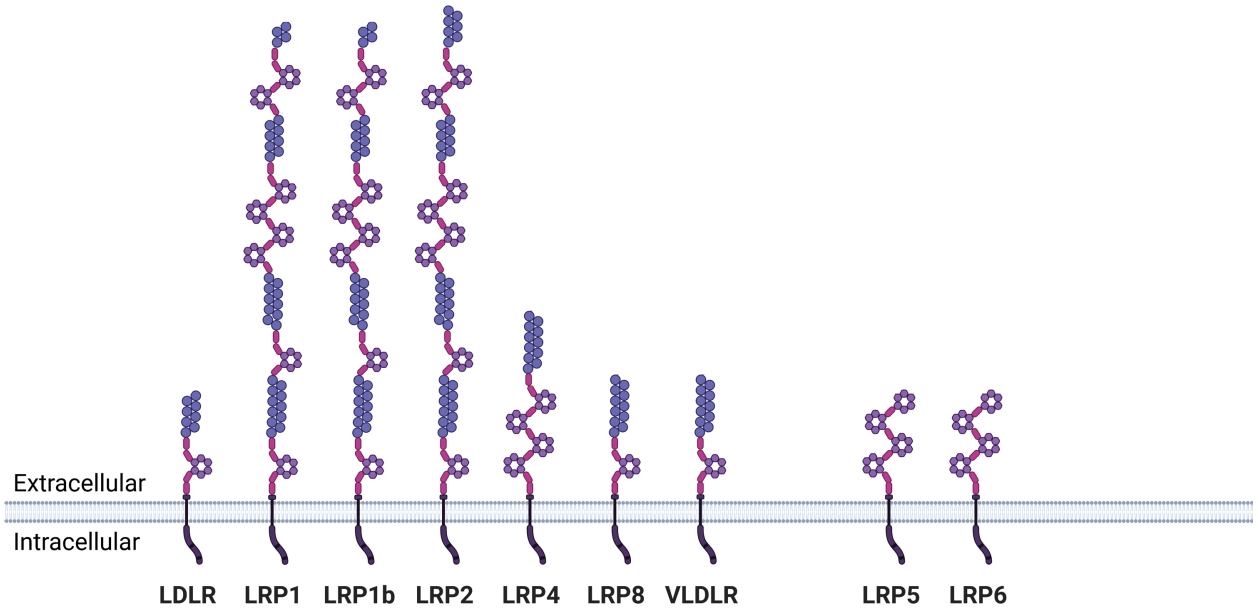

Figure 3. The LRP family and related proteins.

LRP5/6 structure

Although not strictly considered core members of the LRP protein family, LRP5 and LRP6 are often included based on their functional and structural similarities with different LRPs (**Figure 3**). LRP5 and LRP6 are highly homologous proteins, sharing ~70% sequence identity (**Appendix A: Figure 43**). LRP6 is a 180-210 kDa protein comprised of ~1600 amino acids. LRP6's large extracellular domain (~1350 amino acids) contains four β-propeller (BP) domains (also known as LDLR type B repeats) intercalated with four EGF-like domains (collectively referred to as E1-4), followed by three LDLR type A repeats, named for their homology to those in the LDLR ligand-binding region (**Figure 4**). LRP6 also contains a short, hydrophobic transmembrane domain followed by an intracellular domain that mediates cytoplasmic signaling (14).

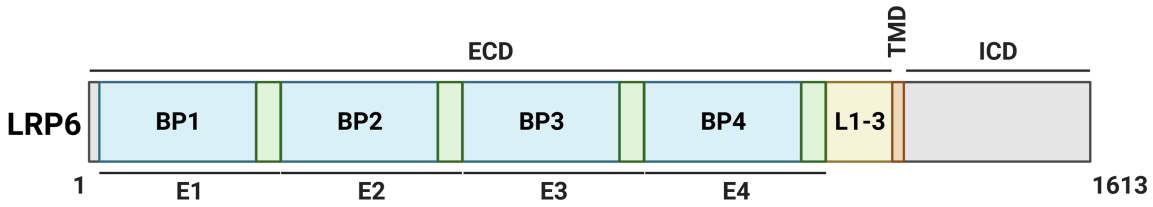

Figure 4. Structure of LRP6. BP: β-propeller, E: β-propeller and EGF-like domain, ECD: extracellular domain, L1-3: LDL type A repeats, ICD: intracellular domain, TMD: transmembrane domain.

The BP domains in LRP6 consist of six groups of four antiparallel β-strands. LRP6's BP1, BP2, and BP3 domains share more sequence homology with each other than with its BP4 domain (**Figure 5**). Accordingly, the BP1, BP2, and BP3 domains of LRP6 include an exposed hydrophobic region surrounded by negatively charged residues, which the BP4 domain lacks (15). Additionally, LRP6's BP1 and BP2 domains fold cooperatively, as do its BP3 and BP4 domains (16). The top surfaces of LRP6's BP1 and BP3 domains contain binding sites for WNTs, WNT inhibitors, and anti-LRP6 antibodies (14).

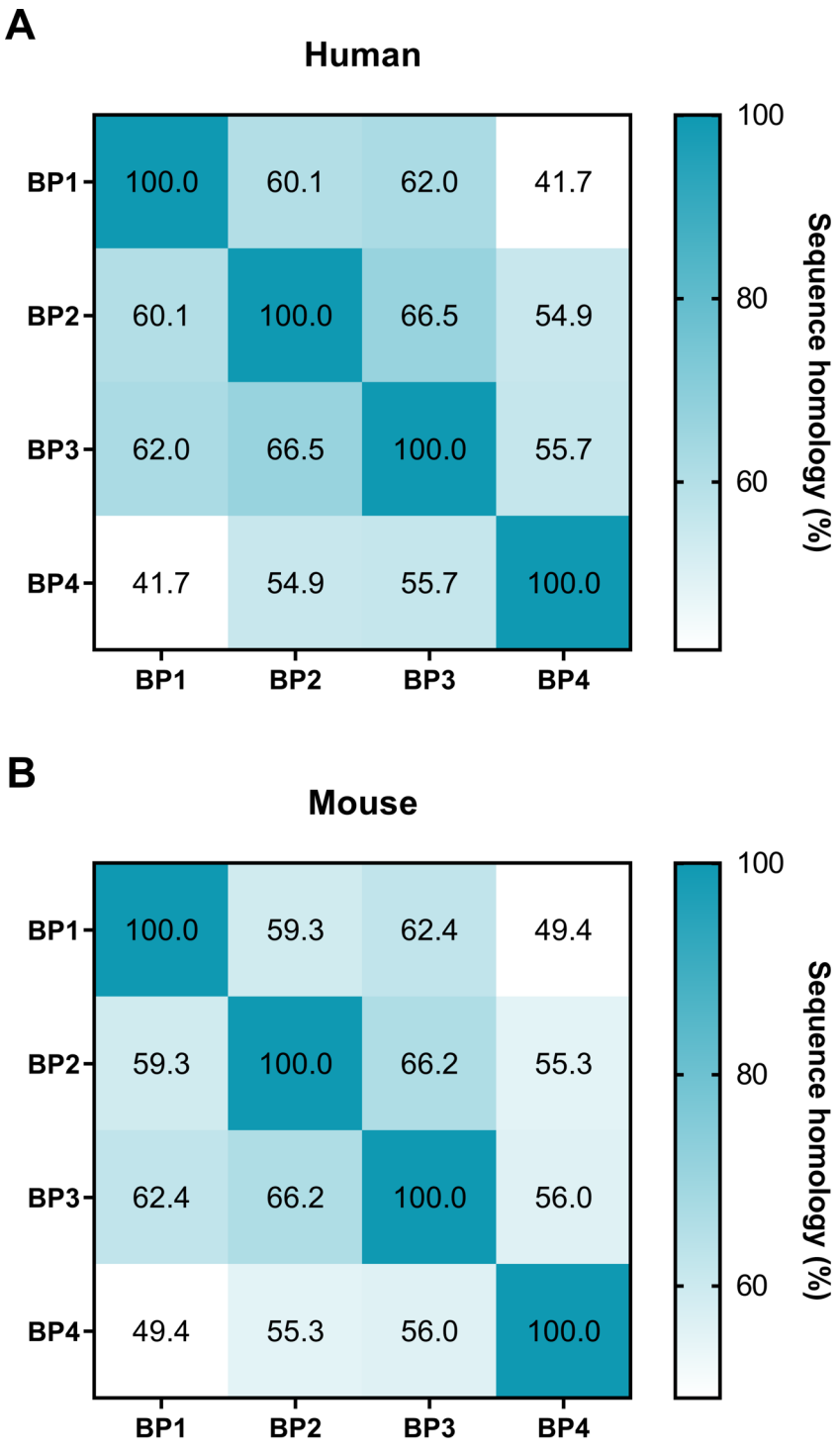

Figure 5. Sequence homology among LRP6 BP domains. (A) Human LRP6, (B) mouse LRP6. BP: β-propeller.

Selenium, selenocysteine, and selenoproteins

The essential micronutrient selenium (Se) exerts many of its biological functions in the form of the 21st proteinogenic amino acid selenocysteine (Sec), which is incorporated into Sec-containing proteins, or selenoproteins (SePs) (17). Sec residues provide many SePs with redox capabilities, as Sec residues are more efficient catalysts than cysteine (Cys) residues found within active sites of non-SeP enzymes. Specifically, the selenol group in Sec is more acidic than the thiol group in Cys ($pK_a \approx 5.2$ vs. 8.5, respectively) and thus more nucleophilic at physiological pH (18). Sec insertion into nascent SePs requires a characteristic stem-loop secondary structure in the 3' untranslated region (UTR) of the SeP transcript, known as a Sec insertion sequence (SECIS), in addition to specialized translation machinery: a Sec-specific tRNA ($tRNA^{Sec}$) able to recode the opal stop codon (UGA) as Sec, SECIS binding protein 2 (SECISBP2), and eukaryotic elongation factor, Sec-tRNA specific (eEFSec) (19–21). Importantly, expression of these specialized translation factors, especially $tRNA^{Sec}$, depends on Se availability (22). In Se deficiency, UGA read-through and Sec insertion fails to occur, resulting in nonsense-mediated mRNA decay (23).

The 25 known human SePs exhibit diversity in localization, function, and characterization. Well-studied SePs include the glutathione peroxidases (GPXs) GPX1, GPX2, GPX3, GPX4, and GPX6; the thioredoxin reductases (TXNRDs) TXNRD1, TXNRD2, and TXNRD3; the iodothyronine deiodinases (DIOs) DIO1, DIO2, and DIO3; methionine sulfoxide reductase B1 (MSRB1); and selenophosphate synthetase 2 (SEPHS2) (24). GPXs reduce hydrogen peroxide (H_2O_2), organic hydroperoxides, and phospholipid hydroperoxides (GPX4) with the coenzyme reduced glutathione (GSH), while TXNRDs reduce oxidized thioredoxins (TXN), organic hydroperoxides, and H_2O_2, among other substrates (25, 26). DIOs deiodinate the inactive thyroid hormone thyroxine (T4) to its active form triiodothyronine (T3), whereas MSRB1 reduces methionine sulfoxide in proteins to methionine (27, 28). SEPHS2 converts hydrogen selenide (H_2Se) and adenosine triphosphate (ATP) to monoselenophosphate (H_2O_3PSe), the Se donor for $tRNA^{Sec}$ synthesis (29). Lesser characterized SePs include the ER-resident selenoproteins F

(SELENOF), K (SELENOK), M (SELENOM), N (SELENON), S (SELENOS), and T (SELENOT), implicated in Ca^{2+} homeostasis (SELENOK, SELENOM, SELENON, SELENOT) and ER-associated protein degradation (ERAD) (SELENOF, SELENOK, SELENOS); the nuclear oxidoreductase selenoprotein H (SELENOH); the ethanolamine phosphotransferase selenoprotein I (SELENOI); the mitochondrial oxidoreductase selenoprotein O (SELENOO); and two SePs of unclear function: selenoproteins V (SELENOV) and W (SELENOW) (30–34).

SELENOP structure, function, and expression

Another well-studied, yet unique member of the SeP family is the secreted glycoprotein selenoprotein P (SELENOP). Although largely produced and secreted by the liver, SELENOP is ubiquitously expressed throughout the body, and at particularly high levels in the brain, testis, gastrointestinal tract, and hematopoietic system (35). Unlike all other known SePs, which incorporate a single Sec residue into their primary structures, SELENOP possesses multiple Secs. Rat, mouse, and human SELENOP contain one Sec in an N-terminal thioredoxin-like fold (UXXC) and nine Secs in a C-terminal Se-rich domain (**Figure 6**) (36). Additionally, SELENOP has three histidine-rich regions, which include one established and two putative heparin binding sites (37, 38). SELENOP is also N-glycosylated at three N-terminal sites and O-glycosylated at one C-terminal site (39).

Figure 6. Structure of SELENOP. HBS: heparin binding site, His-rich: histidine-rich regions, LRP8 BS: lipoprotein receptor-related protein 8 (LRP8) binding site, U: selenocysteine.

Sec insertion into SELENOP involves two separate SECIS elements in the *SELENOP* mRNA. Notably, SECIS 1 is markedly more efficient than SECIS 2. In general, SECIS 2 recodes *SELENOP*'s first UGA codon, while SECIS 1 recodes *SELENOP*'s subsequent UGA codons (40). Failure to recode *SELENOP*'s UGA codons yields premature termination products that correspond to the major SELENOP isoforms previously described. Four SELENOP isoforms have been identified in rat plasma that result from termination at the second, third, or seventh UGA codons, or translation of the full *SELENOP* transcript (41, 42). The two SELENOP isoforms reproducibly observed in mouse and human plasma are thought to represent full-length and truncated isoforms of the protein, yet these isoforms await further characterization (43–46). However, the SELENOP isoforms produced by the tissues of other organisms remain unknown.

SELENOP serves dual roles as an antioxidant and Se transport protein through its N- and C-terminal Sec-containing domains, respectively. In cell-free systems, SELENOP reduced TXNRD1 with either tert-Butyl hydroperoxide (tBuOOH) or H_2O_2 as substrates. Importantly, substitution of SELENOP's N-terminal Sec with serine (Ser) abolished this activity (47). Additionally, SELENOP functions as an extracellular phospholipid hydroperoxidase *in vitro*. Specifically, SELENOP reduced phosphatidylcholine hydroperoxide (PCOOH) using TXN or GSH as electron donors, and protected plasma proteins from oxidation by peroxynitrite ($ONOO^-$) (48, 49). In support of SELENOP's intracellular redox function, small intestinal organoids ("enteroids") from *Selenop* knockout (KO) mice displayed decreased viability and oxidative buffering capacity as compared to enteroids from wild-type (WT) mice (50). Similarly, SELENOP knockdown (KD) in human ulcerative colitis (UC) organoids increased reactive oxygen species (ROS) levels at baseline and decreased viability after H_2O_2 treatment (51).

In contrast to its role as an antioxidant, SELENOP's role in Se transport, via the Sec residues in its protein structure, has been studied far more extensively. SELENOP, largely produced by the liver and secreted into the plasma, supplies Se to distant tissues for local SeP synthesis (36). In fact, SELENOP's

ten Sec residues are estimated to comprise ~60% of total plasma Se content (52). As such, SELENOP levels, together with Se levels and GPX activity, constitute the three major biomarkers of whole-body Se status (36). In mice, liver-specific *Selenop* deletion reduced plasma SELENOP, Se, and GPX activity by 96%, 91%, and 87%, respectively, as compared to controls. Moreover, in support of a role for liver-derived SELENOP in Se delivery to distant tissues, liver-specific *Selenop* KO decreased Se levels by 12% in brain, 30% in testis, 52% in muscle, and 65% in kidney (53).

Cells internalize extracellular, secreted SELENOP bound to cell-surface LRPs via clathrin-mediated endocytosis (54). Several SELENOP receptors have been identified in various tissues, namely LRP1, LRP2, and LRP8 (55–58). LRP1 has been reported as the SELENOP receptor in muscle, as mice with muscle-specific LRP1 deficiency showed reduced SELENOP levels in skeletal muscle after SELENOP injection, as compared to WT, SELENOP-injected mice (55). LRP2 serves as the SELENOP receptor in the kidney: LRP2 and SELENOP co-localized in the proximal renal tubules of WT, but not *Lrp2*$^{-/-}$, mouse fetal kidneys (56). LRP8 has been identified as the SELENOP receptor in brain and testis (58, 59). Male *Lrp8*$^{-/-}$ and *Selenop*$^{-/-}$ mice developed similar, severe neurological dysfunction and spermatozoa defects on Se-deficient diet (57, 58, 60, 61). Accordingly, SELENOP was absent from the brains and testes of *Lrp8*$^{-/-}$ mice (58, 59). Although the SELENOP receptor(s) in the gastrointestinal tract remains undefined, *Lrp1*, *Lrp5*, and *Lrp6* are moderately expressed throughout the mouse colon (**Figure 7**).

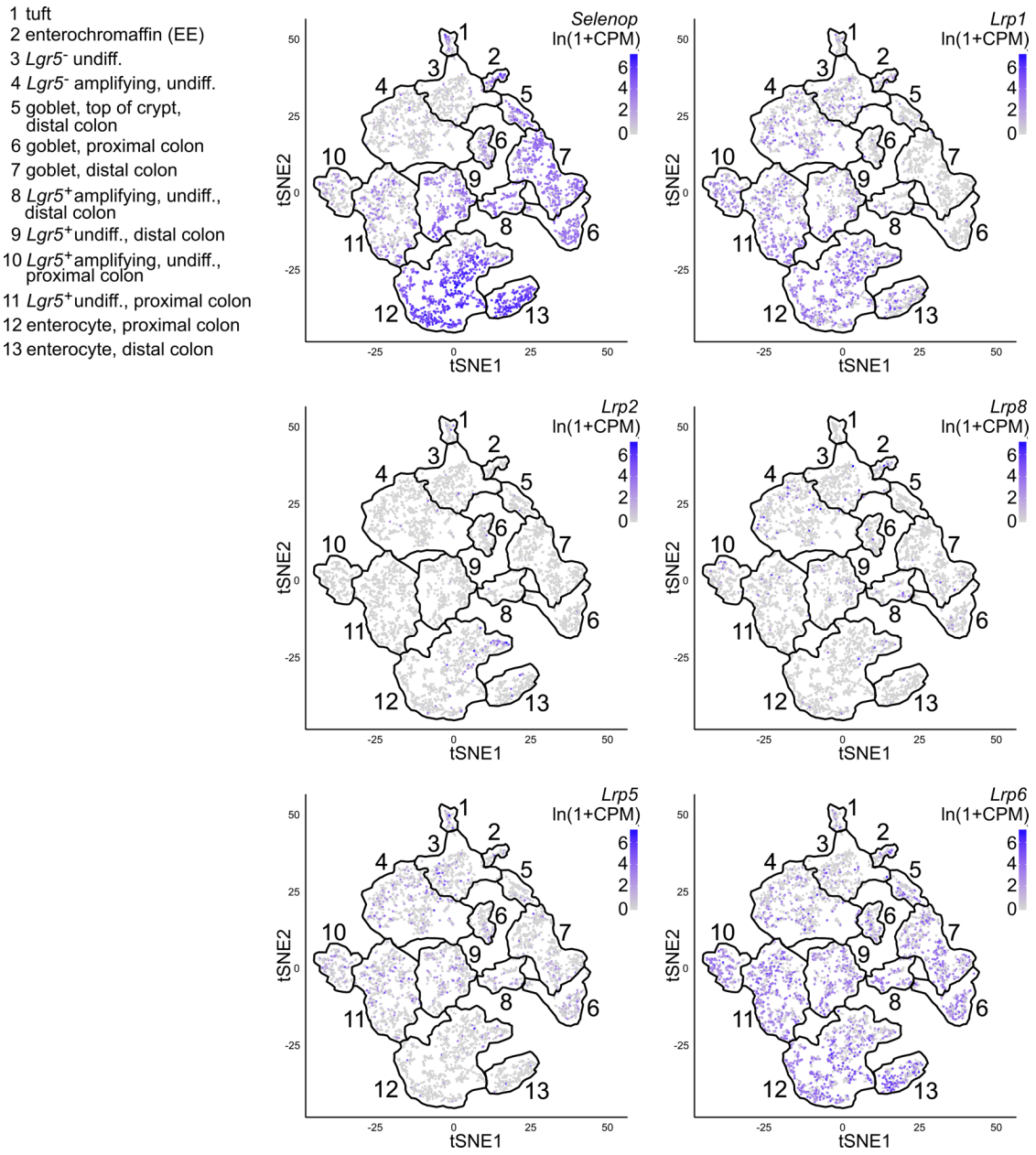

Figure 7. *Selenop* and *Lrp* expression in the mouse colon. Tabula Muris scRNA-seq data queried for *Lrp1*, *Lrp2*, *Lrp5*, *Lrp6*, *Lrp8*, and *Selenop*. n=7 mice.

Interestingly, LRP2 and LRP8 bind different isoforms of SELENOP: LRP2 binds shorter isoforms via SELENOP's N-terminal domain, whereas LRP8 binds longer isoforms via SELENOP's C-terminal domain (56, 62). The selectivity of different LRPs for distinct SELENOP isoforms may impart tissue- and context-specific functional consequences to these interactions. Although the specific residues involved in LRP1: SELENOP and LRP2:SELENOP interactions remain unclear, LRP8:SELENOP interactions required three specific residues (Cys^{324}, Gln^{325}, Cys^{326}) located between SELENOP's fifth and sixth Sec (62). After LRP-mediated endocytosis, SELENOP is rapidly lysosomally degraded to free Sec for sequential metabolism by Sec lyase (SCLY) and SEPHS2. SCLY and SEPHS2 generate H_2Se and H_2O_3PSe; H_2O_3PSe, in turn, donates the Se to convert a $tRNA^{Ser}$ into a $tRNA^{Sec}$ for Sec incorporation into nascent SePs (63).

SELENOP in intestinal homeostasis

In the mouse intestinal epithelium, *Selenop* expression is highest in differentiated cells, including tuft, goblet, enteroendocrine, and enterocyte cell populations (51). Accordingly, $Selenop^{-/-}$ enteroids exhibited greater stemness than $Selenop^{+/+}$ enteroids, namely increases in plating efficiency, proliferation, and spheroid formation. In support of SELENOP's redox function, H_2O_2 treatment increased ROS levels and decreased survival to a greater extent in $Selenop^{-/-}$ enteroids as compared to $Selenop^{+/+}$ enteroids (50). In contrast to global *Selenop* KO, intestinal epithelial-specific *Selenop* deletion ($Selenop^{\Delta IE}$) failed to modify intestinal homeostasis. Specifically, $Selenop^{+/+}$, $Selenop^{\Delta IE/+}$, and $Selenop^{\Delta IE/\Delta IE}$ mice exhibited no differences in colonic proliferation, DNA damage, or apoptosis. Moreover, colon organoids ("colonoids") established from $Selenop^{+/+}$ and $Selenop^{\Delta IE/\Delta IE}$ mice displayed similar viability at days one and four post-plating. Additionally, $Selenop^{+/+}$ and $Selenop^{\Delta IE/\Delta IE}$ colonoids demonstrated similar levels of *Gpx1*, *Gpx2*, and *Gpx3* transcript as well as GPX1 and GPX2 protein (51). The discrepancies between baseline $Selenop^{-/-}$ enteroid and $Selenop^{\Delta IE/\Delta IE}$ colonoid phenotypes may result from different levels of *Selenop* expression, and thus different impacts of *Selenop* deficiency, in the small intestine and colon. Moreover, global, congenital *Selenop* KO may alter intestinal epithelial cell-intrinsic signaling pathways to a greater

extent than tissue- and temporal-specific *Selenop* deletion.

SELENOP in CAC

In addition to SELENOP's role in intestinal homeostasis, our group has studied SELENOP extensively in colitis and colitis-associated cancer (CAC). In human colitis, transcriptional *SELENOP* downregulation in epithelial cells correlated with disease severity, from low-grade dysplasia to CAC (51). CAC can be experimentally modeled in mice by treatment with the mutagen azoxymethane (AOM) followed by repeated exposure to the colitogen dextran sodium sulfate (DSS). In this initiation-promotion model, AOM generates O^6-methylguanine DNA adducts that can result in guanine to adenine transitions or crosslinks, while DSS compromises intestinal epithelial barrier integrity, which allows microorganisms to translocate and stimulate immune cells in the underlying lamina propria (64, 65).

In the AOM/DSS model, whole-body *Selenop* deficiency protected against tumorigenesis. That is, $Selenop^{-/-}$ mice developed fewer colon tumors with lesser dysplasia than $Selenop^{+/+}$ mice. Moreover, $Selenop^{-/-}$ tumors exhibited increased apoptosis and DNA damage, as well as decreased proliferation, as compared to $Selenop^{+/+}$ tumors. Interestingly, $Selenop^{+/-}$ mice displayed the greatest tumor burden, with more colon tumors than either $Selenop^{+/+}$ or $Selenop^{-/-}$ mice. In agreement with this, $Selenop^{+/-}$ tumors demonstrated increased proliferation as compared to either $Selenop^{+/+}$ or $Selenop^{-/-}$ tumors. Such unanticipated observations can be attributed to the "double-edge sword" effect of oxidative stress, in which mild to moderate oxidative stress promotes tumorigenesis through elevated genomic instability, yet extremely high oxidative stress induces apoptosis and thus eliminates initiated cells (50).

Subsequent experiments revealed that both SELENOP's antioxidant and Se transport domains mediate these phenotypes. As previously mentioned, substitution of SELENOP's N-terminal Sec with Ser ($Selenop^{U40S}$) abolishes its redox activity (47). $Selenop^{U40S/U40S}$ mice developed more, larger colon tumors with greater proliferation and DNA damage than $Selenop^{+/+}$ mice after an AOM/DSS protocol. Similarly, deletion of SELENOP's Se transport domain ($Selenop^{\Delta 240\text{-}361}$) promoted tumorigenesis. Specifically,

Selenop$^{\Delta 240\text{-}361/\Delta 240\text{-}361}$ mice developed more colon tumors with greater proliferation, dysplasia, and DNA damage than *Selenop*$^{+/+}$ mice (50).

Our most recent investigations sought to identify the tissue-specific source of tumor-protective SELENOP in experimental CAC. The liver represents one major source of SELENOP; however, liver-specific *Selenop* deletion (*Selenop*$^{\Delta Hep}$) did not modify tumorigenesis. *Selenop*$^{+/+}$ and *Selenop*$^{\Delta Hep/\Delta Hep}$ mice developed colon tumors at similar frequencies and of equivalent sizes after an AOM/DSS protocol. Myeloid cells, and particularly intraepithelial macrophages, constitute another source of SELENOP. Nonetheless, myeloid-specific *Selenop* deletion (*Selenop*$^{\Delta Mye}$) did not impact tumorigenesis. *Selenop*$^{+/+}$, *Selenop*$^{\Delta Mye/+}$, and *Selenop*$^{\Delta Mye/\Delta Mye}$ mice exhibited no differences in colon tumor size, number, or incidence after AOM/DSS treatment. Moreover, *Selenop*$^{+/+}$, *Selenop*$^{\Delta Mye/+}$, and *Selenop*$^{\Delta Mye/\Delta Mye}$ tumors displayed similar levels of macrophage and neutrophil infiltration. Intestinal epithelial cells comprise a third source of SELENOP. Indeed, intestinal epithelial-specific *Selenop* deletion promoted tumorigenesis. *Selenop*$^{\Delta IE/\Delta IE}$ mice developed more, larger colon tumors with greater dysplasia than *Selenop*$^{+/+}$ mice after an AOM/DSS protocol. The greater tumor burden observed in *Selenop*$^{\Delta IE/\Delta IE}$ mice may have resulted from increased tumor initiation, as *Selenop*$^{\Delta IE/\Delta IE}$ mice had more endoscopically visible colon tumors than either *Selenop*$^{+/+}$ or *Selenop*$^{\Delta IE/+}$ mice after the second DSS cycle. In further agreement with this, *Selenop*$^{\Delta IE/\Delta IE}$ colons showed increased intratumoral apoptosis as well as DNA damage, both within tumors and adjacent normal crypts (51).

SELENOP in sporadic CRC

In sporadic colorectal cancer (CRC), primary adenomas demonstrated decreases in SELENOP protein and mRNA expression as compared to adjacent normal colorectal tissues (66–68). Moreover, SELENOP expression was negatively correlated with tumor stage, as stage III and IV primary colorectal carcinomas displayed significantly lower SELENOP protein levels than stage II tumors (66). However, neither patients with colorectal carcinomas nor adenomas exhibited differences in serum SELENOP levels as compared to healthy controls (68, 69).

In addition to SELENOP expression profiling, whole exome sequencing identified six single nucleotide polymorphisms (SNPs) in the *SELENOP* gene that may impact CRC risk. Two such SNPs, the G/A polymorphisms rs3877899 in the *SELENOP* coding sequence and rs7579 in the *SELENOP* 3' UTR, can shift SELENOP isoform expression ratios. Namely, CRC patients with the GG genotype of rs3877899 or the GA genotype of rs7579 had lower plasma levels of the full-length, 60 kDa SELENOP isoform as compared to healthy controls (45) . Moreover, the GA genotype of rs7579 was positively correlated with CRC risk (70). Four additional SNPs in *SELENOP* have been associated with advanced colorectal adenoma risk: one polymorphism in the 5' UTR (C/G at – 4166) and three polymorphisms in the 3'UTR (A/G at 31,174 bp 3' of STOP, rs12055266; G/A at 43,881 bp 3'of STOP, rs3797310; and C/T at 44,321 bp 3' of STOP, rs2972994) (71). However, the relevance of these four SNPs to SELENOP function and/or expression awaits further elucidation.

Summary

WNT signaling plays important homeostatic roles in the intestinal epithelium. Canonical, but not noncanonical, WNT signaling utilizes the WNT co-receptor LRP5/6 and the key downstream transcriptional effector β-catenin. LRP5/6 is a close relative of the LRP protein family, whose members bind a vast array of structurally and functionally diverse ligands, and thus modulate innumerable signaling pathways. LRP1, LRP2, and LRP8 mediate cellular uptake of SELENOP, which serves as both a local antioxidant and a Se source for SeP synthesis. SELENOP, and particularly intestinal epithelial-derived SELENOP, protects against experimental CAC. However, SELENOP's expression in and contributions to sporadic CRC are understudied.

CHAPTER 2: METHODS

RNA isolation, cDNA synthesis, and RT-qPCR

Colon/small intestine epithelia were isolated as previously described (72). Cells/organoids were homogenized in TRIzol™ Reagent (15596018, Invitrogen) prior to RNA isolation with the RNeasy® Mini (74106, Qiagen) or Micro (74004, Qiagen) Kit, as appropriate. cDNA was synthesized from 2 µg total RNA with qScript™ cDNA SuperMix (95048100, Quantabio). TaqMan™ RT-qPCR was performed in triplicate with TaqMan™ probes listed in **Table 1** (Applied Biosystems) and TaqMan™ Universal PCR Master Mix (4304437, Applied Biosystems). SYBR Green RT-qPCR was performed in triplicate with primers listed in **Table 2** (Integrated DNA Technologies) and PerfeCTa® SYBR® Green SuperMix ROX (9505502K, Quantabio). RT-qPCR results were analyzed by the delta-delta Ct method and normalized to *Gapdh/GAPDH*, *GUSB*, or *Tbp*.

Gene	Assay ID
Dio1	Mm00839358_m1
Dio2	Mm00515664_m1
Dio3	Mm00548953_s1
Gapdh	Mm99999915_g1
Gpx1	Mm00656767_g1
Gpx2	Mm00850074_g1
Gpx3	Mm00492427_m1
Gpx4	Mm00515041_m1
GUSB	Hs00939627_m1
Msrb1	Mm00489121_m1
Selenof	Mm00474111_m1
Selenoh	Mm01335355_g1
Selenoi	Mm01210813_m1
Selenok	Mm00785961_s1
Selenom	Mm00459806_m1
Selenon	Mm01188435_m1
Selenoo	Mm00662744_m1
Selenop	Mm00486048_m1
Selenos	Mm01318786_m1
Selenot	Mm01615823_m1
Selenov	Rn01475733_m1
Selenow	Mm01268252_m1
Sephs2	Mm00545980_s1
Tbp	Mm00446973_m1
Txnrd1	Mm00443675_m1
Txnrd2	Mm00496766_m1
Txnrd3	Mm00462552_m1

Table 1. TaqMan™ RT-qPCR probes.

Gene	Primer Names	Primer Sequences (5' to 3')	Reference
Axin2	mAxin2_RT_F mAxin2_RT_R	TGACTCTCCTTCCAGATCCCA TGCCCACACTAGGCTGACA	Short et al. (2019) *Oncogene*.
AXIN2	hAXIN2_RT_F hAXIN2_RT_R	CAACACCAGGCGGAACGAA GCCCAATAAGGAGTGTAAGGACT	Thompson et al. (2019) *Carcinogenesis*
Gapdh	mGapdh_RT_F mGapdh_RT_R	CCGCATCTTCTTGTGCA CGGCCAAATCCGTTCA	Short et al. (2019) *Oncogene*.
GAPDH	hGAPDH_RT_F hGAPDH_RT_R	GGCCTCCAAGGAGTAAGACC AGGGGTCTACATGGCAACTG	Thompson et al. (2019) *Carcinogenesis*
Lgr5	mLgr5_RT_F mLgr5_RT_R	CCAATGGAATAAAGACGACGGCAACA GGGCCTTCAGGTCTTCCTCAAAGTCA	Luong-Gardiol et al. (2019) *Cancer Cell.*
LGR5	hLGR5_RT_F hLGR5_RT_R	GAGTTACGTCTTGCGGGAAAC TGGGTACGTGTCTTAGCTGATTA	Liao et al. (2020) *Stem Cell Rep.*
Sox9	mSox9_RT_F mSox9_RT_R	GAGCCGGATCTGAAGAGGGA GCTTGACGTGTGGCTTGTTC	Wang et al. (2020) *Cancer Cell.*
SOX9	hSOX9_RT_F hSOX9_RT_R	AGCGAACGCACATCAAGAC CTGTAGGCGATCTGTTGGGG	Li et al. (2015) *PLoS One.*

Table 2. SYBR Green RT-qPCR primers.

RNA *in situ* hybridization (RNAscope®)

Chromogenic RNA *in situ* hybridization was performed with bacterial *DapB* (negative control) (310043), human *PPIB* (positive control) (313901), mouse *Ppib* (positive control) (313911), human *SELENOP* (512831), or mouse *Selenop* (549611) RNAscope® probes (Advanced Cell Diagnostics) and RNAscope® 2.5 HD – BROWN reagents (322300, Advanced Cell Diagnostics) per the manufacturer's protocol.

scRNA-seq data analysis and visualization

Gut Cell Atlas single-cell RNA sequencing (scRNA-seq) expression data (73) were explored at https://www.gutcellatlas.org. Human colorectal polyp/cancer scRNA-seq data (74, 75) (HTA10, HTA11) are publicly available through the Human Tumor Atlas Network (https://data.humantumoratlas.org). Human CRC scRNA-seq data (76) (GSE178341) are publicly available through NCBI's Gene Expression Omnibus (https://www.ncbi.nlm.nih.gov/geo/). These scRNA-seq datasets were analyzed in Python using scanpy, pandas, and numpy packages as previously described (75). Briefly, raw scRNA-seq counts were normalized by median library size, log-like transformed with Arcsinh, and Z-score standardized per gene. CytoTRACE analysis (77) was conducted as previously described (75).

Polyp, normal, and cancer tissue datasets from (75) were integrated with the Single-Cell Regulatory Network Inference and Clustering (SCENIC) pipeline (78, 79). From the SCENIC-derived, Z-score-standardized AUCell values, the "scanpy.tl.umap" function was used to compute UMAP coordinates, 50-principal component decompositions with no feature selection, and k-nearest-neighbor graphs with k equal to the square root of the number of cells projected. The UMAP visualization for the dataset from (74) was produced by the same procedure but with normalized count values. Strip plots were generated from down-sampled data of the corresponding bar plots, to keep cell number for all dataset categories equal to the cell number of the smallest category.

Human enteroid culture

Human jejunal organoids were a gift from Dr. James Goldenring (Vanderbilt University, Nashville, TN). These enteroids were established from deidentified tissue collected at Vanderbilt University Medical Center (VUMC) and provided by the Western Division of the Cooperative Human Tissue Network (CHTN) in accordance with the VUMC Institutional Review Board (IRB). Enteroids were refed with Intesticult™ Organoid Growth Medium (06010, STEMCELL Technologies) every 4 days. For ELISA experiments, enteroids were refed every 2-3 days with media described in **Table 3**. Enteroids were split and replated every 7-10 days as described below.

Enteroids were collected by centrifugation at 200 *g* for 5 minutes at 4° C, gently sheared ~20x by pipetting, then centrifuged again as above. Enteroid fragments were resuspended in growth factor reduced (GFR) Matrigel® (354230, Corning), plated in four ~12 µL plugs per well, incubated at 37° C for 30 minutes, and fed with 500 µL Intesticult™ Organoid Growth Medium.

Condition	Basal Media	Supplements	Additives
Stem cell	Advanced DMEM/F12 (12634010, Gibco) 1X B-27™ Supplement (17504044, Gibco) 1X GlutaMAX™ (35050061, Gibco) 1X N-2™ Supplement (17502048, Gibco) 1 mM HEPES (15630080, Gibco) 2% (v/v) penicillin/streptomycin (15140122, Gibco)	20% (v/v) R-spondin-conditioned media (from R-spondin-expressing cells gifted by Dr. Jeff Whitsett, The University of Cincinnati, Cincinnati, OH) 10% (v/v) Noggin-conditioned media (from Noggin-expressing cells gifted by Dr. G.R. van den Brink, Amsterdam, NL)	None
Enterocyte			2 µM IWP 2 (3533, Tocris Bioscience) 2 mM valproic acid (P4543, Sigma-Aldrich)
Paneth cell			3 µM CHIR 99021 (4423, Tocris Bioscience) 10 µM DAPT (2634, Tocris Bioscience)
Goblet cell			10 µM DAPT (2634, Tocris Bioscience) 2 µM IWP 2 (3533, Tocris Bioscience)

Table 3. Human enteroid media components.

ELISAs

3-4 mL human enteroid conditioned media was concentrated using Amicon® Ultra-4 10 kDa centrifugal filters (Millipore, UFC801024) to yield a final volume of ~500 µL. 293 STF and RKO-dCas9-VPR cell lines were cultured to ~50% confluency in 6-well plates, then refed with serum-free Dulbecco's Modified Eagle Medium (DMEM) (11995065, Gibco) for 96 hours. SELENOP sandwich enzyme-linked immunosorbent assays (ELISAs) were performed with N22 and N11 capture and detection antibodies, respectively, as described previously (80).

RNA-seq data analysis

RNA sequencing (RNA-seq) expression and mutation data from colon and rectal adenocarcinomas in The Cancer Genome Atlas (TCGA) Pan-Cancer Atlas (81) were explored at https://www.cbioportal.org (82, 83). RNA-seq expression data from Mutant Enteroid miRNA and Gene Expression (ME-MIRAGE) (84) were explored at https://jwvillan.shinyapps.io/ME-MIRAGE.

Murine tumorigenesis protocol

Lrig1-CreERT2/$^{+}$ (*Lrig1*$^{tm1.1(cre/ERT2)Rjc}$/J, 018418, The Jackson Laboratory), *Apc*$^{fl/+}$(*Apc*^{tm1Tyj}/J, 009045, The Jackson Laboratory), *Selenop*$^{-/-}$ (*Selenop*^{tm1Rfb}/J, 008201, The Jackson Laboratory), and *Selenop*$^{fl/fl}$ (B6.Cg-*Selenop*$^{tm3.1Rfb}$/Mmnc, 37485, Mutant Mouse Resource & Research Centers) mice were previously generated (53, 85–87) and backcrossed to a C57BL/6J background. *Lrig1-CreERT2/*$^{+}$*; Apc*$^{fl/fl}$*; Selenop*$^{+/-}$ or *Selenop*$^{fl/+}$ mice were bred with *Selenop*$^{+/-}$ or *Selenop*$^{fl/+}$ mice, respectively, to generate female and male littermates for experiments. *Lrig1-CreERT2/*$^{+}$*; Apc*$^{fl/+}$*; Selenop*$^{+/+}$, *Selenop*$^{+/-}$, and *Selenop*$^{-/-}$ mice were provided Se-supplemented (1.00 mg Se/kg) defined diet (Envigo) ad libitum. *Lrig1-CreERT2/*$^{+}$*; Apc*$^{fl/+}$*; Selenop*$^{+/+}$, *Selenop*$^{fl/+}$, and *Selenop*$^{fl/fl}$ mice were provided Se-sufficient (0.15 mg Se/kg) defined diet (Envigo) *ad libitum*. Bedding from all cages was mixed and redistributed two weeks before experiments and every two weeks thereafter to minimize microbiome variation. All mice were housed with 12-hour dark/light cycles.

Cohorts of 8-10-week-old *Lrig1-CreERT2/$^{+}$; Apc$^{fl/+}$; Selenop* mice were administered three daily i.p. injections of 2 mg tamoxifen (T5648, Sigma-Aldrich) dissolved in corn oil (Mazola). Mice were colonoscopically monitored for tumors on days 50, 64, 78, and 92 after initial tamoxifen injection, then euthanized on day 100 (88) by experimenters blinded to genotype. Small intestine and colon tissues were macroscopically imaged and analyzed, then Swiss-rolled and formalin-fixed for unstained and hematoxylin and eosin (H&E)-stained slide preparation by the VUMC Translational Pathology Shared Resource (TPSR). Colon tumor volume was calculated from length (L) and width (W) measurements with the formula W^2*L/2 (89). H&E-stained slides were examined for dysplasia severity by a gastrointestinal pathologist blinded to genotype.

Murine tumoroid culture

Tumor organoids ("tumoroids") were established from *Apc$^{\Delta IE/+}$; Selenop$^{+/+}$* and *Selenop$^{-/-}$* mice as described previously (90). Tumoroids were refed with basal media supplemented with 20% R-spondin-conditioned media and 10% Noggin-conditioned media every 3 days. Tumoroids were split and replated every 7-10 days as described below.

Tumoroids were collected by centrifugation at 200 *g* for 5 minutes at 4° C, gently sheared twice through a 25G needle, then centrifuged again as above. For subculture and expansion, tumoroid fragments were resuspended in GFR Matrigel® and plated in 50 µL plugs. For enzymatic dissociation experiments, tumoroids were resuspended in TrypLE™ Express (12604013, Gibco) with 10 µM Y-27632 (1254, Tocris Bioscience) and 50 µg/mL DNase I (D5025, Sigma-Aldrich), incubated at 37° C for 3 minutes, and filtered through a 70 µm cell strainer. Enzymatic dissociation was halted by addition of PBS (without Ca^{2+} or Mg^{2+}) and centrifugation as above. Tumoroid cells were then resuspended in GFR Matrigel® and plated at a density of 5,000 live cells per 50 µL plug. Tumoroid fragments/cells were incubated at 37° C for 30 minutes, then fed with 500 µL basal media supplemented with 20% (v/v) R-spondin-conditioned media and 10% (v/v) Noggin-conditioned media.

Murine tumoroid image quantification

Tumoroids were imaged after five days with an EVOS® FL2 Auto Imaging System (ThermoFisher Scientific). Tumoroid number was quantified in ImageJ (91) by an experimenter blinded to genotype.

Murine tumoroid protein extraction

Tumoroids were collected by centrifugation at 200 *g* for 5 minutes at 4° C, resuspended in Cell Recovery Solution (354253, Corning), and incubated on ice for 30 minutes. Tumoroids were centrifuged as above, resuspended in CelLytic MT (C3228, Sigma-Aldrich) with phosphatase inhibitor cocktail 2 (P5726, Sigma-Aldrich), phosphatase inhibitor cocktail 3 (P0044, Sigma-Aldrich), and protease inhibitor cocktail (P8340, Sigma-Aldrich), incubated on ice for 15 minutes, and centrifuged at 16000 *g* for 10 minutes at 4° C. Supernatant protein concentrations were quantified with a BCA Protein Assay Kit (23225, Pierce).

Murine enteroid culture

Enteroids were established and cultured as previously described (92).

Human tumoroid culture

Human tumoroids were established and cultured as previously described (93). Known clinical characteristics are described in **Table 4**.

Line	Location	Age	Race	Sex	Stage	Dysplasia	Mutations	MSI/MSS	CMS
32385	Right	61	Black	Female	T3N0	HGD		MSI	1/3
35349	Sigmoid	57	White	Female	T3N0	HGD	$KRAS^{G12D}$, $TP53^{R248W}$	MSS	2/4
40299	Sigmoid	67	White	Female	T3N1b	LGD		MSS	4
82742	Right	79	Black	Male	T4aN2b	HGD		MSS	2

Table 4. Clinical characteristics of human colon tumors. Stage and dysplasia were determined by the attending pathologist. All patients were treatment-naïve. For line 35349, mutational analysis was performed on biopsy tissue prior to resection. Lines 32385, 40299, and 82742 were not subjected to further mutational analysis. Microsatellite instability was analyzed by PCR and IHC per clinical standard of care. CMS: consensus molecular subtype, HGD: high-grade dysplasia, LGD: low-grade dysplasia, MSI: microsatellite instability, MSS: microsatellite stable.

SELENOP treatments

Human tumoroids were treated with 0 or 500 ng/mL purified human SELENOP for five days prior to RNA extraction. 293 STF cells were treated with 0 or 100 ng/mL purified human SELENOP for 16 hours prior to TOPFlash assays.

Cell lines and maintenance

293T (CRL-3216), Caco-2 BBE (CRL-2102), HepG2 (HB-8065) and RKO (CRL-2577) cells were purchased from ATCC, which confirms cell line identity by short tandem repeat analysis. 293 Super TOPFlash (293 STF) cells were a gift from Drs. Ethan Lee (Vanderbilt University, Nashville, TN) and Jeremy Nathans (Johns Hopkins University, Baltimore, MD) (94, 95). Although 293 STF cells were not authenticated in our laboratory, they demonstrate expected G418-resistance and WNT-induced TOPFlash reporter activity. 293T-FLAG-LRP6 cells were a gift from Drs. Victoria Ng (Vanderbilt University, Nashville, TN) and Ethan Lee (Vanderbilt University, Nashville, TN). MC38 cells were a gift from Dr. Barbara Fingleton (Vanderbilt University, Nashville, TN). YAMC cells, generated and described by (96), were obtained from the VUMC Digestive Disease Research Center (DDRC) GI Organoid Subcore.

293 STF, 293T, Caco-2 BBE, HepG2, MC38, and RKO cell lines were maintained in DMEM (11995065, Gibco) supplemented with 10% (v/v) fetal bovine serum (FBS) (07068085, Avantor) and 1% (v/v) penicillin/streptomycin (15140122, Gibco), and cultured at 37° C in 5% CO_2. YAMC cell lines were maintained in Roswell Park Memorial Institute (RPMI) 1640 Medium (61870036, Gibco) supplemented with 10% (v/v) FBS, 1% (v/v) penicillin/streptomycin, and 10 U/mL recombinant mouse interferon-γ (IFN-γ) (485MI100/CF, R&D Systems), and cultured at 33° C in 5% CO_2. All cells used for experiments were passaged <15 times and regularly tested for mycoplasma contamination with a Mycoplasma PCR Detection Kit (G238, abm).

Lentiviral transduction

293T cells were cultured to ~50% confluency in 10-cm plates, then co-transfected with 1 μg pMD2.G (12259, Addgene) envelope plasmid, 1 μg psPAX2 (12260, Addgene) packaging plasmid, and 2 μg 7TFP (24308, Addgene), lenti dCAS-VP64_Blast (61425, Addgene), lentiGuide-Puro-NONTARGET (97), lentiGuide-Puro-hSELENOP (97), lentiGuide-Puro-mSELENOP (97), pLV-mCherry (VectorBuilder), pLV-hSELENOP (VectorBuilder), pLX304-V5-mSELENOP (97), or pLX304-V5-mSELENOP_Δ258-299 (97) using polyethylenimine (24314, Polysciences, Inc.). Cells were refed 16 hours after transfection, and lentiviral supernatants were passed through 0.45 μm filters 48 hours later. Target cells were transduced overnight in filtered lentivirus containing 5 μg/mL polybrene (TR1003G, Millipore). For tumoroids, filtered lentiviral supernatants were concentrated with Lenti-X Concentrator™ (631232, Takara Bio) per the manufacturer's protocol. Target tumoroids were transduced for 4 hours in concentrated lentivirus with 8 μg/mL polybrene and 10 μM Y-27632. Forty-eight hours later, cells/tumoroids were selected with the following concentrations of puromycin (P8833, Sigma-Aldrich) or blasticidin (ant-bl-05, InvivoGen): 1 μg/mL puromycin (293 STF, MC38, and RKO cells), 3 μg/mL puromycin (tumoroids), 5 μg/mL puromycin (YAMC cells), 5 μg/mL blasticidin (tumoroids) or 10 μg/mL blasticidin (YAMC STF cells).

CRISPRa cell line generation

RKO and MC38 cells were cultured to ~50% confluency in 10-cm plates, then co-transfected with 1 μg pCMV-HA-m7pB (98) transposase plasmid and 2.5 μg PB-TRE-dCas9-VPR (63800, Addgene) transposon plasmid using Lipofectamine® 2000 (11668019, Invitrogen). Cells were selected with 100 μg/mL hygromycin B (10687010, Gibco) 72 hours later. *SELENOP* or *Selenop* promoter-targeted CRISPR activation (CRISPRa) single guide RNAs (sgRNAs) were designed with the CRISPick tool (Broad Institute). The top four ranked candidates were ordered as oligonucleotides (Integrated DNA Technologies), cloned into lentiGuide-Puro (52963, Addgene) as described in (99), and sequence-verified by GENEWIZ with U6 GENEWIZ universal primers. As lentiGuide-Puro-hSELENOP_3 and lentiGuide-Puro-mSELENOP_3 yielded the greatest *SELENOP/Selenop* overexpression in RKO- and MC38-dCas9-VPR cells, respectively, these sgRNAs were used for subsequent experiments. All sgRNA sequences are listed in **Table 5**.

sgRNA Name	sgRNA Designations	sgRNA Sequences (5' to 3')
NONTARGET	NONTARGET_CRa_F_1	CACCGGACCTTCATTGAAGAAAAGC
	NONTARGET_CRa_R_1	AAACGCTTTTCTTCAATGAAGGTCCGGTGC
hSELENOP_1	hSELENOP_CRa_F_1	CACCGGGAAGGGCTAAGGGTAAACA
	hSELENOP_CRa_R_1	AAACTGTTTACCCTTAGCCCTTCCCGGTGC
hSELENOP_2	hSELENOP_CRa_F_2	CACCGGTTTGGGAAAGAAGGCAACT
	hSELENOP_CRa_R_2	AAACAGTTGCCTTCTTTCCCAAACCGGTGC
hSELENOP_3	hSELENOP_CRa_F_3	CACCGTTCTTTCCCAAACTATAACA
	hSELENOP_CRa_R_3	AAACTGTTATAGTTTGGGAAAGAACGGTGC
hSELENOP_4	hSELENOP_CRa_F_4	CACCGTGGGAAAGAAGGCAACTTGG
	hSELENOP_CRa_R_4	AAACCCAAGTTGCCTTCTTTCCCACGGTGC
mSELENOP_1	mSELENOP_CRa_F_1	CACCGACTTTGGACTGCACCTCAGA
	mSELENOP_CRa_R_1	AAACTCTGAGGTGCAGTCCAAAGTCGGTGC
mSELENOP_2	mSELENOP_CRa_F_2	CACCGCTGCATTTGCAAGGTCGCAG
	mSELENOP_CRa_R_2	AAACCTGCGACCTTGCAAATGCAGCGGTGC
mSELENOP_3	mSELENOP_CRa_F_3	CACCGGCTGAGGCAGTACTTACTGA
	mSELENOP_CRa_R_3	AAACTCAGTAAGTACTGCCTCAGCCGGTGC
mSELENOP_4	mSELENOP_CRa_F_4	CACCGGTTGTTTACCTCGCCCTCTG
	mSELENOP_CRa_R_4	AAACCAGAGGGCGAGGTAAACAACCGGTGC

Table 5. sgRNA sequences.

WNT3A treatments

293 STF and RKO cell lines were treated with 400 ng/mL and 200 ng/mL recombinant human WNT3A (rhWNT3A) (5036WNP10/CF, R&D Systems), respectively, for 16 hours prior to TOPFlash assays. MC38 and YAMC cell lines were treated with 35 ng/mL and 100 ng/mL recombinant mouse WNT3A (rmWNT3A) (1324WN010/CF, R&D Systems), respectively, for 16 hours prior to TOPFlash assays. 293T lysates were treated with 500 ng rmWNT3A prior to immunoprecipitation (IP). 293T and RKO cells were treated with 400 ng/mL and 200 ng/mL rhWNT3A, respectively, for 96 hours prior to RNA extraction.

TOPFlash reporter assays

293 STF, RKO STF, and YAMC STF cell lines were seeded in 12-well plates (100,000 cells/well). Thirty-two hours after plating, 293 STF and RKO STF cell lines were treated without or with rhWNT3A and 0, 20, 40, 60, 80, or 100 ng/mL purified human SELENOP for 16 hours, whereas YAMC STF cell lines were treated without or with rmWNT3A for 16 hours. Cells were lysed in 1X Glo Lysis Buffer (E2661, Promega), and lysates were mixed 1:1 with Steady-Glo® luciferase reagent (E2510, Promega) or CellTiter-Glo™ luminescent cell viability reagent (G7570, Promega). Luminescence was measured with a GloMax® Discover microplate reader (Promega). Steady-Glo® readings were normalized to CellTiter-Glo™ readings to account for cell viability.

RKO-dCas9-VPR and MC38-dCas9-VPR cell lines were seeded in 12-well plates (50,000 cells/well). Twenty-four hours later, cells were co-transfected with 0.50 μg M50 Super 8x TOPFlash reporter plasmid (12456, Addgene) and 0.05 μg pRL-TK control reporter plasmid (E2241, Promega) using Lipofectamine® 2000. Forty-eight hours later, cells were treated without or with WNT3A for 16 hours. Cells were lysed in Dual-Glo® luciferase reagent (E2920, Promega), luminescence was measured with a GloMax® Discover microplate reader, Dual-Glo® Stop & Glo® reagent (E2920, Promega) was

added, and luminescence was measured again. Dual-Glo® readings were normalized to Stop & Glo® readings to control for transfection efficiency.

siRNA transfections

293 STF or RKO STF cells were seeded in 6-well or 12-well plates (300,000 or 100,000 cells/well, respectively). Twenty-four hours later, cells were transfected with 100 nM control A (sc37007, Santa Cruz Biotechnology), pooled *APC* (sequences published in (94), Dharmacon), or *SELENOP* small interfering RNAs (siRNAs) (sc-40930a, Santa Cruz Biotechnology) using Lipofectamine® RNAiMAX (13778075, Invitrogen).

FLAG IPs

293T cells were cultured to ~50% confluency in 10-cm plates, then co-transfected with 2 μg FLAG-mLRP6 plasmids (97) and 2 μg mSELENOP plasmids (62, 97) with polyethylenimine. Forty-eight hours later, cells were incubated on ice for 10 minutes in FLAG® IP Lysis Buffer (L3412, Sigma-Aldrich) with phosphatase inhibitor cocktail 2, phosphatase inhibitor cocktail 3, and protease inhibitor cocktail, then transferred to microcentrifuge tubes and centrifuged at 16000 *g* for 10 minutes at 4° C. Supernatant protein concentrations were quantified with a BCA Protein Assay Kit. 2 mg total protein was used for IP with ANTI-FLAG® M2 Affinity Gel (A2220, Sigma-Aldrich) per the manufacturer's protocol. Bound proteins were eluted with 150 ng/μL 1X FLAG® Peptide (F3290, Sigma-Aldrich) at 4° C for 30 minutes.

Proximity ligation assays

293T cells were cultured to ~10% confluency in 8-well chamber slides (PEZGS0816, Millipore), then transfected with 0.1 μg pcDNA6-N-3XFLAG-Lrp6 (123595, Addgene) and 0.1 μg pCMV6-V5-mSELENOP (62) plasmids using polyethylenimine. After 48 hours, cells were fixed in 3% (w/v) paraformaldehyde (158127, Sigma-Aldrich), briefly washed in PBS with 10 mM glycine (G36050, Research Products International), and permeabilized in PBS with 0.2% (v/v) Triton™ X-100 (T8787,

Sigma-Aldrich). Proximity ligation assays were then performed with antibodies (**Table 6**) and the Duolink® In Situ Red Starter Kit Mouse/Rabbit (DUO92101, Sigma-Aldrich) per the manufacturer's protocol. Slides were imaged with a Nikon Eclipse E800 upright microscope and NIS-Elements BR software.

Antibody	Supplier	Catalog #	Species/Isotype	Dilution
anti-α-catenin	Sigma-Aldrich	C2081	Rabbit polyclonal	1:500
anti-β-catenin	BD Biosciences	610154	Mouse monoclonal (IgG1)	1:500
anti-FLAG	Sigma-Aldrich	F1804	Mouse monoclonal (IgG1)	1:500
anti-V5	Cell Signaling Technology	13202	Rabbit monoclonal (IgG)	1:500
IgG1	Cell Signaling Technology	5415	Mouse monoclonal (IgG1)	1:500
IgG	Cell Signaling Technology	3900	Rabbit monoclonal (IgG)	1:500

Table 6. Antibodies for proximity ligation assays.

Heparin and $NaClO_3$ treatments

293T or 293T-FLAG-LRP6 cells were cultured to ~50% confluency in 10-cm plates, then treated with 1 mg/mL heparin (H3393, Sigma-Aldrich) or 50 mM sodium chlorate ($NaClO_3$) (244147, Sigma-Aldrich) for 48 hours prior to FLAG IPs.

SELENOP-conditioned media preparation

HepG2 cells were seeded in 10-cm plates (3,000,000 cells/plate). After 48 hours, SELENOP-conditioned media was collected and centrifuged at 500 *g* for 5 minutes at 4° C.

Cell surface biotinylation and isolation experiments

293T cells were cultured to ~80% confluency in 10-cm plates, then treated with 3 mL complete DMEM or SELENOP-conditioned media for 2 hours. Cells were biotinylated and lysed with a Cell Surface Biotinylation and Isolation Kit (A44390, Pierce) per the manufacturer's protocol. Lysate concentrations were quantified with a BCA Protein Assay Kit. Equal amounts of total protein were used

for pulldown with NeutrAvidin™ Agarose (29200, Pierce), and bound proteins were eluted with DTT (A39255, Pierce).

Plasmid construction

pCMV6-V5-mSELENOP (full-length) and pCMV6-mSELENOP (tU3, tU4, tU5, tU6, tU7, and tU9) constructs were a gift from Dr. Suguru Kurokawa and are described elsewhere (62). pCMV6-V5-mSELENOP tU1, tU2, tU3, tU4, Δ258-267, Δ268-277, Δ278-287, Δ288-299, and Δ258-299 plasmids were generated via round-the-horn polymerase chain reaction (PCR) as described in (100) with pCMV6-V5-mSELENOP (full-length) and the primers listed in **Table 7**. All pCMV6-V5-mSELENOP constructs were sequence-verified by GENEWIZ with T7 and M13R GENEWIZ universal primers.

pLX304-V5-mSELENOP plasmids (full-length and Δ258-299) were generated by Gateway® cloning (101) (ThermoFisher Scientific) per the manufacturer's protocol. Briefly, V5-mSELENOP was flanked by attB sites via PCR amplification from pCMV6-V5-mSELENOP (full-length or Δ258-299) with primers listed in **Table 7** and Q5® Hot Start High-Fidelity 2X Master Mix (M0494S, New England BioLabs). attB-flanked PCR products were purified with the QIAquick PCR Purification Kit (28104, Qiagen) prior to BP reactions with Gateway™ pDONR™221 (12536017, Invitrogen) using Gateway™ BP Clonase™ II Enzyme mix (11789020, Invitrogen). LR reactions were then performed with the BP reactions and pLX304 (25890, Addgene) using Gateway™ LR Clonase™ II Enzyme mix (11791020, Invitrogen). All pLX304-V5-mSELENOP constructs were sequence-verified by Plasmidsaurus.

pcDNA6-FLAG-mLRP6 ΔECD, ΔE1-4, ΔE1/2, ΔE3/4, and ΔL1-3 plasmids were generated via round-the-horn PCR as described in (100) with pcDNA6-N-3XFLAG-Lrp6 (123595, Addgene) and the primers listed in **Table 7**. All pcDNA6-FLAG-mLRP6 constructs were sequence-verified by GENEWIZ with T7 and BGHR GENEWIZ universal primers. pReceiver-M14-mLRP5-3XFLAG was purchased from GeneCopoeia (EX-Mm34003-M14). pLEX307-V5-GFP was previously generated in our lab (93).

Construct	Primer Designations	Primer Sequences (5' to 3')
pCMV6-V5-mSELENOP_tU1	mSELENOP_tU_F	TACGACTAAGCAAGAATGGAGTACAGAATTAAGTG
	mSELENOP_tU1_R	TAAGCTGGCTTGAAGAAGAGCAACCACTGTCACTT
pCMV6-V5-mSELENOP_tU2	mSELENOP_tU_F	TACGACTAAGCAAGAATGGAGTACAGAATTAAGTG
	mSELENOP_tU2_R	TAAGCTCTCTAAGTGACCCTGCCTGTGCTGGCCCC
pCMV6-V5-mSELENOP_tU3	mSELENOP_tU_F	TACGACTAAGCAAGAATGGAGTACAGAATTAAGTG
	mSELENOP_tU3_R	TAAGAGCTTCCTCTGGGCAAGTGAAAGGTGCAAGC
pCMV6-V5-mSELENOP_tU4	mSELENOP_tU_F	TACGACTAAGCAAGAATGGAGTACAGAATTAAGTG
	mSELENOP_tU4_R	TAAAGCAATTGCAGACCCTGACTTCTCAAATATGA
pCMV6-V5-mSELENOP_Δ258-267	mSELENOP_d258-267_F	TGTAAGTTGTCTAAGGAGTCCGAGGCAGCCCCCAG
	mSELENOP_d258-267_R	GAGCTTCCTCTGGGCAAGTGAAAGGTGCAAGCCTT
pCMV6-V5-mSELENOP_Δ268-277	mSELENOP_d268-277_F	CCCAGCAGCTGCTGCTGTCACTGCCGCCACCTCAT
	mSELENOP_d268-277_R	CAGGAGCTGGTTGATGCACCCCCTTCGACAGAGCT
pCMV6-V5-mSELENOP_Δ278-287	mSELENOP_d278-287_F	TTTGAGAAGTCAGGGTCTGCAATTGCTTGTCAGTG
	mSELENOP_d278-287_R	GGCTGCCTCGGACTCCTTAGACAACTTACACAGGA

pCMV6-V5-mSELENOP_Δ288-299	mSELENOP_d288-299_F	CAGTGTGCGGAAAACCTCCCATCCT
	mSELENOP_d288-299_R	TATGAGGTGGCGGCAGTGACAGCAG
pCMV6-V5-mSELENOP_Δ258-299	mSELENOP_d288-299_F	CAGTGTGCGGAAAACCTCCCATCCT
	mSELENOP_d258-267_R	GAGCTTCCTCTGGGCAAGTGAAAGGTGCAAGCCTT
pLX304-V5-mSELENOP	attB1-mSELENOP_F	GGGGACAAGTTTGTACAAAAAAGCAGGCTTCACCATGTGGAGAAGCCTAGGGCTTGCC
	attB2-mSELENOP_R	GGGGACCACTTTGTACAAGAAAGCTGGGTCTTAGTTTGAATGACATTTACACTT
pLX304-V5-mSELENOP_Δ258-299	attB1-mSELENOP_F	GGGGACAAGTTTGTACAAAAAAGCAGGCTTCACCATGTGGAGAAGCCTAGGGCTTGCC
	attB2-mSELENOP_R	GGGGACCACTTTGTACAAGAAAGCTGGGTCTTAGTTTGAATGACATTTACACTT
pcDNA6-FLAG-mLRP6_ΔECD	mLRP6_dECD_F	ACCAACACAGTTGGTTCCGTTATTGGAGTAATTGT
	mLRP6_dECD_R	GGATCCGAATTCTCTAGACTTGTCGTCATCGTCTT
pcDNA6-FLAG-mLRP6_ΔE1-4	mLRP6_dE4_F	GAGCCTCCAACGTGTTCTCCTCAGCAGTTTACCTG
	mLRP6_dE1_R	CGCTCTCAGCAGCACGCAGAAGCTGCAGGCCAGGA
pcDNA6-FLAG-mLRP6_ΔE1/2	mLRP6_dE2_F	GTCCCCGAGGCTTTCCTTCTGTTCTCGAGGAGAGC
	mLRP6_dE1_R	CGCTCTCAGCAGCACGCAGAAGCTGCAGGCCAGGA
pcDNA6-FLAG-mLRP6_ΔE3/4	mLRP6_dE4_F	GAGCCTCCAACGTGTTCTCCTCAGCAGTTTACCTG
	mLRP6_dE3_R	GGGGACAATGCATGTCTTCATGTCACCGATGAGCT

pcDNA6-FLAG-mLRP6 _ΔL1-3	mLRP6_dL1-3_F	CCAACTGAGGAGCCAGCACCACAAGCCACCAACAC
	mLRP6_dL1-3_R	TGGAGGCTCTCCACAGGACAGCTCATCCTGAAGCA

Table 7. PCR primers for plasmid construction.

V5 IPs

293T cells were cultured to ~50% confluency in 10-cm plates, then transfected with 4 μg pLEX307-V5-GFP (93) or pCMV6-V5-mSELENOP (62) with polyethylenimine. Forty-eight hours later, cells were incubated on ice for 10 minutes in CelLytic™ MT with phosphatase inhibitor cocktail 2, phosphatase inhibitor cocktail 3, and protease inhibitor cocktail, then transferred to microcentrifuge tubes and centrifuged at 16000 *g* for 10 minutes at 4° C. Supernatant protein concentrations were quantified with a BCA Protein Assay Kit. 2 mg total protein was treated without or with rmWNT3A prior to IP with Anti-V5-tag mAb-Magnetic Beads (M16711, MBL International) per the manufacturer's protocol. Bound proteins were eluted in 4X Laemmli Sample Buffer (1610747, Bio-Rad) with 6% (v/v) 2-mercaptoethanol (M6250, Sigma-Aldrich) at 95° C for 5 minutes.

Western blots

Protein samples were diluted in 4X Laemmli Sample Buffer with 6% (v/v) 2-mercaptoethanol, then incubated at 95° C for 5 minutes. 40-80 μg protein was loaded into each lane of a 4-20% Mini-PROTEAN® TGX Precast Protein Gel (4561094, Bio-Rad), alongside Precision Plus Protein Dual Color Standards (1610374, Bio-Rad) for SDS-PAGE. SDS-PAGE-separated proteins were transferred to a 0.45 μm nitrocellulose membrane (NBA085C001EA, PerkinElmer), blocked with Intercept® (TBS) Blocking Buffer (927-60001, LI-COR) at room temperature for 30 minutes, then probed with primary antibodies (**Table 8**) diluted in 50% Intercept® (TBS) Blocking Buffer/50% TBS with 0.1% (v/v) Tween-20 (P1379, Sigma-Aldrich) (TBS-T) at 4° C overnight. Membranes were washed with TBS-T, then probed with secondary antibodies (**Table 8**) diluted in TBS-T at room temperature for 30 minutes. Membranes were washed again with TBS-T, imaged with an Odyssey Clx near-infrared fluorescence imaging system (LI-COR), and quantified with Image Studio (LI-COR). Densitometric values for proteins of interest were normalized to those of their corresponding loading controls.

1° antibody	Supplier	Catalog #	Species/Isotype	Dilution
anti-APC	Santa Cruz Biotechnology	sc-7930	Rabbit polyclonal	1:1000
anti-β-tubulin	Cell Signaling Technology	2146	Rabbit polyclonal	1:2000
anti-FLAG	Sigma-Aldrich	F1804	Mouse monoclonal (IgG1)	1:1000
anti-GAPDH	Cell Signaling Technology	5174	Rabbit monoclonal (IgG)	1:3000
anti-GPX1	Sigma-Aldrich	SAB5700925	Rabbit monoclonal (IgG)	1:1000
anti-GPX2	abcam	ab137431	Rabbit polyclonal	1:1000
anti-GPX3	Novus	NBP1-06398	Rabbit polyclonal	1:1000
anti-LRP6	Cell Signaling Technology	2560	Rabbit monoclonal (IgG)	1:1000
anti-LRP6	Cell Signaling Technology	3395	Rabbit monoclonal (IgG)	1:1000
anti-Na^+/K^+-ATPase	Cell Signaling Technology	3010	Rabbit polyclonal	1:1000
anti-SELENOK	Dr. Peter Hoffmann University of Hawaii Honolulu, HI, USA	N/A	Rabbit monoclonal (IgG)	1:250
anti-SELENOP	Vanderbilt Antibody and Protein Resource	N11	Mouse monoclonal (IgG1)	1:1000
anti-SELENOP	Dr. Suguru Kurokawa Osaka Ohtani University, Tondabayashi, Osaka, JP	N/A	Rabbit polyclonal	1:1000
anti-V5	abcam	ab27671	Mouse monoclonal (IgG2a)	1:1000
anti-V5	Cell Signaling Technology	13202	Rabbit monoclonal (IgG)	1:1000
anti-WNT3A	abcam	ab28472	Rabbit polyclonal	1:1000
2° antibody	**Supplier**	**Catalog #**	**Species/Isotype**	**Dilution**
anti-mouse IgG	LI-COR	92668020	Goat polyclonal	1:10000
anti-rabbit IgG	LI-COR	92632211	Goat polyclonal	1:10000

Table 8. Antibodies for Western blots.

Protein homology analysis

Mouse LRP5 (AAC36468.1), human LRP6 (AAI43726.1), mouse LRP6 (AAH60704.1), human LRP8(Q14114), mouse LRP8 (EDL30769), human SELENOP (CAA77836.2), and mouse SELENOP (CAA68140.2) protein sequences were downloaded from the NCBI Protein database (https://www.ncbi.nlm.nih.gov/protein). Pairwise sequence alignments were performed with the EMBOSS Needle tool (102) offered by the European Bioinformatics Institute at the European Molecular Biology Laboratory (https://www.ebi.ac.uk/Tools/psa/emboss_needle).

Predictive modeling of protein-protein complexes

Human LRP6 (AAI43726.1), human SELENOP (CAA77836.2), and human WNT3A (BAB61052.1) protein sequences were downloaded from the NCBI Protein database (https://www.ncbi.nlm.nih.gov/protein). LRP6:SELENOP and LRP6:WNT3A structures were predicted using ColabFold (103) within ChimeraX (v1.6.1) (104).

Immunofluorescence (IF)

Selenop$^{+/+}$ and *Selenop*$^{-/-}$ colon, liver, and small intestine tissues were flash frozen in Tissue-Tek® O.C.T. Compound (4583, Sakura Finetek), then mounted onto slides by the VUMC TPSR. Tissue sections were fixed in 1% (w/v) paraformaldehyde, washed in PBS, permeabilized in PBS with 0.2% (v/v) Triton X-100, washed in PBS, and blocked in PBS with 10% (v/v) normal goat serum (NGS) (01-6201, Invitrogen) for 45 minutes at room temperature. Tissue sections were incubated in primary antibodies (**Table 9**) diluted in PBS/5% NGS overnight at 4° C. Tissue sections were then washed in PBS/1% NGS, incubated in secondary antibodies (**Table 9**) diluted in PBS/5% NGS for 1 hour at room temperature, then washed in PBS/1% NGS.

1° antibody	Supplier	Catalog #	Species/Isotype	Dilution
anti-caveolin	BD	610406	Mouse monoclonal (IgG1)	1:250
anti-clathrin	BD	610499	Mouse monoclonal (IgG1)	1:250
anti-GFP	Novus	NB600-308	Rabbit monoclonal (IgG)	1:500
anti-E-cadherin	BD	610182	Mouse monoclonal (IgG2a)	1:400
anti-SELENOP	Sigma-Aldrich	HPA036287	Rabbit polyclonal	1:200
anti-SELENOP	Burk Lab	N/A (Clone 695)	Rabbit polyclonal	1:200
2° antibody	**Supplier**	**Catalog #**	**Species/Isotype**	**Dilution**
anti-mouse IgG2a AlexaFluor® 488	Invitrogen	A-21131	Goat polyclonal	1:500
anti-mouse IgG1 AlexaFluor® 568	Invitrogen	A-21124	Goat polyclonal	1:1000
anti-rabbit IgG AlexaFluor® 488	Invitrogen	A-11008	Goat polyclonal	1:1000
anti-rabbit IgG AlexaFluor® 568	Invitrogen	A-11011	Goat polyclonal	1:500

Table 9. Antibodies for IF.

293T cells were seeded on #1 thickness, 22 x 22 mm coverslips (102222, ThermoFisher Scientific) in a 6-well plate (20,000 cells/well). Twenty-four hours later, cells were transfected with 1 µg pCS2 LRP6-eGFP (180143, Addgene) using Lipofectamine® 3000 (L3000001, Invitrogen). After 48 hours, cells were fixed in 3% (w/v) paraformaldehyde, briefly washed in PBS with 10 mM glycine, permeabilized in PBS with 0.2% (v/v) Triton™ X-100, and blocked in PBS with 3% (w/v) dry milk powder (M17200, Research Products International). Cells were incubated in primary antibodies (**Table 9**) diluted in PBS/3% milk for 30 minutes, briefly washed in PBS, incubated in secondary antibodies (**Table 9**) diluted in PBS/3% milk for 30 minutes, and briefly washed in PBS.

Coverslips were mounted onto slides with ProLong™ Gold Antifade Mountant with DAPI (P36931, Invitrogen), and allowed to dry overnight. Slides were imaged with a Nikon Eclipse E800 upright microscope and NIS-Elements BR software.

Polarized epithelial monolayer experiments

Caco-2 BBE cells were seeded on Transwell® permeable supports (3450, Corning) in a 6-well plate (500,000 cells/insert). Ohmic resistance was measured at indicated timepoints with a Millicell® ERS-2 Voltohmmeter (MERS00002, Millipore), and transepithelial electrical resistance (TEER) was calculated with the formula [sample resistance (Ω) - blank resistance (Ω)] * Transwell® surface area (cm^2). For apical/basolateral ELISA experiments, cells were cultured with complete media in both compartments for 14 days, then refed with serum-free media containing 0 or 0.5 μM sodium selenite (Na_2SeO_3) (S5261, Sigma-Aldrich) in the apical or basolateral compartments for 2 days prior to ELISA. For basolateral ELISA experiments, cells were cultured with complete media in both compartments for 4 days, then refed with serum-free media containing 0.5 μM Na_2SeO_3 for 1, 3, or 5 days prior to ELISA. For RT-qPCR experiments, cells were cultured with complete media in both compartments for 5 or 10 days prior to RNA extraction.

Figure design

Schematics were created with Biorender.com under the Vanderbilt University School of Medicine Basic Sciences institutional license. All other figures were designed in Inkscape (v1.2.2).

Statistical analysis

Statistical analyses for scRNA-seq data were performed in Python with scipy.stats and seaborn packages. All other statistical analyses were performed in GraphPad Prism (v9.5.1). Sample sizes and statistical tests are reported in figure legends.

Study approval

All animal experiments were carried out in accordance with protocols approved by the VUMC IACUC. All human tissues were provided by the Western Division of the CHTN in accordance with the VUMC IRB.

CHAPTER 3: SELENOP MODIFIES SPORADIC COLORECTAL CARCINOGENESIS AND WNT SIGNALING ACTIVITY THROUGH LRP5/6 INTERACTIONS

Rationale

We previously discovered tumor-protective roles for SELENOP in CAC (50, 51). However, CAC only constitutes 1-3% of total CRC cases, whereas sporadic (non-hereditary) CRC comprises 65-85% of total CRC cases (105, 106). In sporadic CRC, genetic and epigenetic alterations influenced by lifestyle, environmental, and dietary factors drive carcinogenesis through activation of oncogenes and inactivation of tumor suppressor genes (107). Conventional sporadic CRCs are characterized by initial inactivation of the tumor suppressor gene *APC* and resultant hyperactivation of WNT signaling (108). In this study, we defined SELENOP's contributions to conventional, sporadic colorectal carcinogenesis.

SELENOP is predominantly expressed by differentiated epithelial cells in the normal colon and small intestine epithelium

We first profiled the selenotranscriptome in WT mouse small intestine and colon epithelial isolates by RT-qPCR. *Selenop* was the most abundant SeP mRNA in the small intestine epithelium (**Figure 8A**), in agreement with prior measurements of SeP mRNA levels in whole small intestine tissue (109). *Selenop* was one of several highly expressed SeP mRNAs, including selenoprotein F (*Selenof*), glutathione peroxidase 1 (*Gpx1*), and glutathione peroxidase 2 (*Gpx2*), in the small intestine and colon epithelium (**Figure 8A**). Additionally, we confirmed GPX1 (**Figure 9A**) and GPX2 (**Figure 9B**) protein expression in these tissues. We observed similar selenotranscript expression patterns in the Gut Cell Atlas scRNA-seq dataset (73) generated from normal human colon and small intestine epithelium (**Figure 10**).

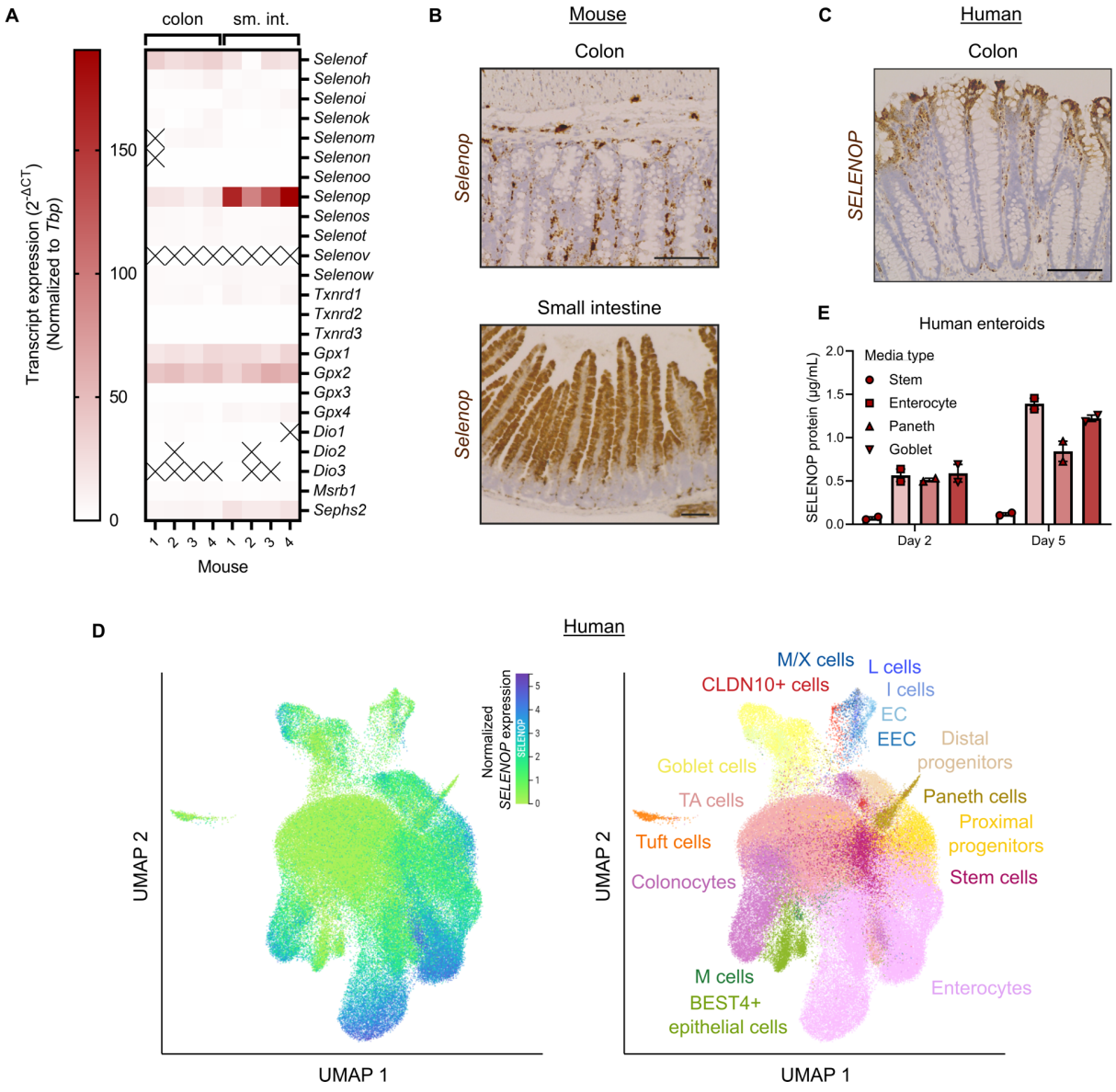

Figure 8. *SELENOP* is predominantly expressed by differentiated epithelial cells in the normal colon and small intestine epithelium. (A) RT-qPCR of mouse colon and small intestine (sm. int.) epithelial isolates for SePs. n=4 mice. (B) RNAscope® of mouse colon and small intestine for *Selenop*. Representative 20x (colon) or 10x (small intestine) images, scale bars = 100 µm. (C) RNAscope® of human colon for *SELENOP*. Representative 20x images, scale bars = 100 µm. (D) Gut Cell Atlas scRNA-seq data from human colon and small intestine epithelium queried for *SELENOP*. EC: enterochromaffin, EEC: enteroendocrine, TA: transit amplifying. n=6 donors. (E) ELISA of conditioned media from human enteroids treated with indicated media for SELENOP. Pooled data from n=2 independent experiments. Data are displayed as mean ± SEM.

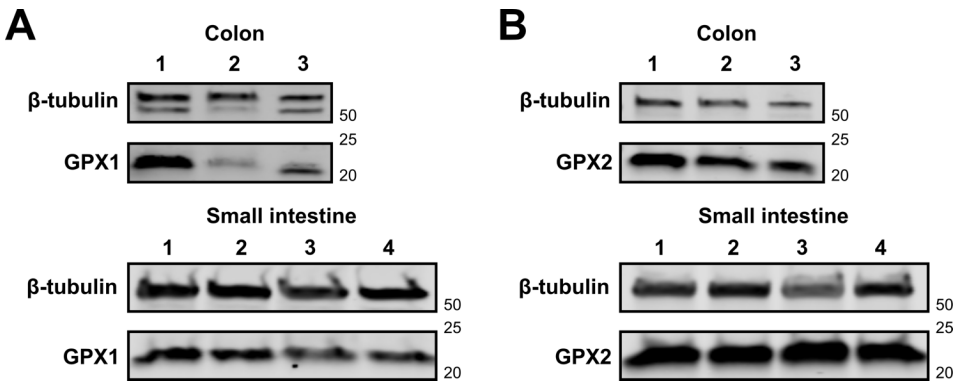

Figure 9. GPX1 and GPX2 protein expression in WT mouse colon and small intestine epithelium. Western blots for (A) GPX1, (B) GPX2, and (A, B) β-tubulin (loading control) in WT mouse colon and small intestine epithelium. n=3-4 mice.

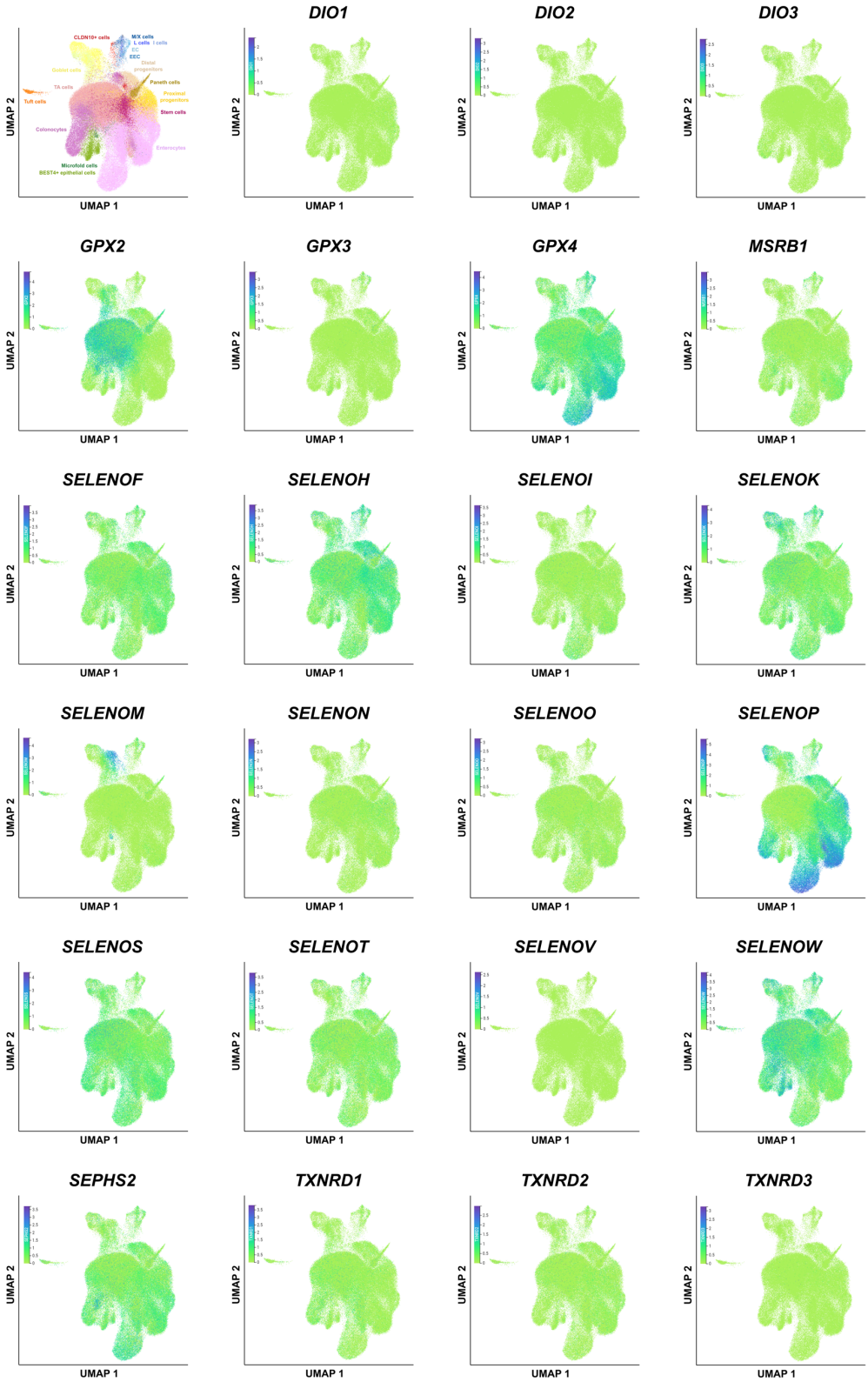

Figure 10. SeP expression in the normal human colon and small intestine. Gut Cell Atlas scRNA-seq data from human colon and small intestine epithelium queried for indicated SePs. EC: enterochromaffin, EEC: enteroendocrine, TA: transit amplifying. n=6 donors.

When we performed RNA *in situ* hybridization on WT mouse tissues with a validated *Selenop* RNAscope® probe (**Figure 11**), we predominantly detected *Selenop* in differentiated epithelial cells of the villi and crypts, as well as in stromal cells (**Figure 8B**). We observed a similar pattern of *SELENOP* expression in human colon tissues (**Figure 8C**). Together, these findings complement previously described *SELENOP* expression patterns in mouse and human colon tissues (51). In the Gut Cell Atlas scRNA-seq dataset (73), *SELENOP* was moderately to highly expressed throughout enterocyte and colonocyte populations, as well as in subsets of proximal progenitor, Paneth, goblet, and enteroendocrine cells (**Figure 8D**). To corroborate these observations, we maintained human enteroids in Se-replete (i.e. with 3% FBS and ~160 nM Na_2SeO_3), directed differentiation media (110), then measured SELENOP protein levels by ELISA. Indeed, SELENOP protein was highly expressed among enteroids differentiated towards enterocytes, goblet cells, or Paneth cells (**Figure 8E**). We observed similar trends in *SELENOP* transcript expression in enteroids skewed towards the enterocyte, goblet cell, or Paneth cell lineages (**Figure 12**).

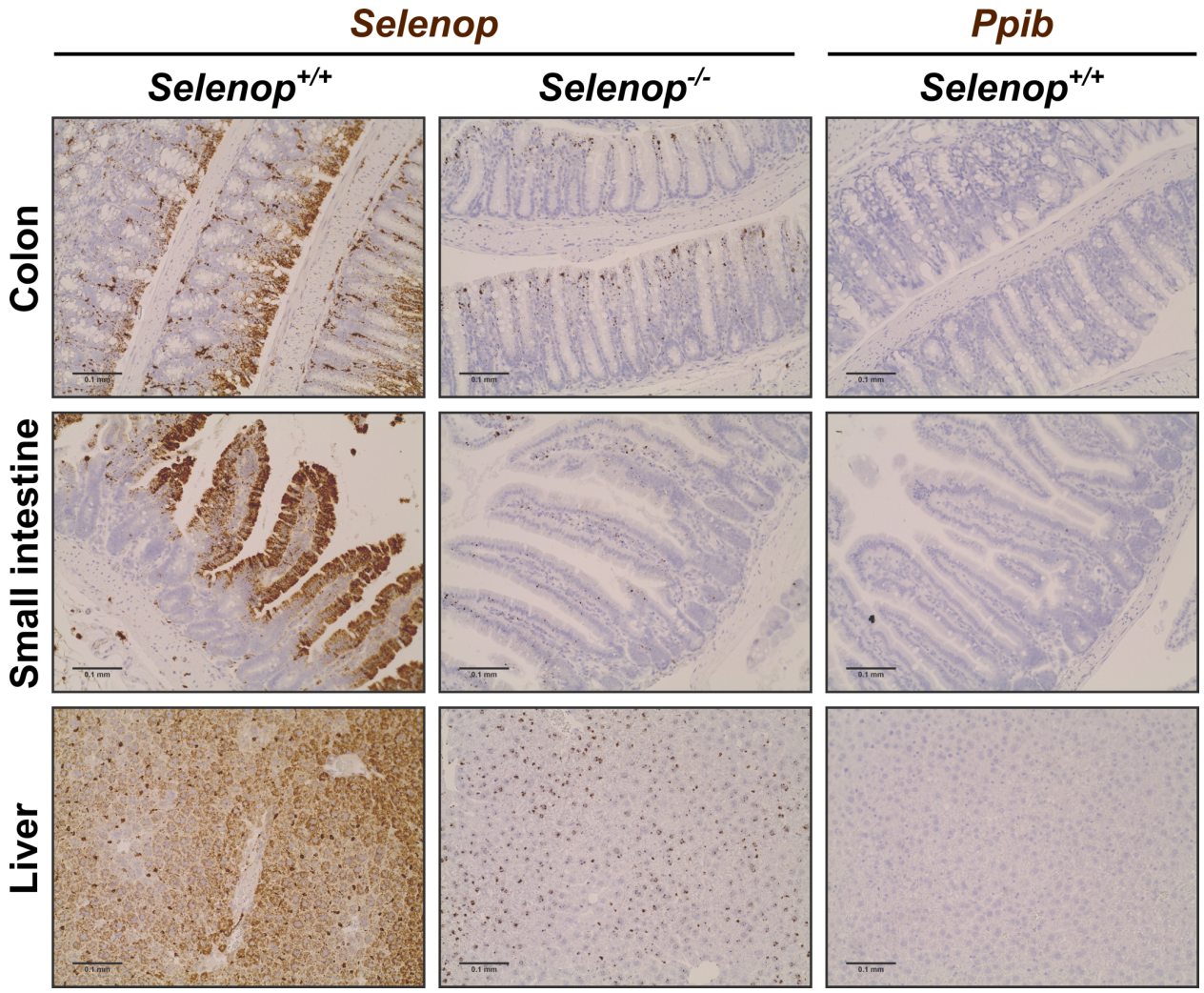

Figure 11. Validation of *Selenop* RNAscope® probe. RNAscope® of *Selenop*$^{+/+}$ and *Selenop*$^{-/-}$ colon, small intestine, and liver for *Selenop* or *Ppib* (negative control). Representative 20x images, scale bars = 100 µm.

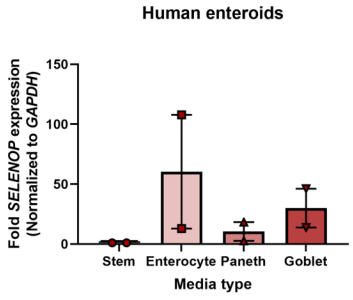

Figure 12. *SELENOP* expression in differentiated human enteroids. RT-qPCR for *SELENOP* of human enteroids subjected to directed differentiation protocols. Pooled data from n=2 independent experiments. Data are displayed as mean ± SEM.

WNT signaling activation downregulates *SELENOP* expression

In a mouse model of sporadic CRC, we consistently observed reduced *Selenop* expression within adenomas as compared to differentiated epithelium, even as early as the microadenoma stage (**Figure 13A**). As WNT hyperactivation drives tumorigenesis in this model, we hypothesized that WNT signaling activity inversely correlates with *SELENOP* expression. To investigate this, we first compared *SELENOP* expression among colorectal adenocarcinomas with or without WNT signaling mutations in RNA-seq datasets from The Cancer Genome Atlas (**Appendix B: Figure 44, Figure 45**). Indeed, *SELENOP* expression was reduced in adenocarcinomas with activating, truncating mutations in *AXIN2* (**Figure 13B**) or *APC* (**Figure 13C**), as compared to adenocarcinomas without these mutations.

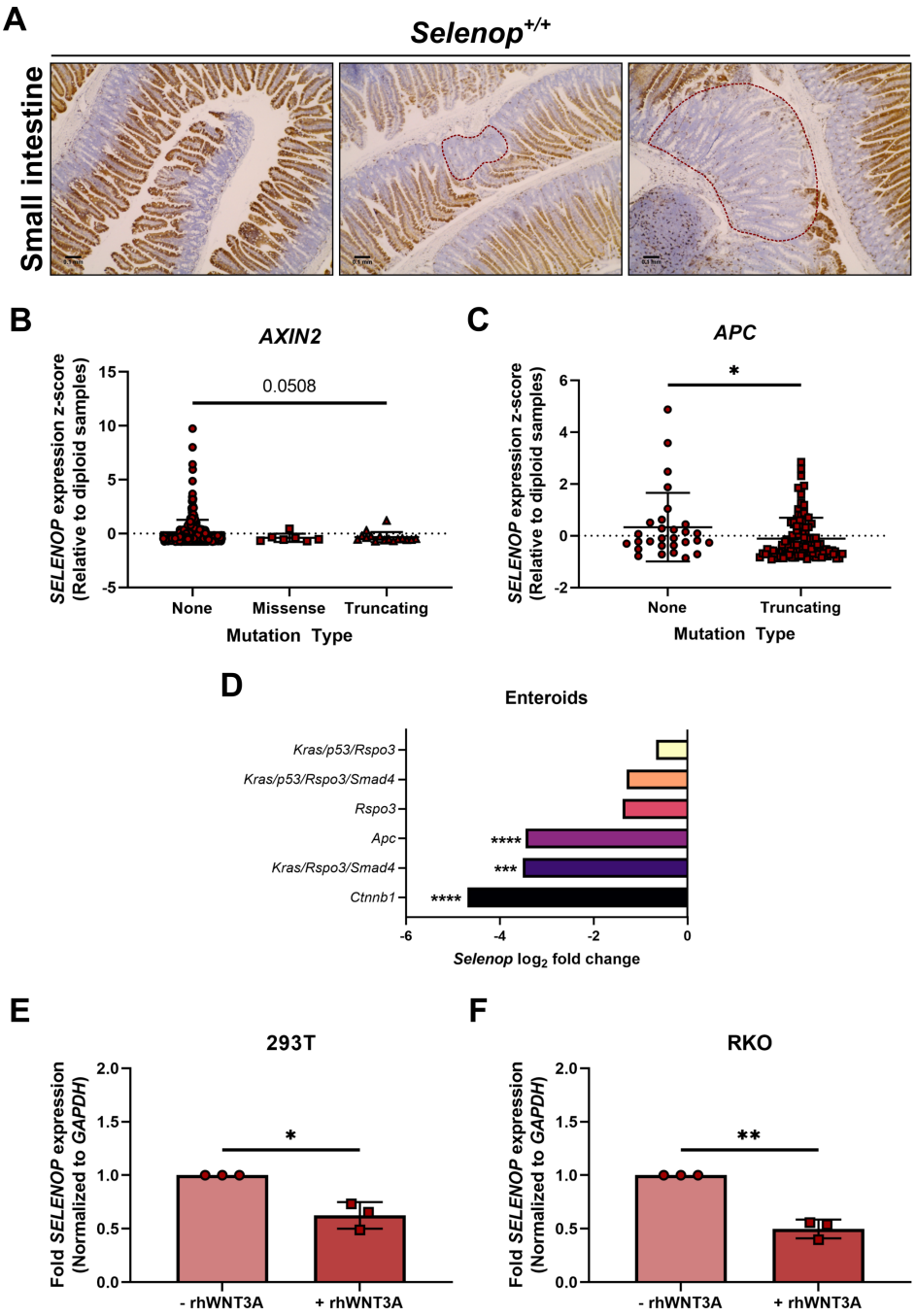

Figure 13. WNT signaling activation downregulates *SELENOP* expression. (A) RNAscope® of *Apc*$^{\Delta IE/+}$; *Selenop*$^{+/+}$ small intestine for *Selenop*. Representative 10x images, scale bars = 100 μm. (B) *SELENOP* expression in colon adenocarcinomas from The Cancer Genome Atlas (TCGA) RNA-seq data stratified by *AXIN2* mutation type. n=391 tumors. (C) *SELENOP* expression in rectal adenocarcinomas from TCGA RNA-seq data stratified by *APC* mutation type. n=226 tumors. (D) *Selenop* expression in WT versus mutant mouse enteroids from Mutant Enteroid miRNA and Gene Expression (ME-MIRAGE) RNA-seq data stratified by genetic modification(s). n=2-5 mice per genotype. (E, F) RT-qPCR for *SELENOP* of (E) 293T or (F) RKO cells treated without or with rhWNT3A. Pooled data from n=3 independent experiments. Kruskal-Wallis test with 2-sided Dunn's multiple comparisons tests (B), 2-sided Mann-Whitney test (C), 2-sided Welch's t tests (D), 2-sided paired t tests (E, F). *p<0.05, **p<0.01, ***p<0.001, ****p<0.0001. Data are displayed as mean ± SD (B, C) or SEM (E, F).

We next examined *Selenop* expression in an RNA-seq dataset from murine enteroids with activating mutations in tumor protein p53 (*p53*), mothers against decapentaplegic homolog 4 (*Smad4*), R-spondin 3 (*Rspo3*), Kirsten rat sarcoma virus (*Kras*), β-catenin (*Ctnnb1*), and/or *Apc*. Here, *Selenop* expression was lower in *Apc*-, *Ctnnb1-,* or *Kras/Rspo3/Smad4*-mutant than WT enteroids (**Figure 13D**), in further support of an inverse relationship between WNT signaling activity and *SELENOP* expression. To test this hypothesis more directly, we treated noncancer (293T) or CRC (RKO) cells with WNT3A, then measured *SELENOP* mRNA levels. In fact, WNT3A treatment decreased *SELENOP* expression in 293T (**Figure 13E**) or RKO (**Figure 13F**) cells. Thus, WNT signaling activation downregulates *SELENOP* expression.

SELENOP **expression progressively increases throughout conventional colorectal carcinogenesis**

We next refined *SELENOP*'s expression pattern in different types of colorectal polyps and cancers. For these analyses, we used a previously published scRNA-seq dataset of conventional adenomas (adenoma-specific cells [ASC]), serrated polyps (serrated-specific cells [SSC]), microsatellite stable (MSS) cancers, and microsatellite instability-high (MSI-H) cancers (75). Stem and absorptive cells are thought to represent the tumor-initiating cell types for conventional adenomas and serrated polyps, respectively, that can beget MSS and MSI-H cancers (75). Here, we observed high *SELENOP* expression in subsets of ASCs, SSCs, and MSS cancer cells (**Figure 14A**). We also leveraged Cellular Trajectory Reconstruction Analysis Using Gene Counts and Expression (CytoTRACE) analysis to computationally predict cellular differentiation state from these data (77). As *SELENOP* expression inversely correlated with WNT signaling activity above, we expected a similar inverse relationship between *SELENOP* expression and stemness. Surprisingly, in ASCs and MSS cancer cells, *SELENOP* expression weakly correlated ($r=0.44$, $p=0.01$) with CytoTRACE-inferred stemness (**Figure 14B**).

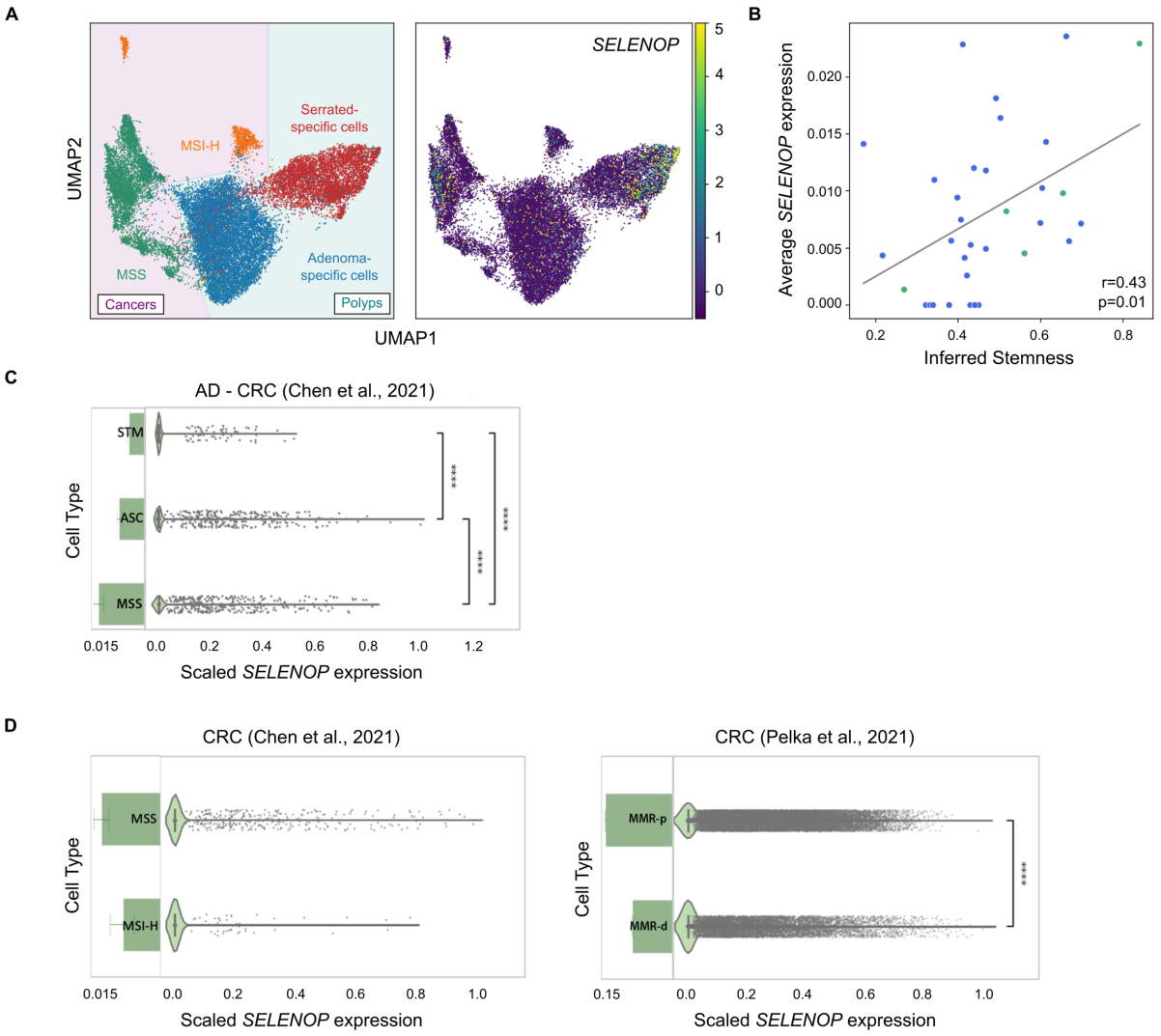

Figure 14. *SELENOP* expression increases throughout conventional colorectal carcinogenesis. (A, B) scRNA-seq data from human colorectal polyps and cancers. (A) *SELENOP* expression in cell clusters. MSI-H: microsatellite instability-high, MSS: microsatellite stable. n=62 polyps, n=7 cancers. n=149,116 cells. (B) *SELENOP* expression versus stemness inferred from CytoTRACE analysis. ASC: adenoma-specific cells. n=29 polyps, n=5 cancers. (C) scRNA-seq data from human colorectal polyps/cancers and normal colon tissues. *SELENOP* expression by cell type. AD: adenoma, CRC: colorectal cancer, STM: stem. n=34 normal samples, n=29 polyps, n=5 cancers. (D) scRNA-seq data from human colorectal cancers. *SELENOP* expression by tumor type. MMRd: mismatch repair deficient, MMRp: mismatch repair proficient. (Left) n=2 MSI-H cancers, n=5 MSS cancers. (Right) n=32 MMRd cancers, n=28 MMRp cancers. Spearman's rank correlation (B), Kruskal-Wallis test with 2-sided Mann-Whitney test (C), 2-sided Mann-Whitney tests (D). ****p<0.0001. Data are displayed as mean ± SD.

When we integrated this dataset with its corresponding patient-matched normal tissue datasets (**Figure 15A**), we observed increases in *SELENOP* expression from normal crypt stem cells to ASCs to MSS cancer cells (**Figure 14C**). Similarly, in a snRNA-seq dataset generated from familial adenomatous polyposis (FAP) and non-FAP patients (74) (**Figure 15B**), *SELENOP* expression was greater in adenocarcinomas than in polyps or unaffected stem cells (**Figure 15C**). While seemingly paradoxical, these findings uphold the inverse relationship between WNT signaling activity and *SELENOP* expression, as stem cells presumably exhibit relatively higher WNT tone than conventional polyps or cancers. We also noted higher *SELENOP* expression in SSCs than in absorptive cells; however, *SELENOP* expression did not differ between absorptive cells and MSI-H cancer cells (**Figure 15D**). Although *SELENOP* expression levels did not differ ($p=0.263$) between MSS and MSI-H cancers in this particular dataset (75) (**Figure 14A, Figure 14D**), *SELENOP* expression was greater in mismatch repair (MMR)-proficient than MMR-deficient cancers in another scRNA-seq dataset (76) (**Figure 14D**), and this correlates with the proportion of stem-like cells present in each cancer type. Overall, these results indicate that slight upregulation of *SELENOP* expression occurs throughout conventional colorectal carcinogenesis as a function of stemness.

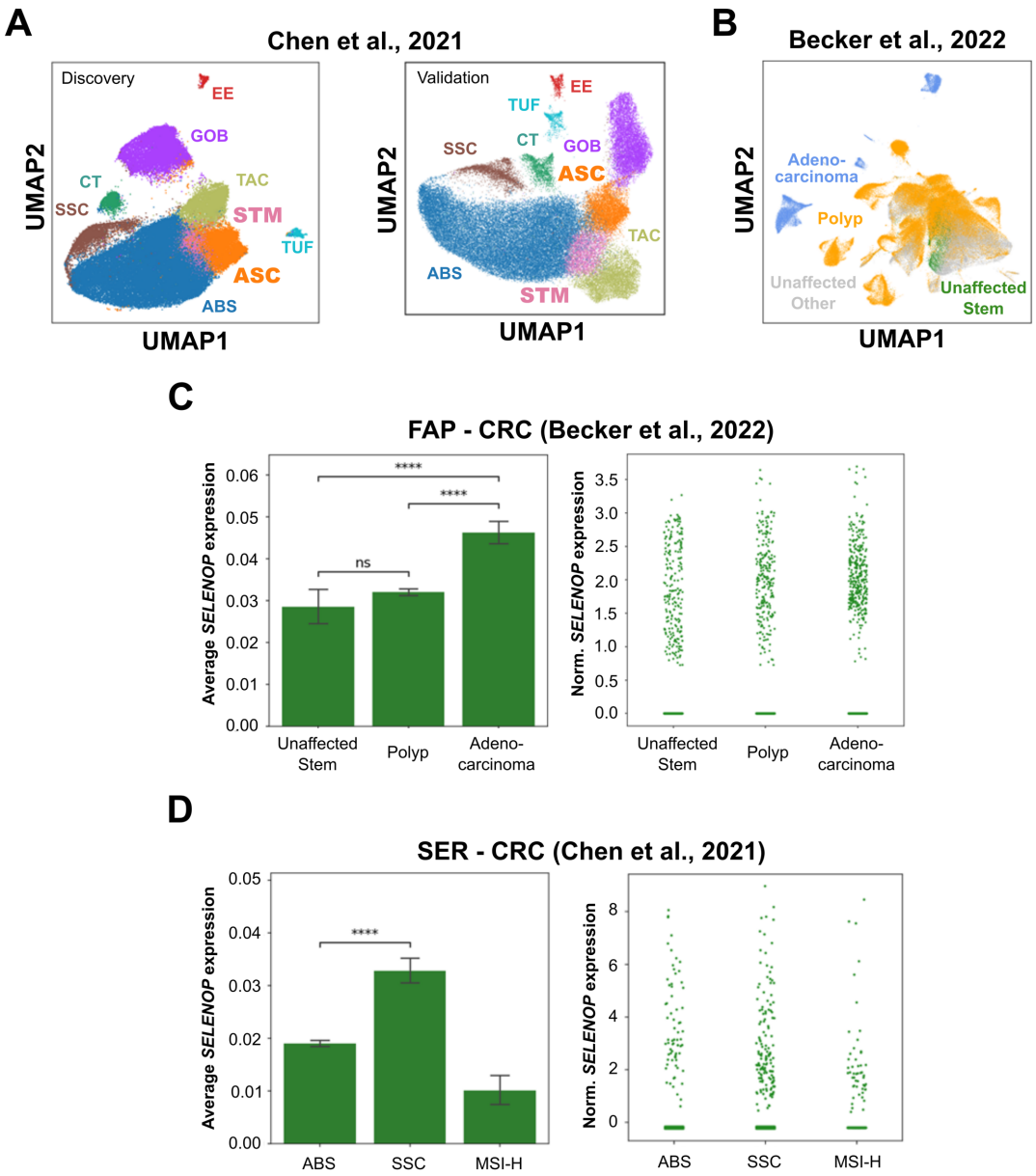

Figure 15. *SELENOP* expression throughout CRC progression. (A) scRNA-seq data from human colorectal polyps and normal colon tissue. (Left) Discovery cohort: n=35 normal samples, n=27 polyps, n=70,691 cells. (Right) Validation cohort: n=31 normal samples, n=28 polyps, n=71,374 cells. ABS: absorptive, ASC: adenoma-specific cells, CT: crypt top, EE: enteroendocrine, GOB: goblet, STM: stem, SSC: serrated-specific cells, TAC: transit amplifying cells, TUF: tuft. (B, C) snRNA-seq data from human colorectal polyps/cancers and normal colon tissue. n=23 normal samples, n=42 polyps, n=5 cancers, n=161,809 cells. (C) *SELENOP* expression by cell type. CRC: colorectal cancer, FAP: familial adenomatous polyposis. (D) scRNA-seq data from human colorectal polyps/cancers and normal colon tissue. *SELENOP* expression by cell type. ABS: absorptive, MSI-H: microsatellite instability-high, SER: serrated polyp, SSC: serrated-specific cells. n=21 normal samples, n=19 polyps, n=2 cancers. Kruskal-Wallis tests with 2-sided Mann-Whitney tests. ****p<0.0001. Data are displayed as mean ± SD.

Intestinal epithelial *Selenop* deletion does not impact *Apc*-dependent tumorigenesis

Since *SELENOP* upregulation correlated with the conventional adenoma-carcinoma sequence, we hypothesized that SELENOP deficiency would reduce stem cell-driven colorectal tumorigenesis. As we previously reported that neither liver- nor myeloid-specific, but rather, intestinal epithelial-specific *Selenop* deletion promoted CAC tumorigenesis (51), we first tested the effects of intestinal epithelial *Selenop* deletion on CRC tumorigenesis. To model this, we crossed *Selenop*$^{fl/fl}$ mice (53) onto the *Lrig1-CreERT2/*$^{+}$*; Apc*$^{fl/+}$ genetic background (111). The tamoxifen-inducible *Lrig1-CreERT2* driver facilitates loss of one *Apc* allele in leucine-rich repeats and immunoglobulin-like domains 1 (*Lrig1*)-positive intestinal epithelial stem cells, and *Apc* loss-of-heterozygosity (LOH) occurs in this model as in human CRC (88). Importantly, these mice were maintained on a defined, Se-sufficient diet (0.15 mg Se/kg) to control for variations in micronutrient composition among different lots of standard chow (111). Tamoxifen-induced *Lrig1-CreERT2/*$^{+}$*; Apc*$^{fl/+}$*; Selenop*$^{+/+}$*, Selenop*$^{fl/+}$*,* and *Selenop*$^{fl/fl}$ cohorts (hereinafter referred to as *Apc*$^{\Delta IE/+}$*; Selenop*$^{+/+}$*, Selenop*$^{\Delta IE/+}$*,* and *Selenop*$^{\Delta IE/\Delta IE}$ mice) were monitored for tumor formation via colonoscopy and sacrificed after 100 days (**Figure 16A**).

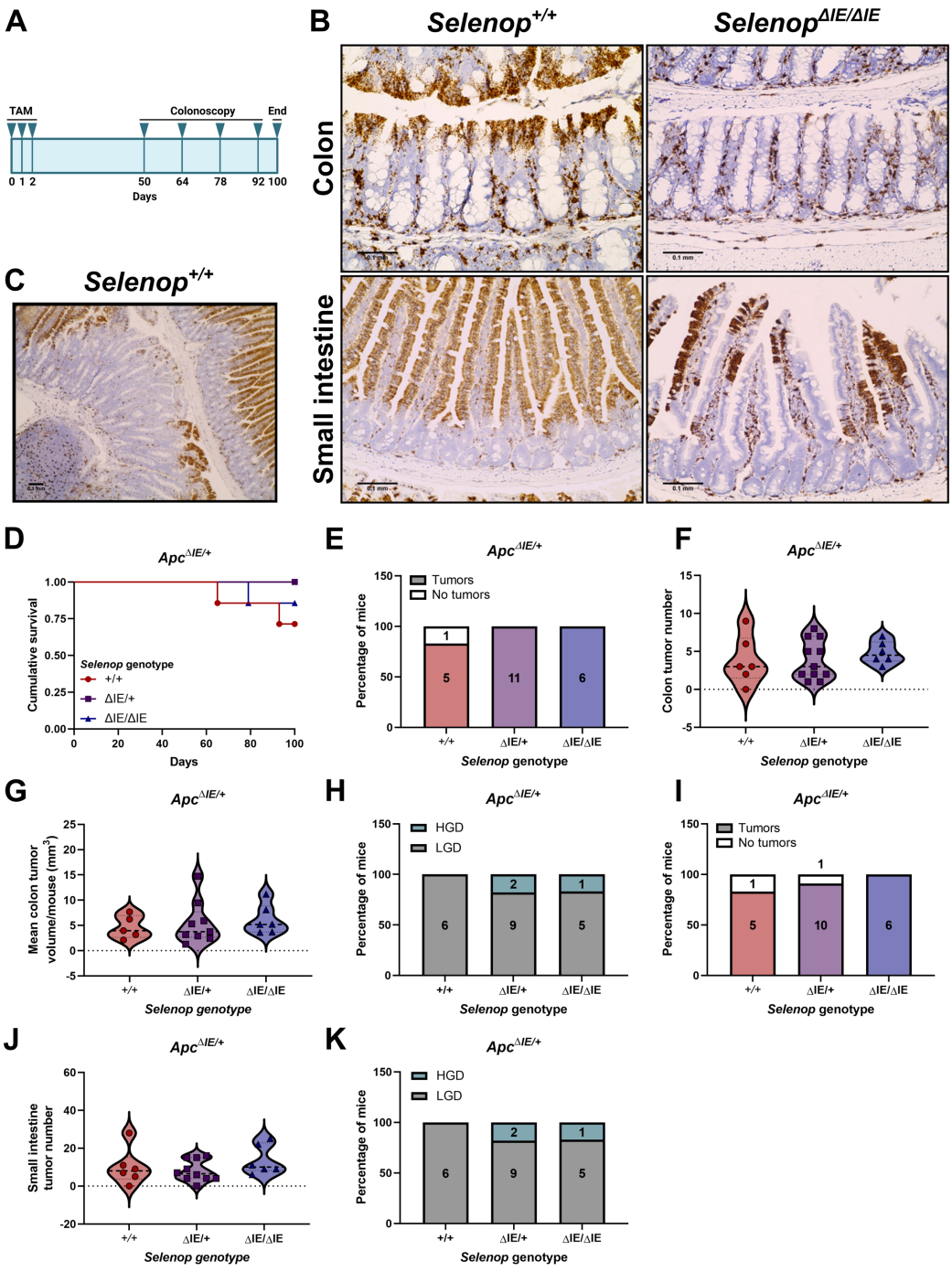

Figure 16. Intestinal epithelial *Selenop* deletion does not impact *Apc*-dependent tumorigenesis. (A) Schematic of murine tumorigenesis protocol. TAM: tamoxifen. (B) RNAscope® of $Apc^{\Delta IE/+}$; $Selenop^{+/+}$ and $Selenop^{\Delta IE/\Delta IE}$ colon and small intestine for *Selenop*. (C) RNAscope® of $Apc^{\Delta IE/+}$; $Selenop^{+/+}$ small intestine adenoma for *Selenop*. (D) Cumulative survival, (E) colon tumor incidence, (F) colon tumor number, (G) colon tumor volume, (H) colon tumor dysplasia scores (HGD: high-grade dysplasia, LGD: low-grade dysplasia), (I) small intestine tumor incidence, (J) small intestine tumor number, and (K) small intestine tumor dysplasia scores of $Apc^{\Delta IE/+}$; $Selenop^{+/+}$ (n=6), $Selenop^{\Delta IE/+}$ (n=11), and $Selenop^{\Delta IE/\Delta IE}$ (n=6) mice. Pooled data from n=2 independent experiments. Representative 20x (B) or 10x (C) images, scale bars = 100 μm. Log-rank test (D), Freeman-Halton tests (E, H, I, K), Kruskal-Wallis tests (F, G, J). n.s.

We first confirmed intestinal epithelial-specific *Selenop* deletion by RNA *in situ* hybridization (**Figure 16B**) with a validated *Selenop* RNAscope® probe (**Figure 11**). *Selenop*$^{\Delta IE/\Delta IE}$ mice displayed near total loss of *Selenop* transcript in the colon epithelium, and markedly reduced, albeit more mosaic loss of *Selenop* transcript in the small intestine epithelium (**Figure 16B**). Notably, we detected stromal *Selenop* mRNA at expected levels in both tissues (**Figure 16B**). As in human colon tumors, we observed loss of *Selenop* mRNA expression in early adenomas (**Figure 16C**).

Interestingly, intestinal epithelial-specific *Selenop* deletion modified neither colonic nor small intestinal tumorigenesis in this model. Specifically, *Apc*$^{\Delta IE/+}$*; Selenop*$^{\Delta IE/\Delta IE}$ mice exhibited no differences in survival (**Figure 16D**), tumor incidence (**Figure 16E, Figure 16I**), tumor number (**Figure 16F, Figure 16J**), or tumor volume (**Figure 16G**) as compared to *Apc*$^{\Delta IE/+}$*; Selenop*$^{+/+}$ mice. Moreover, *Apc*$^{\Delta IE/+}$*; Selenop*$^{+/+}$ and *Apc*$^{\Delta IE/+}$*; Selenop*$^{\Delta IE/\Delta IE}$ tumors showed similar degrees of dysplasia (**Figure 16H, Figure 16K**). Therefore, unlike in experimental CAC, intestinal epithelial-derived SELENOP does not confer major protection against *Apc*-dependent tumorigenesis.

Selenop KO decreases colon tumor incidence and size in *Apc*-dependent tumorigenesis

As we observed strong stromal *Selenop* expression in *Apc*$^{\Delta IE/+}$*; Selenop*$^{\Delta IE/\Delta IE}$ tissues, we hypothesized that secreted, non-epithelial-derived SELENOP compensated for the absence of intestinal epithelial-derived SELENOP in this model. Thus, we next tested the effects of global *Selenop* KO in the *Lrig1-CreERT2/*$^{+}$*; Apc*$^{fl/+}$ adenoma model (85). Importantly, these mice were maintained on a defined, Se-supplemented diet (1.00 mg Se/kg) to control for micronutrient variations among different lots of standard chow (111) and avert neurological dysfunction observed in *Selenop*$^{-/-}$ mice (60). Tamoxifen-induced *Lrig1-CreERT2/*$^{+}$*; Apc*$^{fl/+}$*; Selenop*$^{+/+}$*, Selenop*$^{+/-}$*,* and *Selenop*$^{-/-}$ cohorts (hereinafter referred to as *Apc*$^{\Delta IE/+}$*; Selenop*$^{+/+}$*, Selenop*$^{+/-}$*,* and *Selenop*$^{-/-}$ mice) were monitored for tumor formation via colonoscopy and euthanized after 100 days (**Figure 17A**).

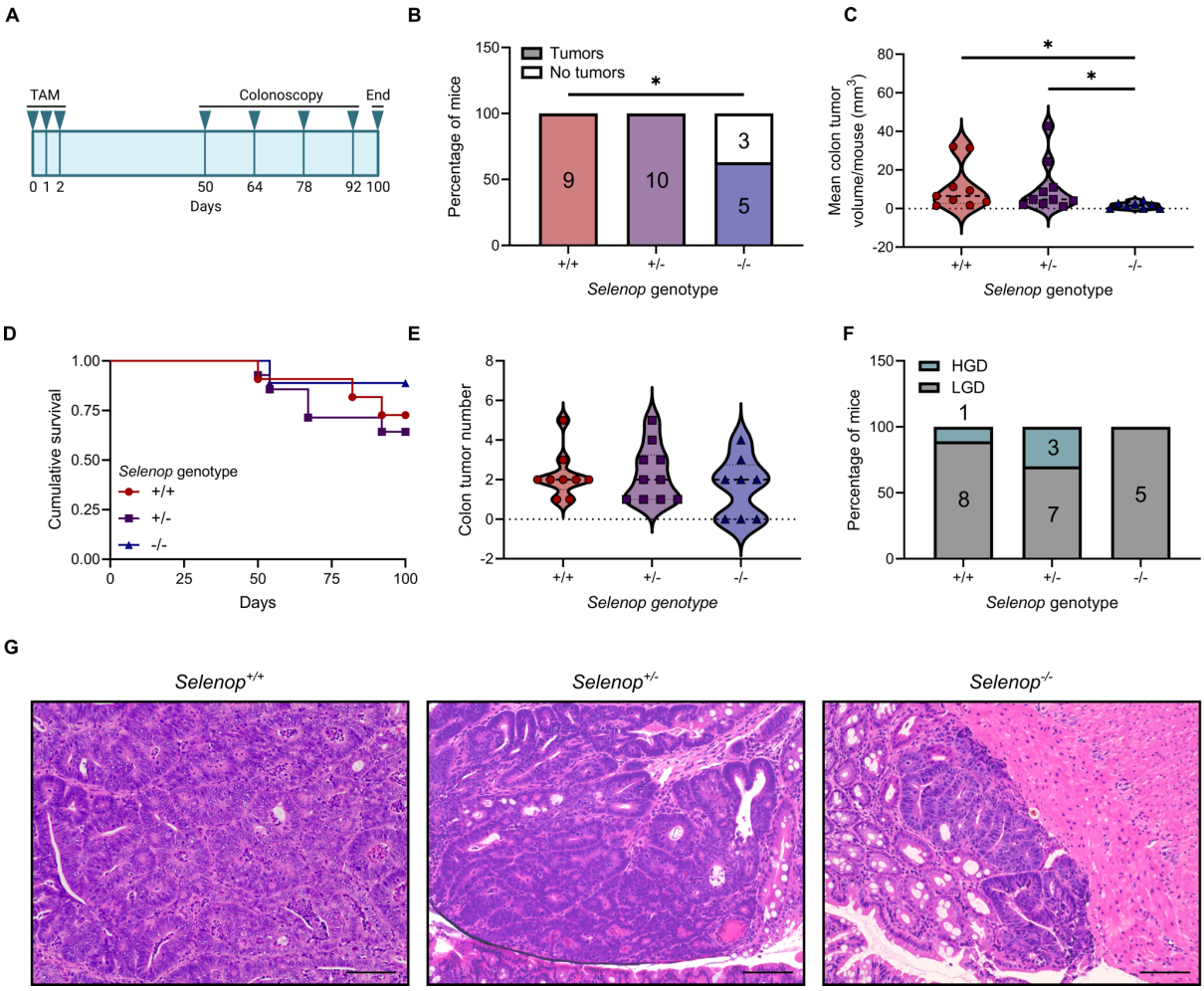

Figure 17. *Selenop* KO decreases colon tumor incidence and size in *Apc*-dependent tumorigenesis. (A) Schematic of murine tumorigenesis protocol. TAM: tamoxifen. (B) Colon tumor incidence, (C) colon tumor volume, (D) cumulative survival, (E) colon tumor number, (F) colon tumor dysplasia scores (HGD: high-grade dysplasia, LGD: low-grade dysplasia), and (G) colon tumor histology of $Apc^{AIE/+}$; $Selenop^{+/+}$ (n=9), $Selenop^{+/-}$ (n=10), and $Selenop^{-/-}$ (n=8) mice. Pooled data from n=2 independent experiments. Representative 20x images (G), scale bars = 100 μm. Freeman-Halton tests (B, F), Kruskal-Wallis tests (C, E) with 2-sided Dunn's multiple comparisons tests (C), log-rank test (D). *p<0.05.

In the colon, we observed decreased tumor incidence (**Figure 17B**) and volume (**Figure 17C**) in *Apc*$^{\Delta IE/+}$*; Selenop*$^{-/-}$ mice as compared to *Apc*$^{\Delta IE/+}$*; Selenop*$^{+/+}$ or *Selenop*$^{+/-}$ mice, despite similar survival (**Figure 17D),** numbers (**Figure 17E**), and dysplasia severity (**Figure 17F, Figure 17G**). Similarly, in the small intestine, we observed decreased tumor area (**Figure 18A**) in *Apc*$^{\Delta IE/+}$*; Selenop*$^{-/-}$ mice as compared to *Apc*$^{\Delta IE/+}$*; Selenop*$^{+/+}$ or *Selenop*$^{+/-}$ mice, despite similar incidence (**Figure 18B**), numbers (**Figure 18C**), and dysplasia severity (**Figure 18D**, **Figure 18E**). Altogether, these results propound tumor-promotive roles for SELENOP in *Apc*-dependent tumorigenesis.

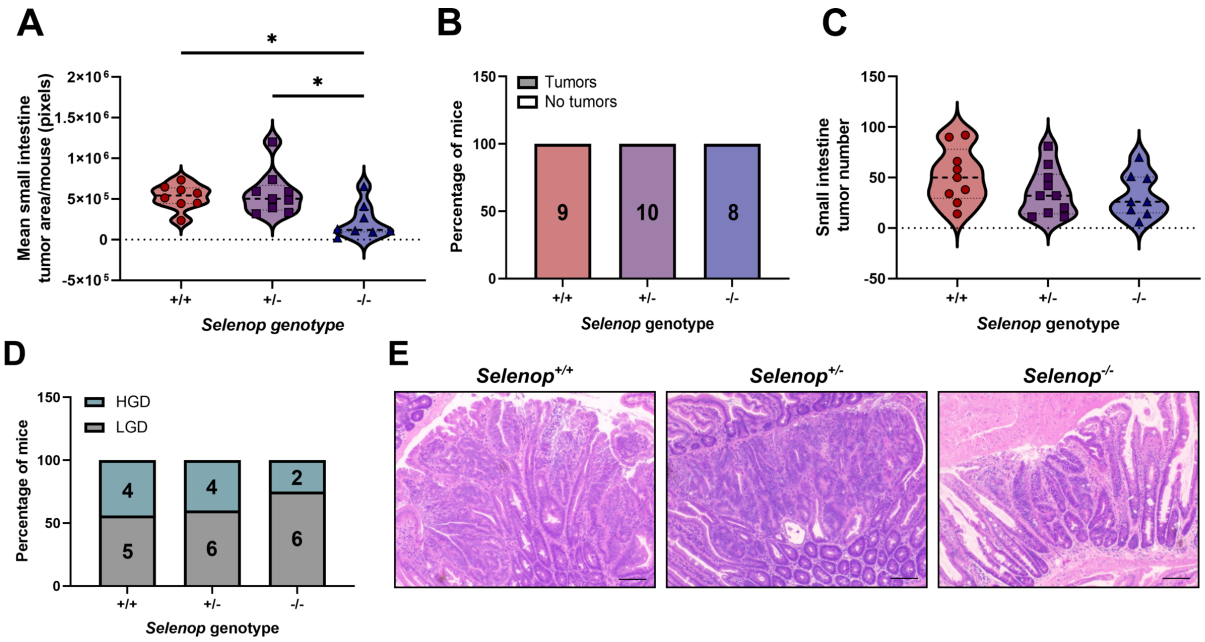

Figure 18. *Selenop* KO decreases small intestine tumor size in *Apc*-dependent tumorigenesis. (A) Small intestine tumor area, (B) small intestine tumor incidence, (C) small intestine tumor number, (D) small intestine tumor dysplasia scores (HGD: high-grade dysplasia, LGD: low-grade dysplasia), and (E) small intestine tumor histology of *Apc*$^{\Delta IE/+}$*; Selenop*$^{+/+}$ (n=9), *Selenop*$^{+/-}$ (n=10), and *Selenop*$^{-/-}$ (n=8) mice. Pooled data from n=2 independent experiments. Representative 20x images (E), scale bars = 100 μm. Kruskal-Wallis tests (A, C), Freeman-Halton tests (B, D). *p<0.05.

Selenop KO decreases tumoroid forming capacity and WNT target gene expression

To interrogate these phenotypes further, we established tumoroids from $Apc^{\Delta IE/+}$; $Selenop^{+/+}$ and $Selenop^{-/-}$ adenomas. Importantly, we maintained all tumoroids in Se-replete media (i.e. with 3% FBS and ~160 nM Na_2SeO_3). Since $Apc^{\Delta IE/+}$; $Selenop^{-/-}$ mice developed smaller colon tumors than $Apc^{\Delta IE/+}$; $Selenop^{+/+}$ mice *in vivo*, we hypothesized that $Apc^{\Delta IE/+}$; $Selenop^{-/-}$ tumoroids would exhibit defects in organoid formation *ex vivo*. To test this, we dissociated $Apc^{\Delta IE/+}$; $Selenop^{+/+}$ and $Selenop^{-/-}$ tumoroids, plated equivalent cell numbers, imaged after five days (**Figure 19A**), and quantified viable tumoroids (**Figure 19B**). Indeed, $Apc^{\Delta IE/+}$; $Selenop^{-/-}$ tumoroids demonstrated lower single cell plating efficiency than $Apc^{\Delta IE/+}$; $Selenop^{+/+}$ tumoroids (**Figure 19B**).

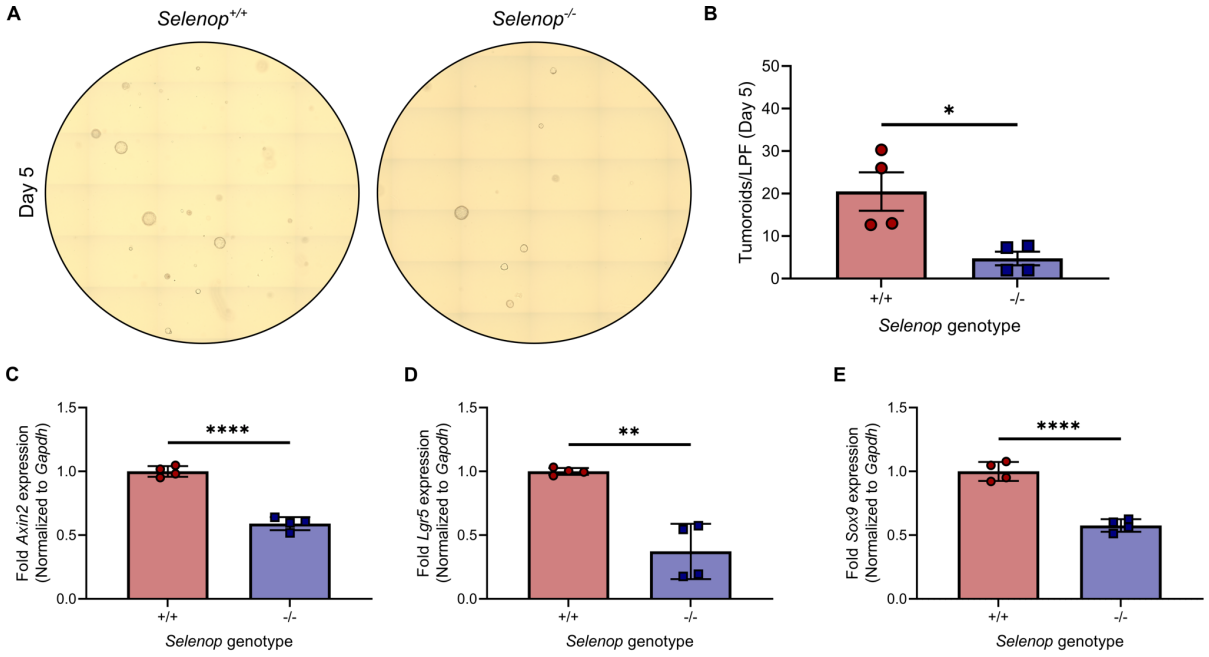

Figure 19. *Selenop* KO decreases tumoroid forming capacity and WNT target gene expression. (A, B) $Apc^{\Delta IE/+}$; $Selenop^{+/+}$ or $Selenop^{-/-}$ tumoroids 5 days after enzymatic dissociation. (A) Representative 10x tile scans. (B) Visible tumoroids per low power field (LPF). (C, D, E) RT-qPCR for (C) *Axin2*, (D) *Lgr5*, and (E) *Sox9* of $Apc^{\Delta IE/+}$; $Selenop^{+/+}$ or $Selenop^{-/-}$ tumoroids. Pooled data from n=2 independent experiments with n=2 mice per genotype. 2-sided unpaired t tests. *p<0.05, **p<0.01, ****p<0.0001. Data are displayed as mean ± SEM.

As untransformed intestinal crypts require exogenous WNT stimulation to form organoids *ex vivo* (112), we hypothesized that $Apc^{\Delta IE/+}$; $Selenop^{-/-}$ tumoroids would exhibit lower WNT signaling activity than $Apc^{\Delta IE/+}$; $Selenop^{+/+}$ tumoroids. In fact, $Apc^{\Delta IE/+}$; $Selenop^{-/-}$ tumoroids demonstrated lower levels of the WNT target genes *Axin2*, *Lgr5*, and sex-determining region Y-box transcription factor 9 (*Sox9*) than $Selenop^{+/+}$ tumoroids (**Figure 19C**, **Figure 19D**, **Figure 19E**). Thus, $Apc^{\Delta IE/+}$; $Selenop^{-/-}$ tumoroids recapitulate aspects of tumor phenotypes observed in $Apc^{\Delta IE/+}$; $Selenop^{-/-}$ mice.

Selenop KO upregulates *Selenok* and *Gpx3* transcript expression in tumoroids

Additionally, we compared the selenotranscriptomes of $Apc^{\Delta IE/+}$; $Selenop^{+/+}$ and $Selenop^{-/-}$ tumoroids to evaluate potential dysregulation of other selenotranscripts in the absence of *Selenop*. Here, $Apc^{\Delta IE/+}$; $Selenop^{-/-}$ tumoroids exhibited higher glutathione peroxidase 3 (*Gpx3*) and selenoprotein K (*Selenok*) transcript levels than $Apc^{\Delta IE/+}$; $Selenop^{+/+}$ tumoroids (**Figure 20A**). However, we did not observe concomitant GPX3 and SELENOK upregulation at the protein level in $Apc^{\Delta IE/+}$; $Selenop^{-/-}$ tumoroids (**Figure 20B**). These discrepancies may result from the mechanistic complexities of Sec insertion, such that selenotranscript levels do not necessarily reflect SeP levels.

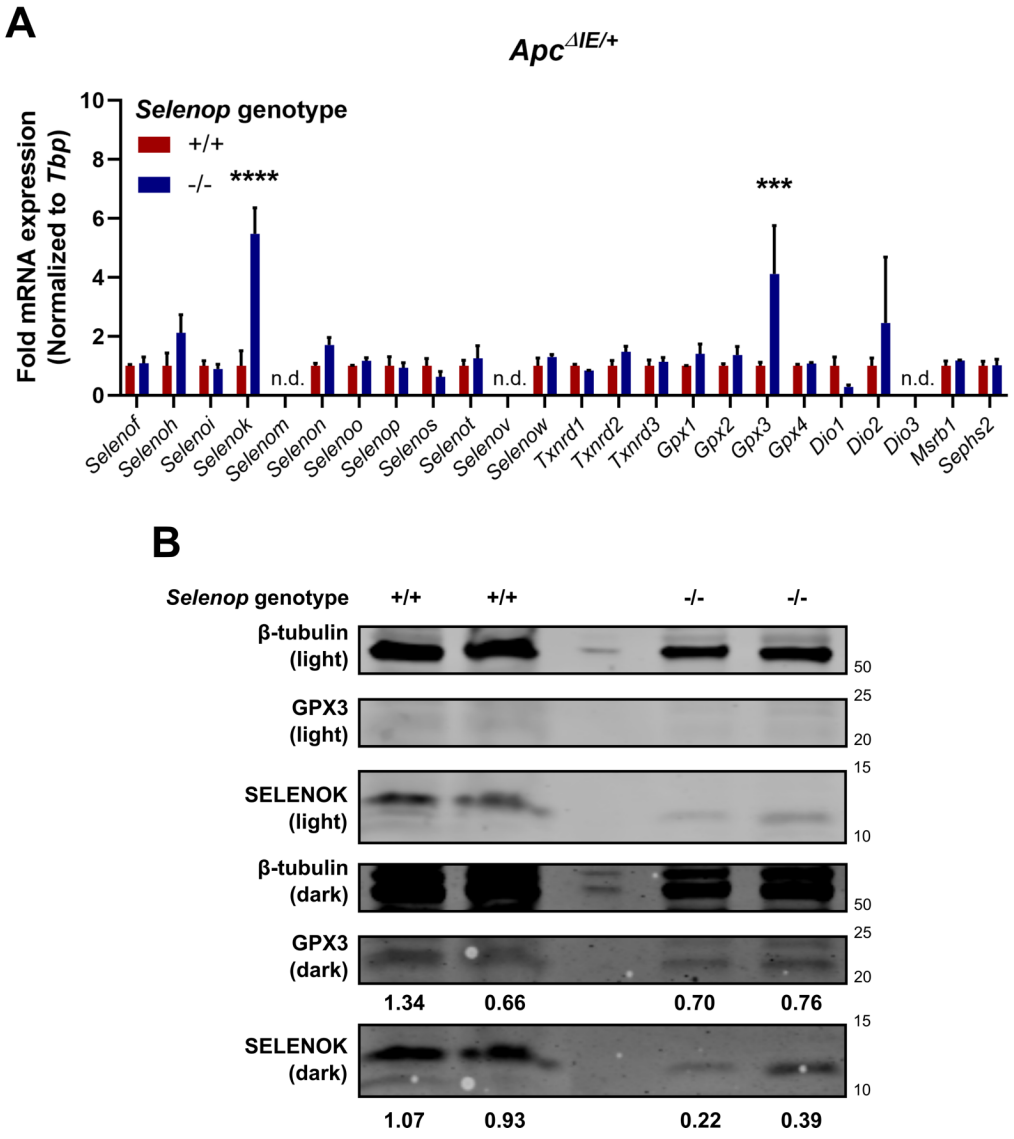

Figure 20. *Selenop* KO upregulates *Selenok* and *Gpx3* transcript expression in tumoroids. (A) RT-qPCR for SePs of $Apc^{\Delta IE/+}$; $Selenop^{+/+}$ and $Selenop^{-/-}$ tumoroids. n.d.: not detected. (B) Western blot for β-tubulin (loading control), GPX3, and SELENOK of lysates from $Apc^{\Delta IE/+}$; $Selenop^{+/+}$ and $Selenop^{-/-}$ tumoroids. Pooled (A) or representative (B) data from n=2 independent experiments with n=2 mice per genotype. 2-sided unpaired t tests with Benjamini, Krieger and Yekutieli adjustment (FDR <0.05). ***q<0.001, ****q<0.0001. Data are displayed as mean ± SEM.

SELENOP restoration increases tumoroid forming capacity and WNT target gene expression

As *Selenop* deficiency dampened WNT tone in tumoroids, we hypothesized that SELENOP restoration would reverse this phenotype. To investigate this, we transduced $Apc^{\Delta IE/+}$; $Selenop^{+/+}$ tumoroids, in which *Selenop* expression is substantially downregulated (**Figure 21**), with a nuclease-deficient Cas9 (dCas9) fused to a transcriptional activator (VP64) and nontarget or *Selenop* promoter-targeted sgRNAs, to drive *Selenop* transcription from the endogenous locus (**Figure 22A**). When we dissociated and plated $Apc^{\Delta IE/+}$; $Selenop^{+/+}$-dCas9-VP64-NONTARGET and SELENOP tumoroids as single cells, more SELENOP-overexpressing cells formed tumoroids after five days, as compared to control cells (**Figure 22B**, **Figure 22C**).

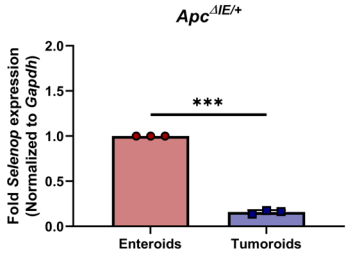

Figure 21. *Selenop* expression is reduced in tumoroids. RT-qPCR for *Selenop* of $Apc^{\Delta IE/+}$; $Selenop^{+/+}$ enteroids and tumoroids. Pooled data from n=3 mice. 2-sided paired t test. ***p<0.001. Data are displayed as mean ± SD.

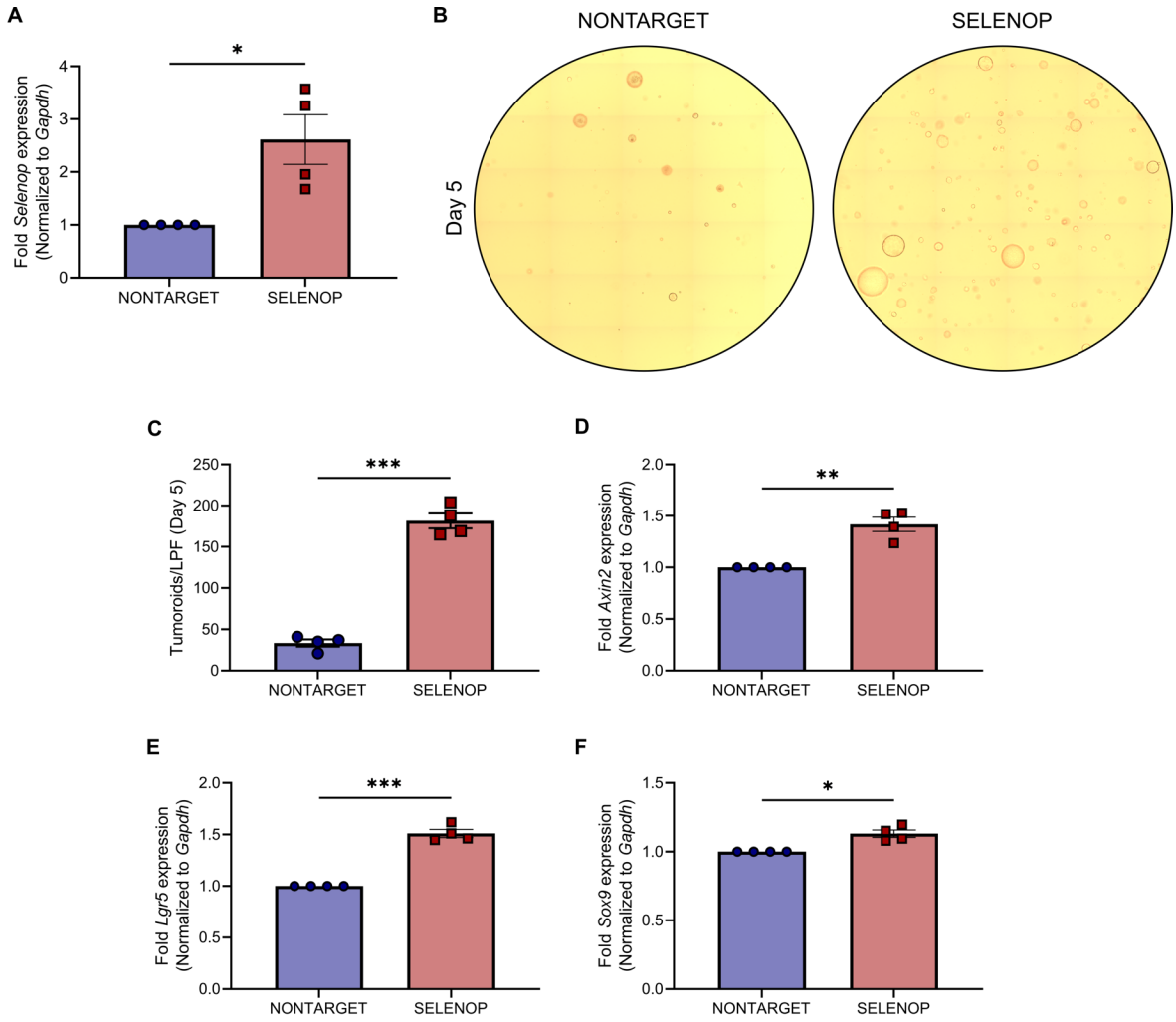

Figure 22. SELENOP restoration increases tumoroid forming capacity and WNT target gene expression. (A) RT-qPCR for *Selenop* of $Apc^{\Delta IE/+}$; $Selenop^{+/+}$-dCas9-VP64-NONTARGET or SELENOP tumoroids. (B, C) $Apc^{\Delta IE/+}$; $Selenop^{+/+}$-dCas9-VP64-NONTARGET or SELENOP tumoroids 5 days after enzymatic dissociation. (B) Representative 10x tile scans. (C) Visible tumoroids per low power field (LPF). (D, E, F) RT-qPCR for (D) *Axin2*, (E) *Lgr5*, and (F) *Sox9* of $Apc^{\Delta IE/+}$; $Selenop^{+/+}$-dCas9-VP64-NONTARGET or SELENOP tumoroids. Pooled data from n=4 independent experiments. 2-sided paired t tests. *p<0.05, **p<0.01, ***p<0.001. Data are displayed as mean ± SEM.

As we and others have reported that additional WNT stimulation increased tumoroid growth even after *Apc* loss-of-function (LOF) (90, 94), we also measured levels of WNT target transcripts by RT-qPCR. Here, SELENOP-overexpressing tumoroids displayed higher *Axin2, Lgr5,* and *Sox9* transcript levels than control tumoroids (**Figure 22D**, **Figure 22E**, **Figure 22F**). Altogether, these results demonstrate that SELENOP overexpression rescues the effects of *Selenop* deficiency on tumoroid forming capacity and WNT target gene expression.

SELENOP increases WNT target gene expression in human tumoroids

Additionally, we tested the effects of SELENOP treatment on WNT target gene expression in human tumoroid lines established from Stage II/III CRC patients (**Table 4**) and cultured in Se-replete media (i.e. with 6% FBS and ~160 nM Na_2SeO_3). Although WNT target transcript levels differed among tumoroid lines, treatment with purified human SELENOP increased *SOX9* levels in lines 32385, 35349, and 40299; *LGR5* levels in line 35349, and *AXIN2* levels in line 40299 (**Figure 23**). Thus, SELENOP also amplifies WNT signaling activity in human CRC tumoroids.

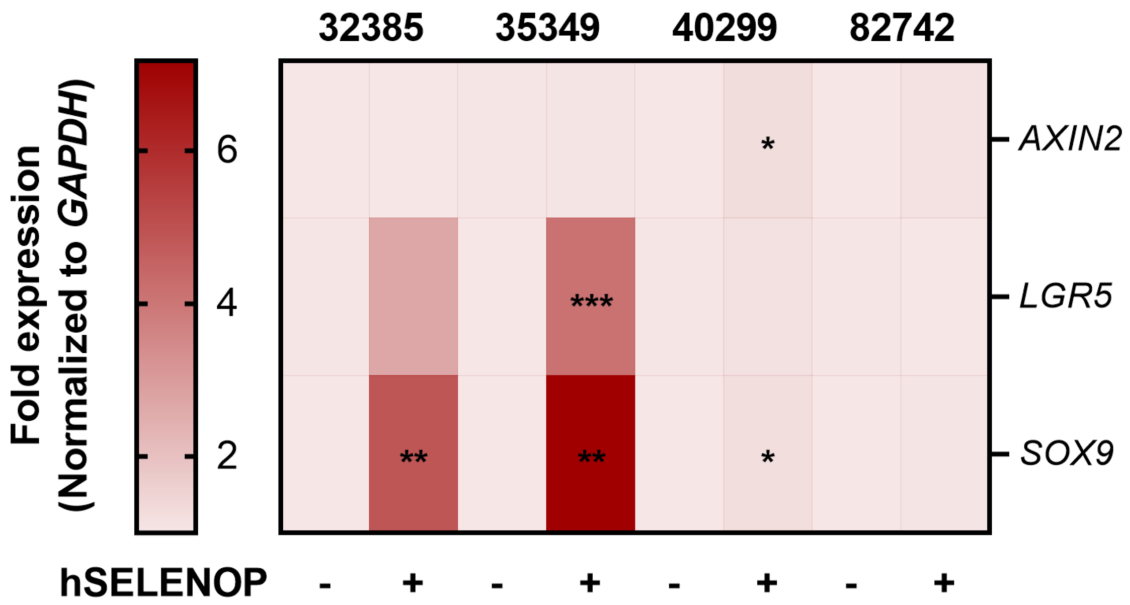

Figure 23. SELENOP increases WNT target gene expression in human tumoroids. RT-qPCR for *AXIN2*, *LGR5*, and *SOX9* of human tumoroids treated without or with hSELENOP. Each five-digit number represents tumoroids established from one patient. Pooled data from n=3 independent experiments. 2-sided paired t tests. *p<0.05, **p<0.01, ***p<0.001. Data are displayed as mean.

SELENOP increases canonical WNT signaling activity in noncancer and CRC cells

As SELENOP under- and overexpression in tumoroids decreased and increased WNT target gene expression, respectively, we hypothesized that SELENOP might directly amplify WNT signaling activity. To investigate this, we used 293 Super TOPFlash (STF) cells, which stably express a luciferase reporter of β-catenin/TCF/LEF-mediated transcription that serves as a direct readout of canonical WNT signaling activity (95). In 293 STF cells, combinatorial treatment with SELENOP and WNT3A increased TOPFlash activity to a greater extent than treatment with WNT3A alone (**Figure 24A**). As 293 STF cells are a noncancer cell line, we subsequently generated RKO (human colon adenocarcinoma) STF cells to confirm this observation and contextualize these findings in CRC. Importantly, RKO cells possess both WT *APC* and *CTNNB1*, and as such display intact WNT signaling (113). Similarly, exogenous SELENOP amplified WNT3A-induced TOPFlash activity in RKO STF cells (**Figure 24B**).

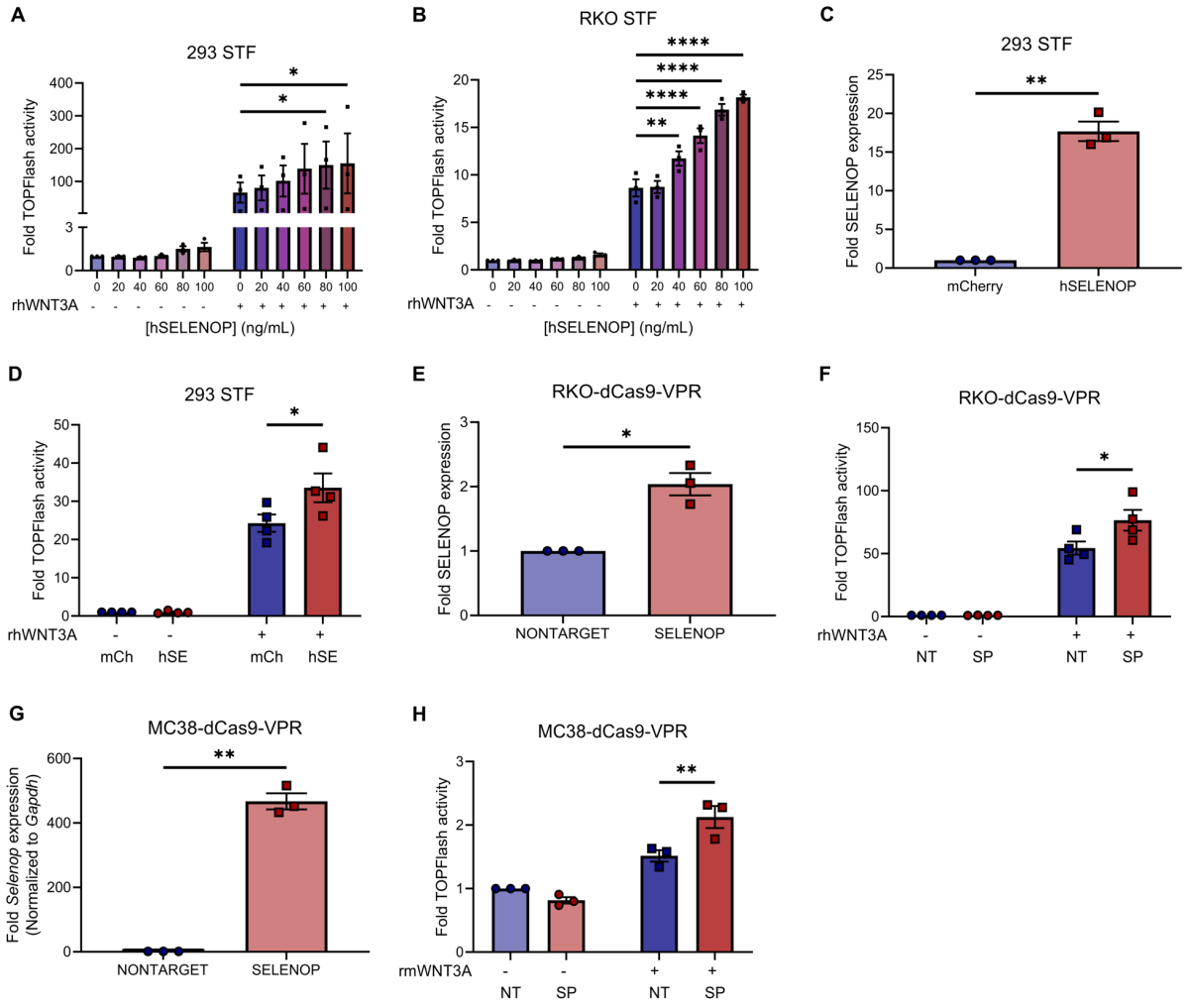

Figure 24. SELENOP increases canonical WNT signaling activity in noncancer and CRC cells. (A, B) TOPFlash activity of (A) 293 STF and (B) RKO STF cells treated without or with rhWNT3A and indicated concentrations of hSELENOP. (C) ELISA for SELENOP of 293 STF-mCherry or hSELENOP conditioned media. (D) TOPFlash activity of 293 STF-mCherry or hSELENOP cells treated without or with rhWNT3A. hSE: hSELENOP, mCh: mCherry. (E) ELISA for SELENOP of RKO-dCas9-VPR-NONTARGET or SELENOP conditioned media. (F) TOPFlash activity of RKO-dCas9-VPR-NONTARGET or SELENOP cells treated without or with rhWNT3A. NT: nontarget, SP: SELENOP. (G) RT-qPCR for *Selenop* of MC38-dCas9-VPR-NONTARGET or SELENOP cells. (H) TOPFlash activity of MC38-dCas9-VPR-NONTARGET or SELENOP cells treated without or with rmWNT3A. Pooled data from n=3-4 independent experiments. 2-way repeated measures ANOVAs with 2-sided Dunnett's multiple comparisons tests (A, B), 2-sided paired t tests (C, E, G), 2-way repeated measures ANOVAs with 2-sided Sidak's multiple comparisons tests (D, F, H). *p<0.05, **p<0.01, ****p<0.0001. Data are displayed as mean ± SEM.

As SELENOP is a secreted protein, we hypothesized that secreted SELENOP would increase WNT signaling activity by an autocrine and/or paracrine mechanism. Indeed, lentiviral SELENOP overexpression in 293 STF cells (**Figure 24C**) promoted WNT3A-induced TOPFlash activity (**Figure 24D**). Similarly, CRISPRa-mediated SELENOP overexpression in RKO cells (**Figure 24E**) or MC38 (mouse colon adenocarcinoma) cells (**Figure 24G**) augmented WNT3A-induced TOPFlash activity (**Figure 24F**, **Figure 24H**). Overall, it appears exogenous or endogenous SELENOP augments canonical WNT signaling activity.

SELENOP interacts with LRP6

We next interrogated the mechanism by which SELENOP increased canonical WNT signaling activity. Interestingly, exogenous SELENOP increased TOPFlash activity even after *APC* KD in 293 STF cells (**Figure 25**). As WNTs bind LRP5/6 and FZD co-receptors to activate WNT signaling (114), while SELENOP binds tissue-specific LRP1, LRP2, or LRP8 receptors for receptor-mediated endocytosis (55, 58, 59, 115, 116), we hypothesized that SELENOP modifies WNT signaling through interactions with LRP5/6. To test this hypothesis, we used 293T cells that stably express FLAG-tagged endogenous LRP6, and we observed that SELENOP co-immunoprecipitated with FLAG-LRP6 in these cells (**Figure 26A**). While both SELENOP and LRP6 are highly conserved between mouse and human (**Appendix C: Figure 46, Appendix D: Figure 47**), overexpressed, V5-tagged mouse SELENOP failed to co-immunoprecipitate with FLAG-LRP6 in these cells, which suggests the SELENOP:LRP6 interaction is species-specific (**Figure 27**). We subsequently confirmed the SELENOP:LRP6 interaction by proximity ligation assay in 293T cells transfected with FLAG-tagged mouse LRP6 (FLAG-mLRP6) and V5-tagged mouse SELENOP (V5-mSELENOP) overexpression constructs (**Figure 28**).

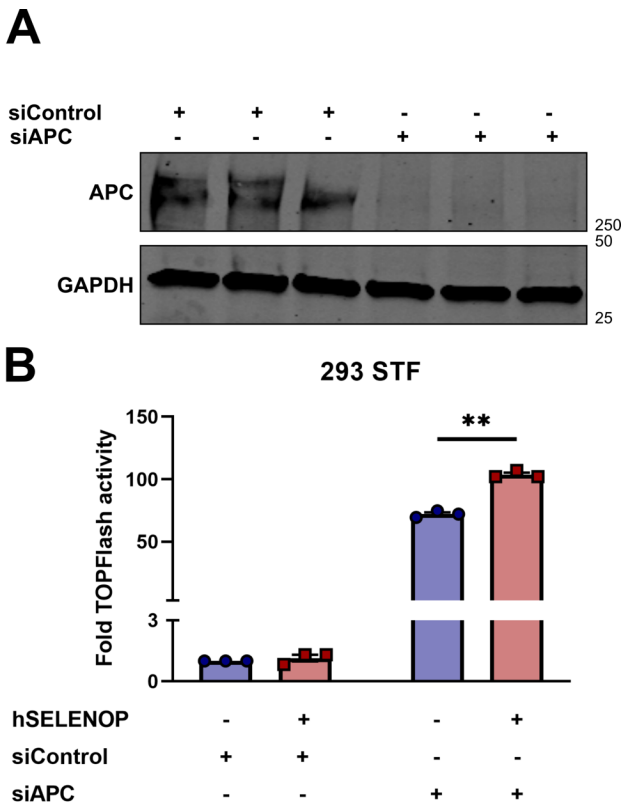

Figure 25. SELENOP acts upstream of APC. (A) Western blot for APC and GAPDH (loading control) of lysates from 293 STF cells transfected with siControl or siAPC. (B) TOPFlash activity of 293 STF cells transfected with siControl or siAPC and treated without or with hSELENOP. Pooled data from n=3 independent experiments. 2-way repeated measures ANOVA with 2-sided Sidak's multiple comparisons test. **p<0.01. Data are displayed as mean ± SEM.

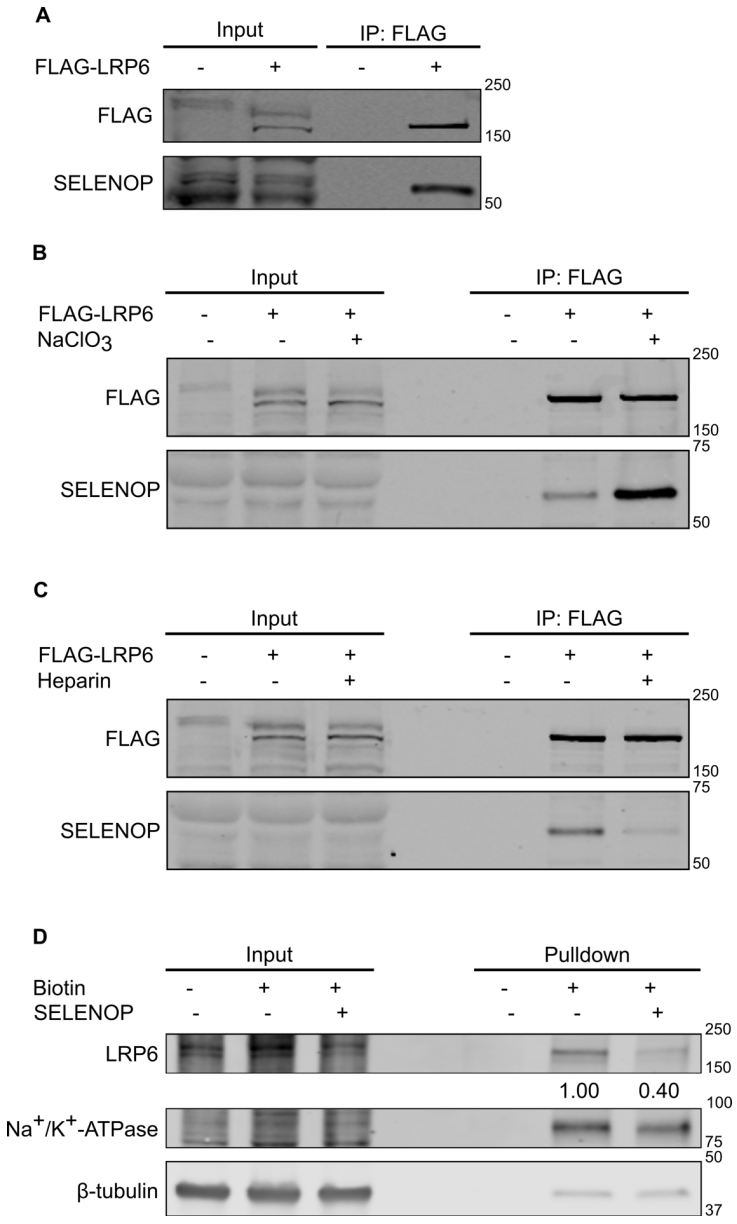

Figure 26. SELENOP interacts with LRP6. (A) Western blot for FLAG and SELENOP of FLAG IPs from 293T or 293T-FLAG-LRP6 cells. (B) Western blot for FLAG and SELENOP of FLAG IPs from 293T or 293T-FLAG-LRP6 cells treated without or with sodium chlorate ($NaClO_3$). (C) Western blot for FLAG and SELENOP of FLAG IPs from 293T or 293T-FLAG-LRP6 cells treated without or with heparin. (D) Western blot for LRP6, Na^+/K^+-ATPase (plasma membrane loading control), and β-tubulin (whole cell loading control) of cell surface biotinylation and isolation from 293T cells treated without or with SELENOP-conditioned media. Representative data from n=3 independent experiments.

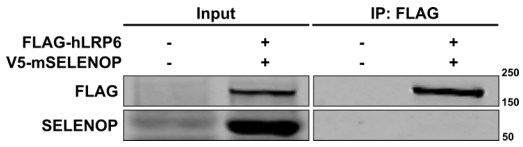

Figure 27. Mouse SELENOP does not interact with human LRP6. Western blot for FLAG and SELENOP of FLAG IPs from 293T or 293T-FLAG-LRP6 cells transfected with V5-mSELENOP. Representative data from n=3 independent experiments.

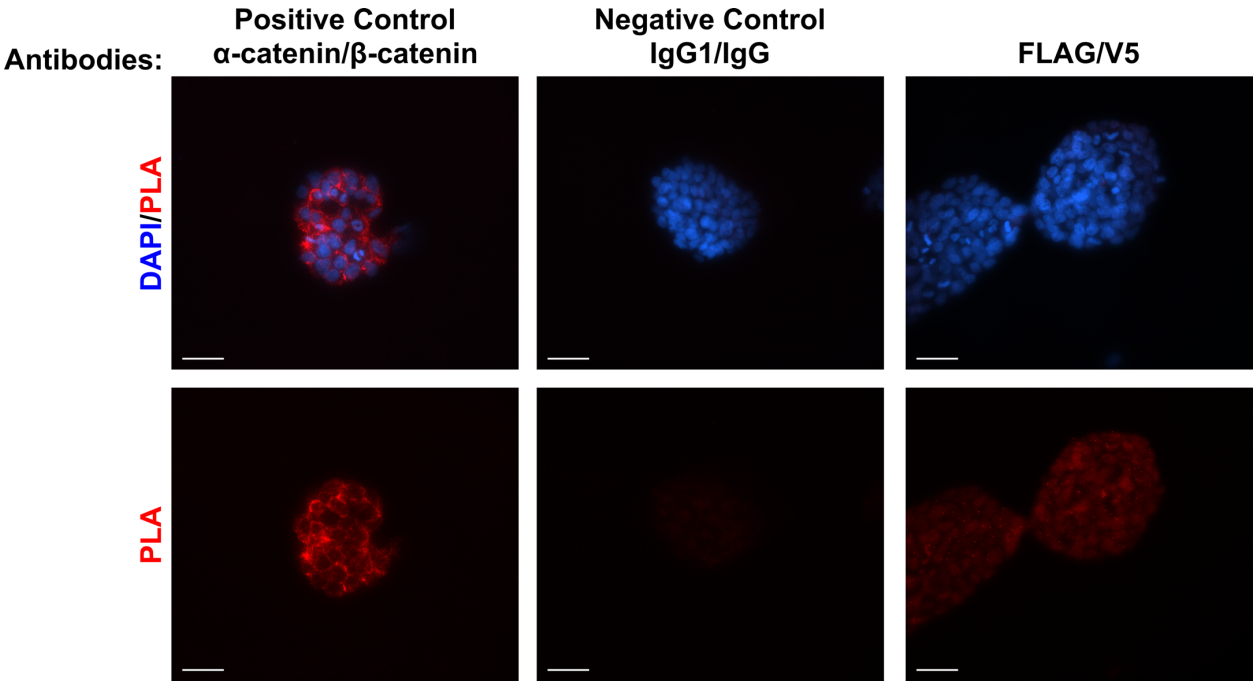

Figure 28. SELENOP interacts with LRP6. Proximity ligation assay of 293T cells co-transfected with FLAG-mLRP6 and V5-mSELENOP. Representative 40x images from n=3 independent experiments, scale bars = 50 µm.

As SELENOP is widely thought to bind heparan sulfate proteoglycans (HSPGs) (37) and HSPGs deliver WNT modulators and ligands to LRP5/6 (117), we hypothesized HSPGs facilitate SELENOP:LRP6 interactions. Surprisingly, inhibition of HSPG synthesis (via $NaClO_3$ treatment) markedly enhanced co-IP of SELENOP and FLAG-LRP6 in 293T-FLAG-LRP6 cells (**Figure 26B**). Conversely, treatment with heparin prevented SELENOP and FLAG-LRP6 co-IP in these cells (**Figure 26C**). Furthermore, we investigated whether SELENOP accelerates LRP5/6 recycling to potentiate WNT signaling activity. We tested this hypothesis through biotinylation and isolation of cell surface proteins with and without SELENOP treatment. Indeed, SELENOP decreased cell surface LRP6 levels (**Figure 26D**). Thus, SELENOP interacts with LRP6 (unless sequestered by HSPGs), promotes LRP6 internalization, and thus amplifies WNT signaling activity.

SELENOP$^{U258\text{-}U299}$ mediates SELENOP:LRP5/6 interactions and SELENOP-induced WNT signaling augmentation

We next mapped the SELENOP:LRP6 interaction on SELENOP using FLAG-mLRP6 and mSELENOP overexpression constructs truncated (t) at SELENOP's third, fourth, fifth, sixth, seventh, or ninth Sec (U) (**Figure 29A**). As expected, full-length mSELENOP co-immunoprecipitated with FLAG-mLRP6 in 293T cells. Interestingly, only truncation at SELENOP's third Sec uncoupled the SELENOP:LRP6 interaction (**Figure 29B**). To further refine the LRP6 interaction domain on SELENOP, we generated V5-mSELENOP overexpression constructs truncated (t) at SELENOP's first, second, third, or fourth Sec (U) (**Figure 29C**). Both full-length and tU4 V5-mSELENOP co-immunoprecipitated with FLAG-mLRP6 in 293T cells; however, truncation at SELENOP's first, second, or third Sec uncoupled this interaction (**Figure 29D**).

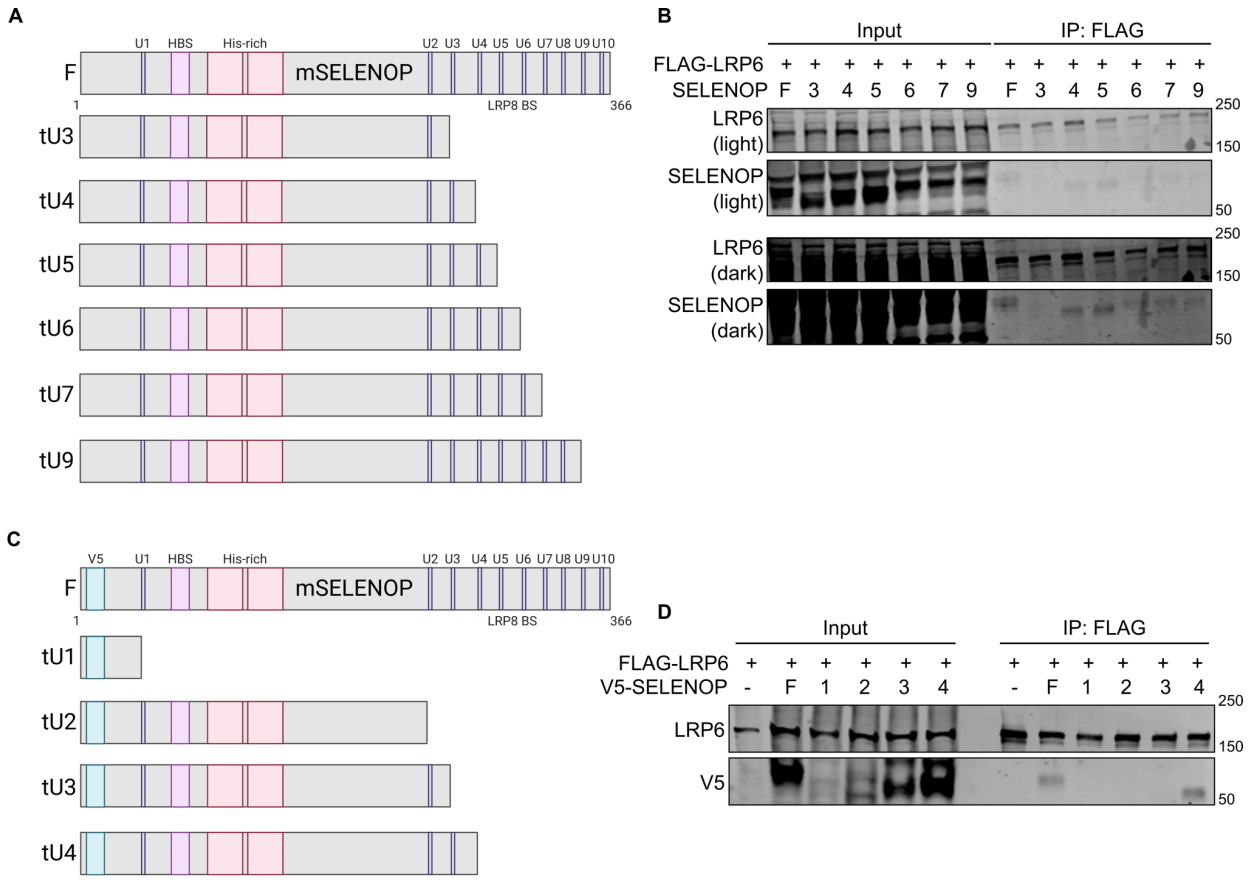

Figure 29. Longer SELENOP isoforms interact with LRP6. (A) Schematic of mouse SELENOP truncation constructs. U: selenocysteine, HBS: heparin binding site, His-rich: histidine-rich region, LRP8 BS: LRP8 binding site. (B) Western blot for LRP6 and SELENOP of FLAG IPs from 293T cells co-transfected with FLAG-mLRP6 and full-length (F) or truncated (at U#) mSELENOP. (C) Schematic of V5-tagged mouse SELENOP truncation constructs. (D) Western blot for LRP6 and V5 of FLAG IPs from 293T cells co-transfected with FLAG-mLRP6 and full-length (F) or truncated (at U#) V5-mSELENOP. Representative data from n=3 independent experiments.

We next generated V5-mSELENOP overexpression constructs with sequential, ~10-aa deletions (Δ) between SELENOP's third (U258) and fourth (U299) Sec, or 42-aa deletion (Δ) from U258 to U299 (**Figure 30A**). Interestingly, full-length, Δ258-267, Δ268-277, Δ278-287, and Δ288-299 V5-mSELENOP all co-immunoprecipitated with FLAG-mLRP6. Only deletion of the entire region from U258 to U299 uncoupled the SELENOP:LRP6 interaction (**Figure 30B**). As LRP6 and LRP5 are highly homologous proteins (**Appendix A: Figure 43**) known to hetero- and homodimerize (14), we hypothesized that SELENOP interacts with LRP5 through its U258-U299 domain. Indeed, full-length, but not Δ258-299 V5-mSELENOP, co-immunoprecipitated with FLAG-mLRP5 (**Figure 31**).

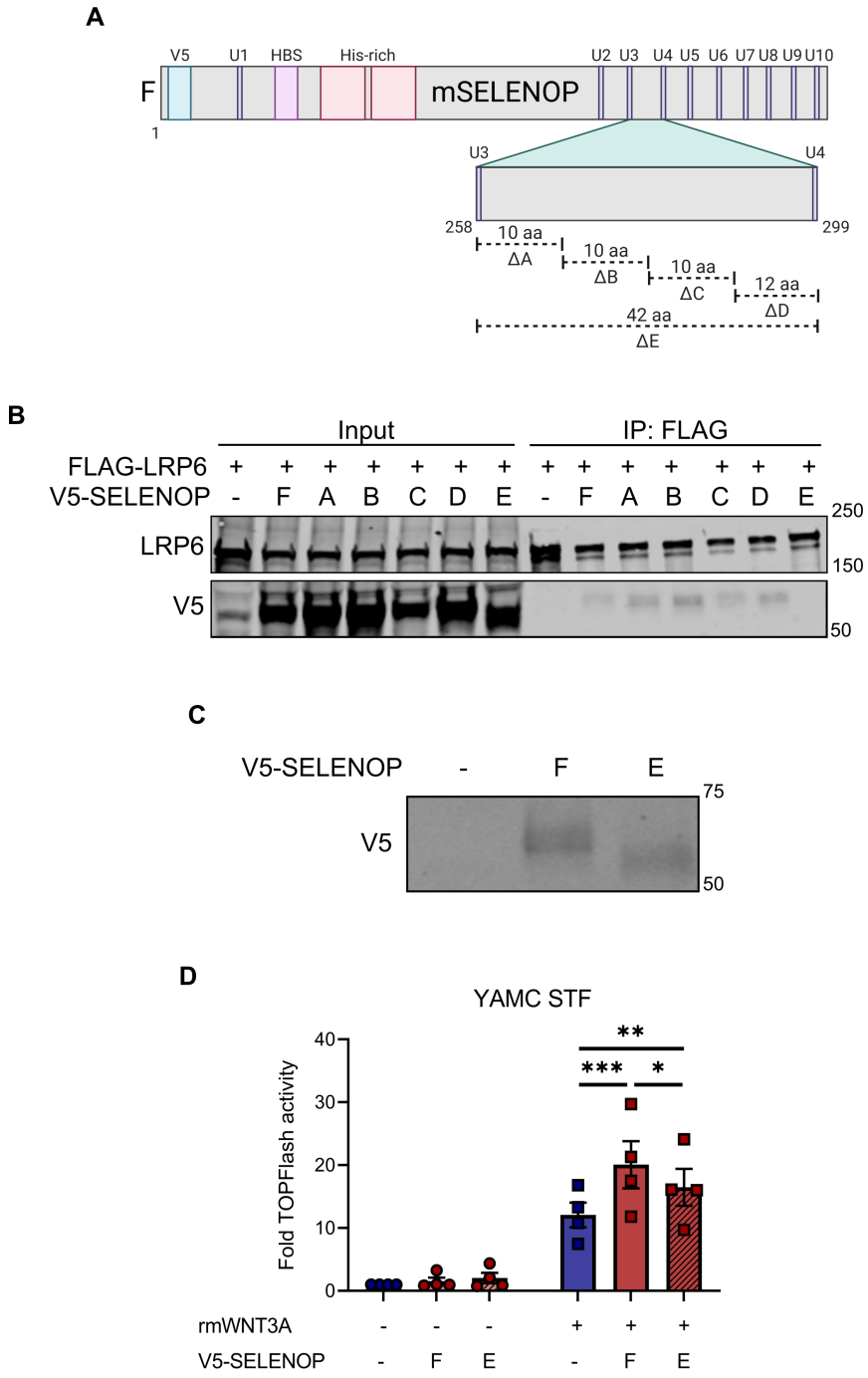

Figure 30. SELENOP$^{U258-U299}$ mediates the SELENOP:LRP6 interaction and SELENOP-induced WNT signaling augmentation. (A) Schematic of V5-tagged mouse SELENOP deletion constructs. U: selenocysteine, HBS: heparin binding site, His-rich: histidine-rich region, LRP8 BS: LRP8 binding site. ΔA: Δ258-267, ΔB: Δ268-277, ΔC: Δ278-287, ΔD: Δ288-299, ΔE: Δ258-299. (B) Western blot for LRP6 and V5 of FLAG IPs from 293T cells co-transfected with FLAG-mLRP6 and full-length (F) or mutant (A-E) V5-mSELENOP. (C) Western blot for V5 and (D) TOPFlash activity of YAMC STF cells transduced with full-length (F) or LRP5/6-uncoupling (E) V5-mSELENOP. Representative (B, C) or pooled (D) data from n=3-4 independent experiments. 2-way repeated measures ANOVA with 2-sided Tukey's multiple comparisons tests. *p<0.05, **p<0.01, ***p<0.001. Data are displayed as mean ± SEM.

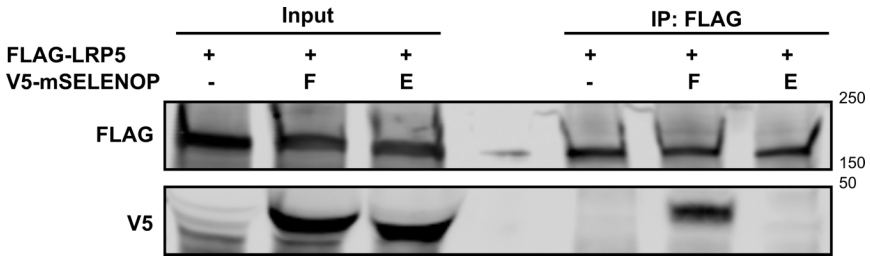

Figure 31. SELENOP$^{U258\text{-}U299}$ mediates the SELENOP:LRP5 interaction. Western blot for FLAG and V5 of FLAG IPs from 293T cells co-transfected with FLAG-mLRP5 and full-length (F) or LRP5/6-uncoupling (E) V5-mSELENOP. Representative data from n=2 independent experiments.

To test our hypothesis that SELENOP increases canonical WNT signaling activity through these specific LRP5/6 interactions, we performed TOPFlash assays on YAMC (immortalized mouse colon) STF cells transduced with full-length or LRP5/6-uncoupling (Δ258-299) V5-mSELENOP overexpression constructs (**Figure 30C**). As expected, overexpression of full-length V5-mSELENOP increased WNT3A-induced TOPFlash activity; however, overexpression of LRP5/6-uncoupling V5-mSELENOP decreased this effect (**Figure 30D**). Altogether, these results indicate that SELENOP$^{U258\text{-}U299}$ mediates SELENOP:LRP5/6 interactions to promote WNT signaling activity.

SELENOP binds multiple domains of LRP6

We next investigated whether the SELENOP:LRP6 interaction requires a specific region of LRP6 with a panel of FLAG-tagged mouse LRP6 deletion mutant constructs (**Figure 32A**). As SELENOP binds LRP8's single BP domain (62), we hypothesized SELENOP binds one (or more) of LRP6's four BP domains. Surprisingly, deletion of LRP6's first and second, third and fourth, or first through fourth BP domains failed to uncouple the SELENOP:LRP6 interaction (**Figure 32B**). Moreover, deletion of LRP6's LDLR repeats failed to uncouple the SELENOP:LRP6 interaction (**Figure 32C**). Thus, SELENOP appears capable of binding multiple domains of LRP6.

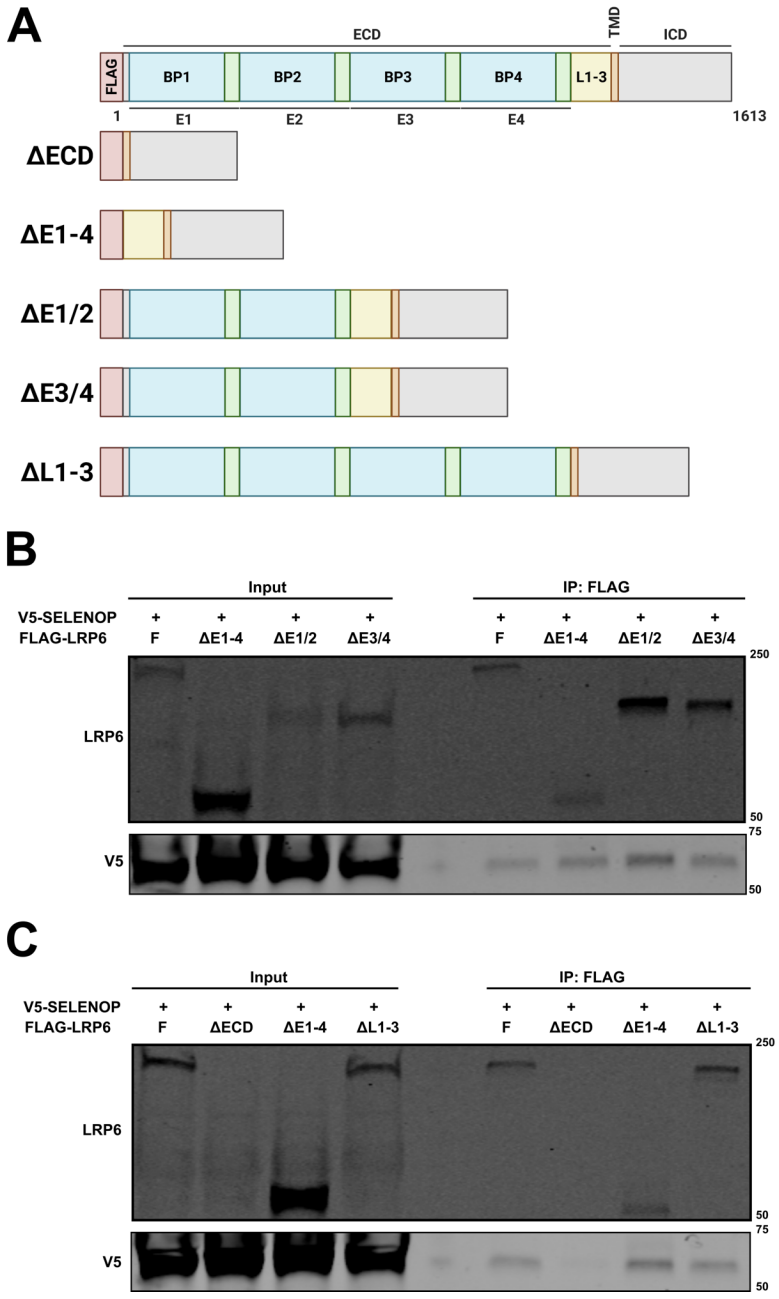

Figure 32. SELENOP binds multiple domains of LRP6. (A) Schematic of FLAG-tagged mouse LRP6 deletion constructs. BP: β-propeller, E: β-propeller and EGF-like domain, ECD: extracellular domain, L1-3: LDLR type A repeats, ICD: intracellular domain, TMD: transmembrane domain. (B) Western blot for LRP6 and V5 of FLAG IPs from 293T cells co-transfected with V5-mSELENOP and full-length (F) or mutant (ΔE1-4, ΔE1/2, ΔE3/4) FLAG-mLRP6. (C) Western blot for LRP6 and V5 of FLAG IPs from 293T cells co-transfected with V5-mSELENOP and full-length (F) or mutant (ΔECD, ΔE1-4, ΔL1-3) FLAG-mLRP6. Representative data from n=3 independent experiments.

SELENOP interacts with WNT3A in an LRP5/6-independent manner

Lastly, we investigated whether LRP6, SELENOP, and WNT3A can co-exist in a protein complex *in vitro*. To accomplish this, we treated lysates from 293T cells co-transfected with FLAG-mLRP6 and V5-mSELENOP overexpression constructs with WNT3A prior to IP. Indeed, both WNT3A and V5-mSELENOP co-immunoprecipitated with FLAG-mLRP6 (**Figure 33A**). This finding raised the possibility that SELENOP interacts with WNT3A, independently of LRP5/6. In similar experiments, WNT3A co-immunoprecipitated with both LRP5/6-uncoupling (Δ258-299) and full-length V5-mSELENOP (**Figure 33B**). Thus, SELENOP interacts with WNT3A in an LRP5/6-independent manner.

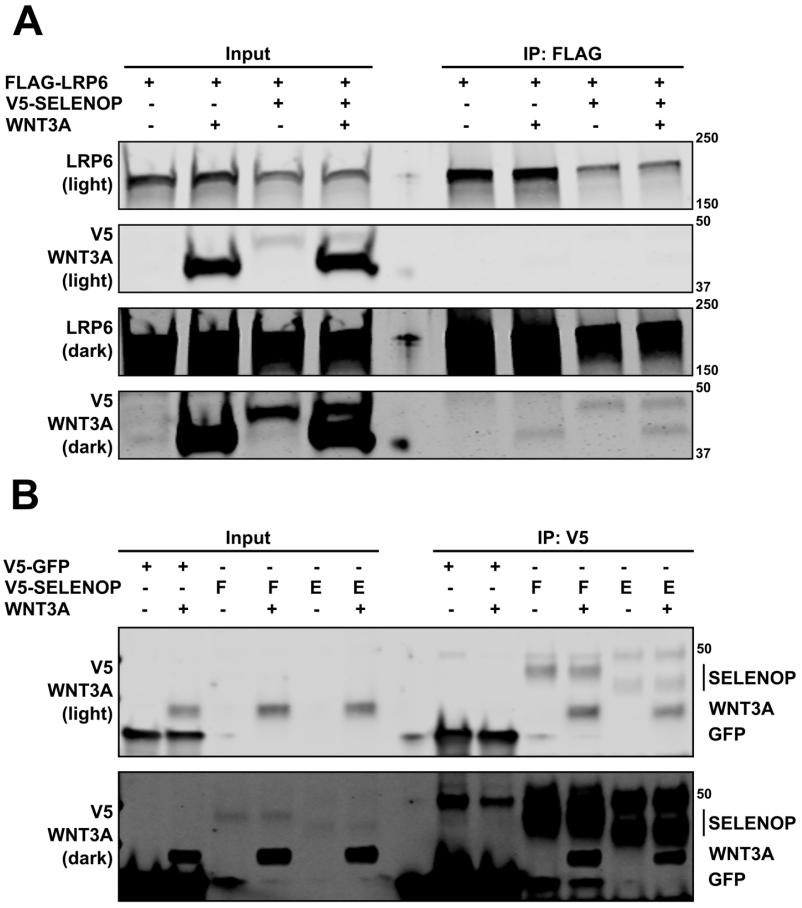

Figure 33. SELENOP interacts with WNT3A in an LRP5/6-independent manner. (A) Western blot for LRP6, V5, and WNT3A of FLAG IPs from 293T cells co-transfected with FLAG-mLRP6 and V5-mSELENOP, then treated without or with rmWNT3A. (B) Western blot for V5 and WNT3A of V5 IPs from 293T cells transfected with V5-GFP, full-length (F), or LRP5/6-uncoupling (E) V5-mSELENOP, then treated without or with rmWNT3A. Representative data from n=3 independent experiments.

CHAPTER 4: DISCUSSION

Summary

In this study, we defined the role of SELENOP in sporadic colorectal carcinogenesis, which is predominantly initiated by mutations that hyperactivate canonical WNT signaling. Since we observed increases in *SELENOP* expression throughout conventional adenoma to carcinoma progression, we hypothesized that SELENOP promotes intestinal tumorigenesis. To test this, we used a mouse model in which intestinal epithelial-specific deletion of the tumor suppressor *Apc* and concomitant WNT signaling hyperactivation drive adenoma formation. In this model, global, but not intestinal epithelial-specific *Selenop* KO was tumor-protective, indicative of compensatory contributions by non-epithelial-derived SELENOP. Underlying these phenotypes, we discovered a novel mechanism in which SELENOP modulates canonical WNT signaling activity through specific interactions with the WNT co-receptors LRP5/6. **Figure 34** graphically depicts the major findings of this study.

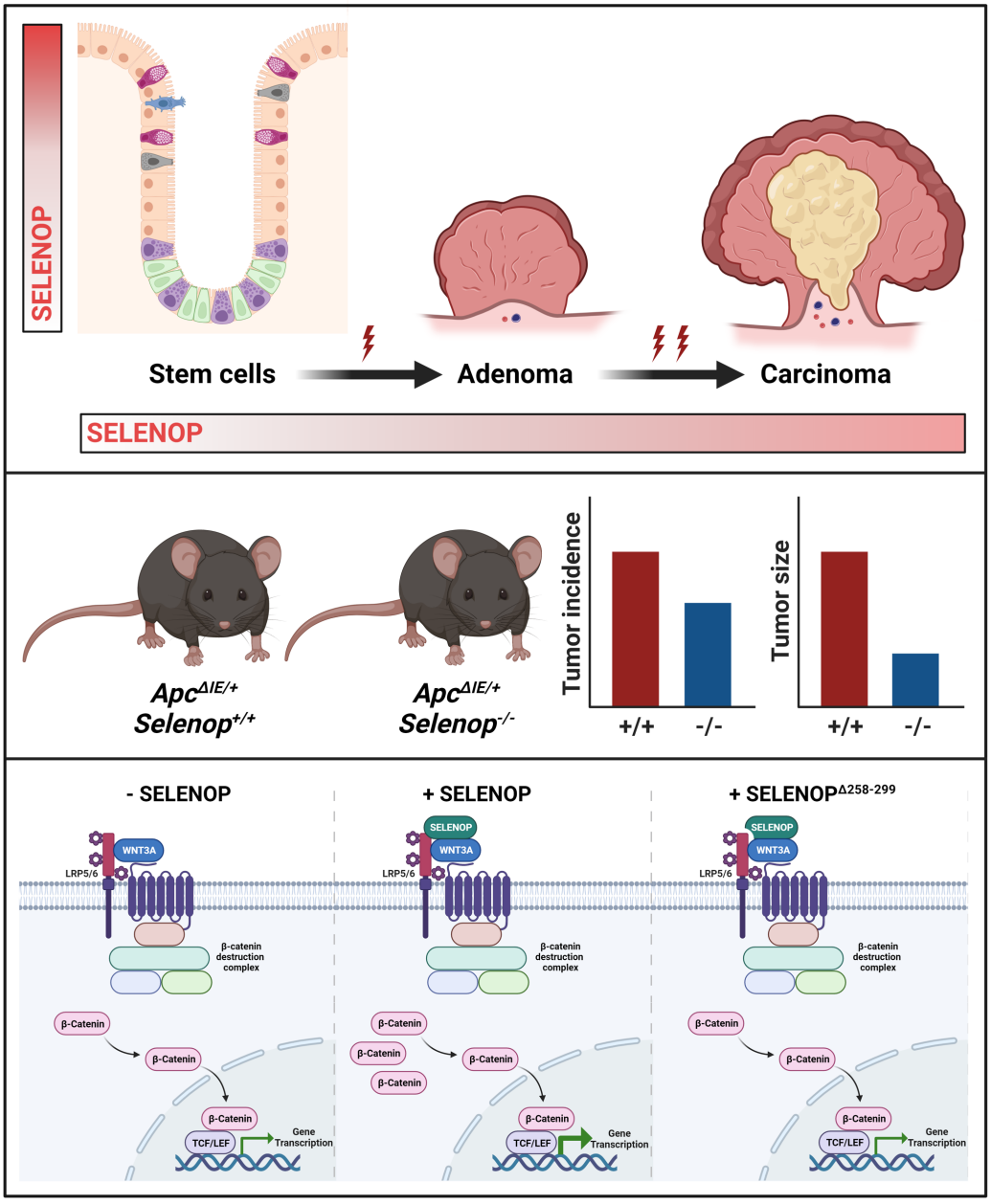

Figure 34. Graphical abstract.

SELENOP expression in the intestine

We identified *Selenop* as the most highly expressed selenotranscript in the normal mouse small intestine epithelium, consistent with a selenotranscriptome profile of whole mouse small intestine (109). To the best of our knowledge, we are the first to characterize SeP mRNA expression specifically in the mouse colon and small intestine epithelium. When we examined *SELENOP* localization *in situ*, we observed a gradient of epithelial *SELENOP* expression up the crypt axis, as well as stromal *SELENOP* expression, in both mouse and human tissues. This expression pattern confirms prior findings in rat, mouse, and human small intestine/colon tissues, and supports *SELENOP*'s recently proposed role as a crypt axis marker (50, 51, 118).

Moreover, we defined the specific cell types responsible for *SELENOP*'s expression pattern using scRNA-seq data from mouse and human intestinal epithelium (73, 119). Here, we predominantly detected *SELENOP* expression in differentiated cell types, including Paneth, goblet, enteroendocrine, and absorptive cells. Given the dearth of data on intestinal epithelial cell type-specific protein expression, we employed directed differentiation of human enteroids to corroborate these observations. Indeed, SELENOP protein levels increased in human enteroids differentiated towards the Paneth cell, goblet cell, or enterocyte lineages.

As previously mentioned, SELENOP functions as a local antioxidant, in addition to its historically established role in Se homeostasis and its newly described role in WNT signaling. Thus, we speculate that high SELENOP expression in differentiated villus and crypt-top epithelial cells protects against the onslaught of ROS they regularly encounter, from xenobiotics, microorganisms, micronutrients, macronutrients, and alcohol (120). In support of this, we observe substantially higher *Selenop* expression in the villus epithelial cells of the small intestine than in the crypt-top epithelial cells of the colon, consistent with the small intestine's much larger role in nutrient absorption.

***SELENOP* expression in CRC**

As molecules implicated in carcinogenesis often display tightly restricted patterns of expression, we next examined *SELENOP* levels throughout CRC progression. Our analyses revealed slight increases in *SELENOP* expression from tumor-initiating stem cells to adenomatous polyps and MSS cancers. Although others have reported reductions in *SELENOP* expression in colorectal tumors as compared to normal colon tissues (66–68, 121), these studies did not stratify *SELENOP* expression by epithelial cell type, and thus failed to account for the *SELENOP* expression gradient from crypt base to top in the normal colon. Namely, in comparisons with bulk normal colon tissues, we believe strong *SELENOP* expression in stromal and differentiated epithelial cells obscures detection of meaningful, albeit subtle, differences in *SELENOP* expression from tumor-initiating cells to polyps and cancers. While *SELENOP* expression was still lower in MSS cancers than in differentiated epithelial cells, we hypothesize that *SELENOP* upregulation throughout progression to malignancy fortifies tumor-promotive WNT signaling activity.

The vast majority of sporadic CRCs arise through either the serrated or conventional pathways. Conventional CRCs, which comprise 60-85% of sporadic CRCs, are characterized by mutational inactivation of the tumor suppressor genes *APC*, *SMAD2/4*, and *TP53*, as well as mutational activation of the oncogene *KRAS*. Importantly, *APC* mutation (and resultant WNT hyperactivation) is widely considered the initiator of conventional colorectal tumorigenesis. Serrated CRCs, which represent 15-40% of sporadic CRCs, are characterized by mutational activation of the oncogenes *KRAS* or v-raf murine sarcoma viral oncogene homolog B1 (*BRAF*), as well as epigenetic inactivation of the tumor suppressor genes MutL protein homolog 1 (*MLH1*) and cyclin-dependent kinase inhibitor 2A (*CDKN2A*) through promoter hypermethylation (108, 122). Conventional CRCs do not typically display microsatellite instability (MSI), but rather chromosomal abnormalities (e.g. aneuploidy, translocations, amplifications) collectively termed chromosomal instability (CIN). In contrast, many serrated CRCs display MSI, but not CIN (123).

Unlike in conventional CRCs, *SELENOP* expression was increased in serrated polyps, but not MSI-H cancers, as compared to tumor-initiating absorptive cells. By way of reminder, MSI generally arises due to epigenetic or mutational inactivation of MMR genes (124). Accordingly, MMR-deficient tumors demonstrated decreased *SELENOP* expression as compared to MMR-proficient tumors. These intriguing results raise the possibility that SELENOP plays distinct roles in conventional versus serrated colorectal carcinogenesis.

In MSI-H colorectal tumors, MMR deficiency generates indels at microsatellite regions that ultimately give rise to myriad neoantigens, which elicit a robust host immune response (125). Accordingly, patients with MSI-H CRCs typically experience longer survival times with lower metastasis risk, as compared to patients with MSS CRCs (126, 127). In further support of a stronger immune response in the setting of MSI, MSI-H CRCs have been found to contain more tumor-associated macrophages (TAMs) and tumor-infiltrating lymphocytes (TILs) than MSS CRCs (128–131). Specifically, MSI-H CRCs exhibited greater numbers of pro-inflammatory M1 macrophages (132), cytotoxic $CD8^+$ T cells (133–137), helper $CD4^+$ T cells (132, 137), and regulatory $FOXP3^+$ T cells (133). These cell types secrete various pleiotropic cytokines; for example, M1 macrophages produce tumor necrosis factor α (TNF-α), interleukin (IL)-6, IL-1β, IL-12, and IL-8 (138). For another, $CD4^+$ T cell subsets can produce IFN-γ, IL-4, IL-5, IL-10, IL-13, IL-17, and IL-35 (139). Notably, several of these cytokines, namely IFN-γ, IL-1β, IL-6, and TNF-α, have been reported to downregulate *SELENOP* transcription *in vitro* (140, 141). Therefore, we speculate that the lower *SELENOP* levels observed in MSI-H versus MSS tumors arises from the greater immune infiltrate and concomitant cytokine production that characterizes MSI-H tumors.

SELENOP in experimental CRC and CAC

Using an *Apc*-dependent mouse adenoma model, we discovered that *Selenop* KO reduced colon tumor size and incidence. Although SELENOP remains relatively understudied in sporadic CRC, the literature supports distinct roles for different SePs in chemically (i.e. AOM) induced experimental CRC.

For example, transgenic mice with a mutation in the $tRNA^{Sec}$ gene that inhibits Sec synthesis, and thus reduces global SeP production, developed fewer early neoplastic lesions called aberrant crypt foci (ACF) than WT mice after AOM treatment (142). Similarly, *Gpx2* or *Selenof* KO mice developed fewer ACFs than WT mice after AOM treatment; in the case of *Gpx2* KO mice, this corresponded with a decrease in tumor number (143, 144). In contrast, *Selenop* KO mice developed more ACFs than *Selenop* WT mice after AOM treatment, although ACF progression to adenomas was not reported in this study (50). Importantly, studies that use ACFs as a primary readout of experimental tumorigenesis warrant cautious interpretation, as ACFs, while widely considered CRC precursors, have been demonstrated to regress spontaneously in several animal models (145–147). To the best of our knowledge, we are the first to investigate the impacts of *Selenop* KO on adenoma, not ACF, development in a genetically, not chemically, induced CRC mouse model.

As in sporadic CRC models, current evidence suggests that different SePs modify CAC by distinct mechanisms. In the AOM/DSS experimental CAC model, *Gpx2* or *Gpx3* KO mice developed more tumors than WT mice (148, 149). In contrast, *Selenof* KO mice developed similar numbers of tumors, yet fewer ACFs, as compared to WT mice after AOM/DSS treatment (150). Notably, *Selenop* KO mice developed fewer, smaller tumors than *Selenop* WT mice after an AOM/DSS protocol (50), which partially parallels our findings in experimental CRC. Additionally, *Selenop* KO tumors from this CAC model displayed dysregulated WNT signaling, including transcriptional upregulation of the known WNT antagonists secreted Frizzled-related proteins (SFRPs) 4 and 5 (50). Similarly, our $Apc^{\Delta IE/+}$; $Selenop^{-/-}$ tumoroids demonstrated defects in organoid formation and decreases in WNT target gene expression, which could be reversed by SELENOP restoration.

However, when we investigated the tissue-specific SELENOP sources responsible for the phenotypes observed in experimental CAC, we discovered that neither liver- nor myeloid-specific, but rather, intestinal epithelial-specific *Selenop* deletion augmented tumorigenesis (51). That is, $Selenop^{\Delta IE/\Delta IE}$ mice developed more, larger tumors at earlier timepoints and with more severe dysplasia than $Selenop^{+/+}$

mice after an AOM/DSS protocol (51). Moreover, *Selenop*$^{\Delta IE/\Delta IE}$ tumors exhibited greater apoptosis and DNA damage than *Selenop*$^{+/+}$ tumors (51). In contrast, in our sporadic adenoma model, we observed no effects of intestinal epithelial-specific *Selenop* deletion on small intestinal or colonic tumorigenesis. Potential explanations for these disparate results involve the etiological differences between CAC and sporadic CRC. In CAC, unlike in sporadic CRC, a chronic inflammatory microenvironment fosters tumorigenesis, as overproduction of ROS by innate immune cells promotes oxidative stress and leads to pro-tumorigenic DNA damage (151). As previously mentioned, SELENOP functions as a Se provider and antioxidant (152), and, as we demonstrate in this study, a WNT modulator. Presumably, intestinal epithelial-derived SELENOP acts as a local antioxidant to mitigate the oxidative stress that constitutes a larger component of CAC than sporadic CRC pathogenesis. Thus, perhaps intestinal epithelial-derived SELENOP plays a larger role in CAC than sporadic CRC.

SELENOP as a WNT modulator

Although SELENOP's effects on WNT signaling were previously undescribed, the literature supports roles for Se itself as both a positive and negative regulator of WNT signaling activity. For example, both sodium selenate and selenomethionine administration activated WNT signaling in hippocampus tissue and primary neurons from a mouse model of Alzheimer's disease (153, 154). However, selenomethionine treatment inhibited WNT signaling in HT-29 human colorectal adenocarcinoma cells (155). Similarly, Se deficiency upregulated transcription of WNT signaling targets and components in the normal mouse colon (156). Conversely, Se supplementation, in the form of Se-enriched broccoli or the synthetic organoselenium compound p-xyleneselenocyanate (p-XSC), reduced intestinal tumorigenesis in the WNT-driven *Apc*$^{Min/+}$ model (157, 158). Thus, the effects of Se on WNT signaling activity may depend on tissue and disease context.

Through this study, we discovered SELENOP as a novel agonist of the canonical WNT signaling pathway. Interestingly, we also observed inverse correlations between WNT signaling activity and *SELENOP* expression in human colorectal adenocarcinomas, mouse intestinal adenomas, and genetically

engineered mouse enteroids. Moreover, WNT3A treatment decreased *SELENOP* levels in both noncancer and human CRC cell lines. Altogether, these results indicate that, while SELENOP upregulates WNT signaling, WNT signaling downregulates *SELENOP* (**Figure 35**). Such a negative feedback loop between WNT and SELENOP upholds the previously described "just-right" or "Goldilocks" WNT signaling model, which postulates an optimal elevation of WNT signaling activity for tumorigenesis, beyond which leads to apoptosis (**Figure 36**).

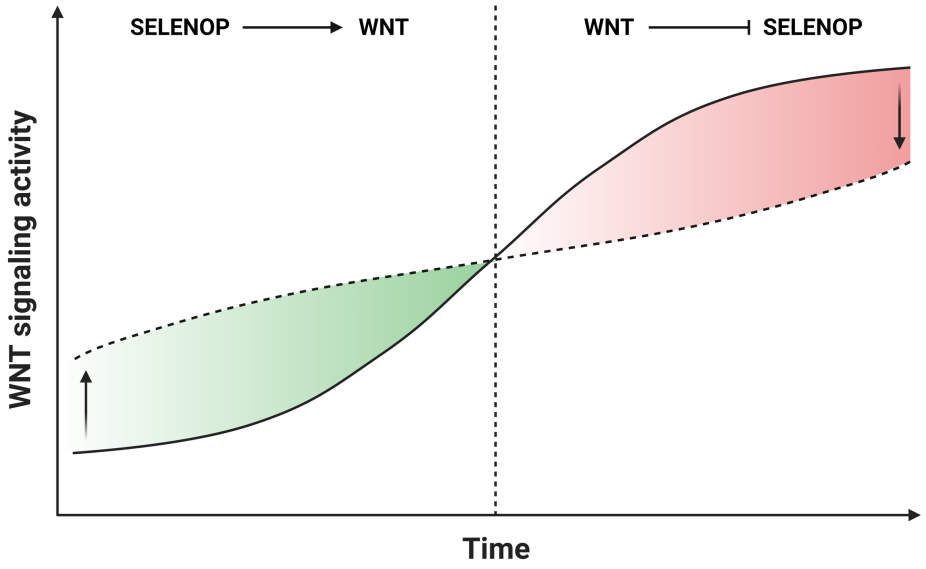

Figure 35. Negative feedback loop between WNT and SELENOP.

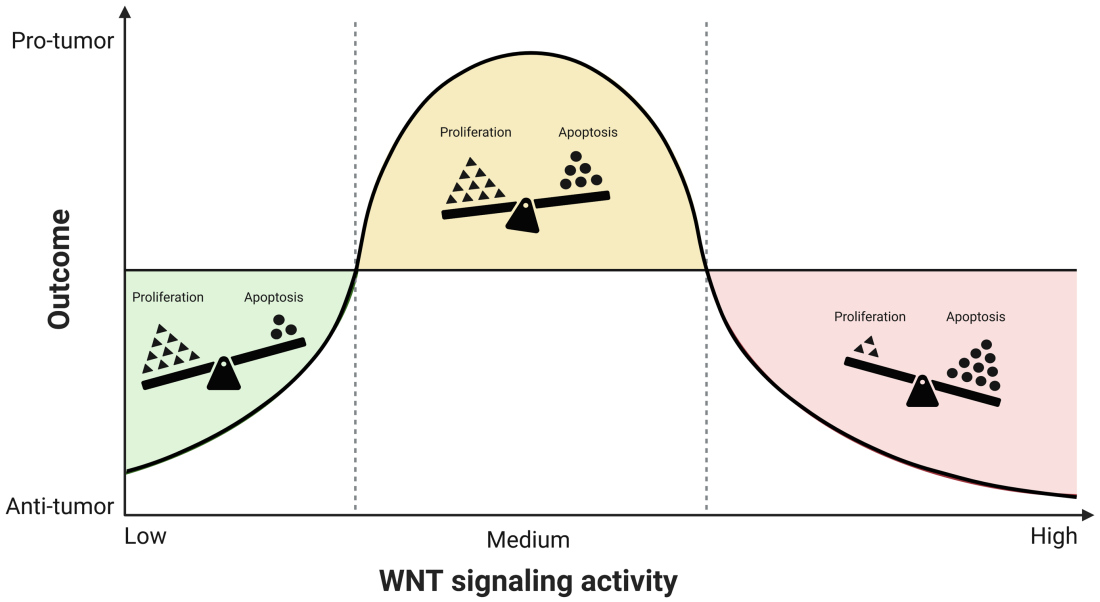

Figure 36. Goldilocks/just-right model of WNT signaling. Adapted from "Impacts of Oxidant and Antioxidant Imbalance on Oxidative Stress Outcome," by BioRender.com (2023). Retrieved from https://app.biorender.com/biorender-templates.

In agreement with the "just-right" WNT signaling model, FAP patients with germline, total LOF *APC* mutations developed colorectal adenomas with somatic, partial LOF *APC* truncations. Conversely, FAP patients with germline, partial LOF *APC* truncations developed colorectal adenomas with somatic, total LOF *APC* mutations (159). That is, germline *APC* mutations appear to select for somatic *APC* mutations which combinatorially afford some residual APC activity, rather than total loss of APC activity, in downregulation of β-catenin. In addition to these human findings, several *in vivo* and *in vitro* studies further support the "just-right" WNT signaling model. For instance, $Apc^{1322T/+}$ mice, which retain only one β-catenin degradation/binding repeat in *Apc*, developed more severe polyposis than $Apc^{Min/+}$ mice, which lack all seven β-catenin degradation/binding repeats in *Apc* (160). Despite the greater tumor burden observed in the $Apc^{1322T/+}$ mice, $Apc^{1322T/+}$ adenomas showed lower levels of nuclear β-catenin, a well-established marker of WNT signaling activity (161), than $Apc^{Min/+}$ adenomas (160). The bifunctional transcriptional regulator CREB-binding protein/p300-interacting transactivator with Asp/Glu-rich C-terminal domain 1 (CITED1) inhibits WNT-induced, β-catenin-dependent transcriptional programs, and

activates bone morphogenetic protein (BMP)-induced, SMAD4-dependent transcriptional programs (162). *Apc*$^{Min/+}$; *Cited1*$^{-}$ mice developed fewer adenomas than *Apc*$^{Min/+}$ mice, and subsequent experiments using conditional, intestinal *Apc* deletion ascribed this phenotype to increases in WNT signaling activity, proliferation, and apoptosis caused by *Cited1* deficiency (163). Similarly, transgenic mice with an activating mutation in *Ctnnb1* exhibited ~3-fold increases in normal villi apoptosis, and, as expected, developed numerous dysplastic lesions (164). Lastly, *in vitro*, β-catenin overexpression in cell lines induced apoptosis, presumably through stabilization of p53 (165, 166). These studies, in conjunction with our findings, suggest a model in which WNT signaling downregulates *SELENOP* expression to prevent further SELENOP-induced WNT activation, and thus maintain submaximal, optimal levels for tumorigenesis.

SELENOP:LRP interactions

LRP1, LRP2, and LRP8 mediate SELENOP uptake in different tissues (55–58, 116). Among these known SELENOP receptors, the interactions between SELENOP and LRP8 are well-studied. SELENOP's LRP8 interaction domain was previously mapped to three specific residues (Cys^{343}, Gln^{344}, Cys^{345}) within the region between SELENOP's fifth and sixth Sec (62). As we mapped SELENOP's LRP5/6 interaction domain to the 42-aa between SELENOP's third and fourth Sec (Sec^{258} - Sec^{299}), SELENOP binds LRP8 and LRP5/6 with distinct sites. To the best of our knowledge, the possibility of species-specific SELENOP:LRP8 interactions have not yet been explored, whereas we demonstrated that mouse SELENOP fails to interact with human LRP6.

In addition to LRP binding sites, SELENOP contains one well-defined (Leu^{79} - Leu^{84}) and two putative, histidine-rich (Thr^{178} - Lys^{189} and His^{194} - Gln^{234}) heparin binding sites (37). As such, SELENOP is widely thought to bind cell-surface HSPGs, which are also necessary for WNT signaling (36, 167). HSPGs prevent aggregation of WNTs (168), as well as facilitate their diffusion along the cell surface by repeated cycles of association and dissociation (117, 167). Although pretreatment with heparin failed to disrupt LRP8:SELENOP interactions in a previous study (62), we hypothesized that HSPGs mediate

LRP5/6:SELENOP interactions, as they do WNT:LRP5/6 interactions. Indeed, pretreatment with heparin prevented LRP6:SELENOP interactions, and inhibition of HSPG synthesis promoted LRP6:SELENOP interactions. Thus, HSPGs may sequester SELENOP from LRP5/6, as they do other WNT modulators and ligands, to fine-tune WNT signaling activity.

The SELENOP:LRP8 interaction was previously mapped to the sole BP domain of LRP8 (62). Accordingly, we hypothesized that SELENOP binds one of the four LRP5/6 BP domains. Rather, we discovered that SELENOP can bind multiple LRP6 BP domains, as neither deletion of LRP6's E1/2 nor E3/4 domains uncoupled SELENOP:LRP6 interactions. Although initially surprising, these findings are not inconsistent with the literature, in which there exists great controversy over whether LRP5/6 ligands bind specifically or promiscuously to the E1/2 or E3/4 domains of LRP5/6. For instance, Bourhis et al. reported that WNT3A only binds LRP6's E3/4 domain, while WNT9B only binds LRP6's E1/2 domain (169). These findings were reproduced and expanded upon by Gong et al., who generated antibodies against either the E1/2 or E3/4 domains of LRP6 and tested their effects on WNT signaling induced by a panel of WNTs. This elegant study stratified the WNTs into three groups: 1) those that bound LRP6's E1/2 domain, 2) those that bound LRP6's E3/4 domain, and 3) those that bound either LRP6's E1/2 or E3/4 domain. WNT1, WNT2, WNT2B, WNT6, WNT8A, WNT9A, WNT9B, and WNT10B bound LRP6's E1/2 domain, whereas WNT3 and WNT3A bound LRP6's E3/4 domain. However, several WNTs, including WNT4, WNT7A, WNT7B, and WNT10, bound both the E1/2 and E3/4 domains of LRP6 (170). Similarly, the secreted WNT inhibitor DKK1 exhibited bipartite binding to LRP6's E1/2 and E3/4 domains (16, 169, 171, 172). Thus, SELENOP may too belong to this third group of ligands with broad binding specificities for LRP6's E1-4 domains.

Although the SELENOP receptor(s) in the gastrointestinal tract remain unidentified, *Lrp5* and *Lrp6* are expressed at much higher levels than *Lrp1*, *Lrp2* or *Lrp8* in the colon (119). Therefore, LRP5/6 may represent *bona fide* receptors for SELENOP uptake in the gut. Our findings that a) SELENOP decreased cell surface LRP6 levels, and b) SELENOP interacted with WNT3A independently of LRP6,

raise the intriguing possibility that LRP6 mediates SELENOP internalization directly (i.e. through SELENOP:LRP6 interactions) or indirectly (i.e. through SELENOP:WNT3A interactions). As SELENOP's expression pattern opposes the WNT3A gradient along the crypt/villus axis, perhaps LRP6 preferentially shuttles SELENOP into WNT-high, SELENOP-low crypt base cells to facilitate synthesis of other SePs and further amplify WNT signaling activity.

Limitations

We characterized *SELENOP*'s mRNA expression pattern by various methods in both mouse and human intestinal tissues; however, we were unsuccessful in our efforts to define SELENOP's protein expression pattern in these tissues. Historically, we have encountered both technical and biological impediments to detecting SELENOP at the protein level. From a technical standpoint, the field suffers from a lack of highly specific and sensitive antibodies that reliably detect SELENOP by Western blot or IF. For instance, even the anti-SELENOP antibodies we used for Western blots in this study could only detect immunoprecipitated or overexpressed, but not endogenous, SELENOP. We have tested both in-house ("695") and commercially available ("HPA") anti-SELENOP antibodies in IF applications, to no avail (**Appendix E**). Specifically, we observe similar, non-specific immunoreactivity in both *Selenop*$^{+/+}$ and *Selenop*$^{-/-}$ liver (**Appendix E: Figure 48**), small intestine (**Appendix E: Figure 49**), and colon (**Appendix E: Figure 50**). Thus, the SELENOP ELISA remains our most reliable method to measure SELENOP protein levels. From a biological standpoint, predominant SELENOP secretion complicates cell type-specific SELENOP protein expression analyses, as intracellular SELENOP comprises only a small fraction of total SELENOP. Thus, future investigations must consider extracellular and intracellular SELENOP to obtain a clearer picture of SELENOP expression in the gut.

We examined the effects of global (*Selenop*$^{-/-}$) and intestinal epithelial-specific (*Selenop*$^{fl/fl}$) SELENOP deficiency in the *Lrig1-CreERT2*$^{/+}$; *Apc*$^{fl/+}$ adenoma model. In this model, *Apc*$^{\Delta IE/+}$ mice develop predominantly low-grade and few high-grade dysplastic adenomas, virtually none of which progress to adenocarcinomas (88, 90). Thus, we cannot draw firm conclusions regarding the role of

SELENOP in more advanced stages of intestinal tumorigenesis based on our findings in this model. To formally investigate this, we could interbreed *Selenop*$^{-/-}$ or *Selenop*$^{fl/fl}$ mice with *Villin-CreERT2*; *Apc*$^{\Delta 716/+}$; *Kras*$^{LSL\text{-}G12D/+}$; *Trp53*$^{LSL\text{-}R270H/+}$ mice, in which the tamoxifen-inducible *Villin-CreERT2* drives oncogenic mutations in *Kras* and *Trp53* (173). These mice also possess a germline truncation mutation in one *Apc* allele; LOH in the second *Apc* allele yields spontaneous formation of intestinal adenomas by three weeks of age (174). *Apc*$^{\Delta 716/+}$; *Kras*$^{G12D/+}$; *Trp53*$^{R270H/+}$ mice develop invasive adenocarcinomas with evidence of epithelial-mesenchymal transition (EMT) within 5-8 weeks post-tamoxifen induction (173). Notably, we have already validated and reported intestinal epithelial-specific *Selenop* deletion with the *Villin-CreERT2* driver in experimental CAC (51).

As *Selenop*$^{-/-}$ mice develop neurological impairments (e.g. spasticity, retropulsion, hyperactivity) on Se-sufficient diets (<0.25 mg Se/kg) (60), we performed global *Selenop* KO tumor studies on Se-supplemented (1.00 mg Se/kg) diet. Importantly, nutritional Se supplementation has been reported to inhibit intestinal tumorigenesis in multiple studies. For example, dietary supplementation with Se-enriched broccoli or the synthetic organoselenium compound p-XSC reduced intestinal neoplasia in the *Apc*$^{Min/+}$ model (157, 158). Similarly, dietary p-XSC, p-methoxybenzylselenocyanate (p-BSC), or Na_2SeO_3 supplementation decreased colon tumor incidence and multiplicity in AOM-treated rats (175, 176). In experimental CAC models, dietary sodium selenite, sodium selenate, selenoneine, or selenomethionine supplementation reduced colon tumor burden (148, 177–180). Thus, supranutritional Se levels in our adenoma studies may have suppressed intestinal tumorigenesis overall (i.e. across all genotypes), and perhaps minimized differences in tumor burden between *Apc*$^{\Delta IE/+}$; *Selenop*$^{+/+}$ and *Selenop*$^{-/-}$ mice. Accordingly, we hypothesize that lower dietary Se concentrations (e.g. 0.25 mg Se/kg – 0.75 mg Se/kg) would exacerbate the *Apc*$^{\Delta IE/+}$; *Selenop* KO phenotypes observed here.

We identified a novel interaction between SELENOP and LRP5/6 *in vitro*. We performed the vast majority of these experiments in noncancer human embryonic kidney cells (293T cells), as they express both SELENOP and LRP5/6 at appreciable levels and possess intact WNT signaling. Although we

observed that endogenous SELENOP co-immunoprecipitated with endogenous LRP6 in these cells, we have not yet confirmed the SELENOP:LRP5/6 interaction in CRC cell lines. Similarly, we have neither interrogated the SELENOP:LRP5/6 interaction nor its functional consequences *in vivo*, as we currently lack an antibody that can detect endogenous levels of mouse SELENOP. Moreover, while we demonstrated that SELENOP-induced WNT signaling augmentation requires LRP5/6:SELENOP interactions, SELENOP's detailed mechanism of action on WNT signaling remains to be elucidated. Does SELENOP binding to LRP5/6 increase its affinity for WNTs, or recruit other WNT agonists? Does SELENOP binding to LRP5/6 promote WNT signalosome formation and/or internalization? Does LRP5/6-bound SELENOP accelerate LRP5/6 receptor recycling? Future studies should aim to address these outstanding questions regarding the interplay between WNT and SELENOP.

CHAPTER 5: FUTURE DIRECTIONS

SELENOP's mechanism of action on WNT signaling

Through this study, we demonstrated SELENOP's role as an LRP5/6-dependent WNT activator. However, the specific details of SELENOP's mechanism of action on WNT signaling require further elucidation. Our finding that SELENOP, LRP6, and WNT3A formed a ternary protein complex (**Figure 33A**) supports SELENOP's involvement in the WNT signalosome. The term "WNT signalosome" refers to a multiprotein complex formed by WNT-induced oligomerization events. Specifically, binding of WNTs to inactive LRP5/6 and Frizzled dimers triggers LRP5/6:Frizzled oligomerization and Dishevelled:Axin co-polymerization (181). This, in turn, recruits other components of the destruction complex and stimulates signalosome internalization, which collectively stabilize cytoplasmic β-catenin. Simply put, the WNT signalosome primarily potentiates WNT signaling activity by sequestering the destruction complex, first at the plasma membrane and then in endocytic vesicles (182).

One mechanism by which SELENOP modulates WNT signaling may involve SELENOP-mediated effects on WNT signalosome formation. WNT signalosomes can be isolated by sucrose density gradient centrifugation, where the presence of different components in heavier fractions corresponds to greater protein coalescence (183). We performed Western blots on previously prepared sucrose density gradient fractions for LRP6, SELENOP, and WNT3A (**Figure 37**). In this experiment, we detected LRP6 and WNT3A at their expected molecular weights, and observed non-specific bands at SELENOP's expected molecular weight (~50-75 kDa). As these cells were not treated with SELENOP, and endogenous SELENOP remains difficult to detect with currently available antibodies via Western blot, our inability to detect SELENOP in WNT3A- and LRP6-containing fractions was not entirely unexpected. To further examine whether SELENOP localizes to the WNT signalosome, it may be necessary to treat cells with WNT3A and SELENOP, fractionate cells by sucrose density gradient centrifugation, immunoprecipitate SELENOP from the pooled heavy fractions, then perform Western blots on the input and IP samples for WNT3A, SELENOP, and LRP6. Similarly, to test whether

SELENOP impacts WNT signalosome formation, we could treat cells with WNT3A and without or with SELENOP, isolate WNT signalosomes by sucrose density gradient centrifugation, then perform Western blots on the fractions for WNT3A, SELENOP, and LRP6. If SELENOP enhances WNT signalosome formation, as we hypothesize based on our findings, we would expect to observe WNT3A and LRP6 in heavier fractions of SELENOP-treated versus untreated cells.

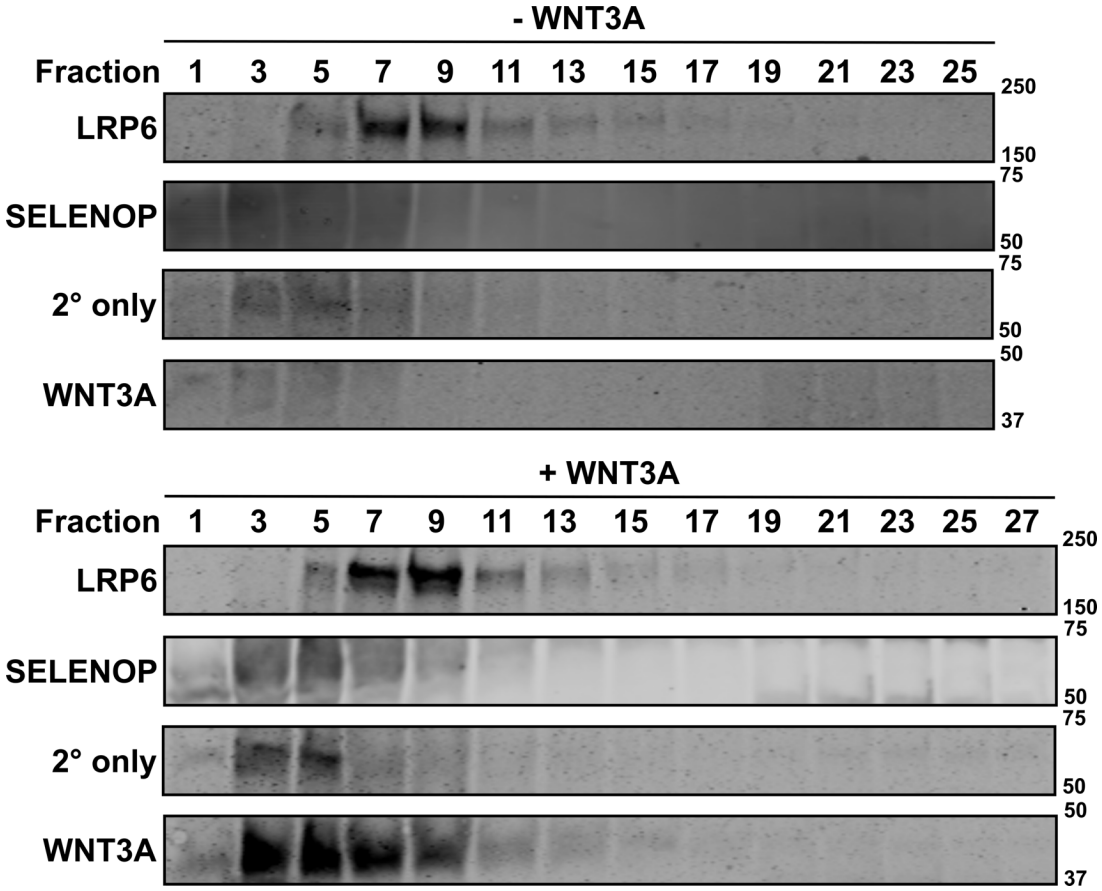

Figure 37. Attempts to detect SELENOP in WNT signalosomes. Western blots for WNT3A, SELENOP, and LRP6 of sucrose density gradient fractions prepared from 293T cells treated without or with WNT3A.

SELENOP may modify WNT signalosome formation through SELENOP-induced conformational changes in LRP5/6. In the unbound state, LRP6's large extracellular domain displayed ~180° of rotational flexibility (184). Ligand binding to LRP5/6's BP domains can transmit conformational changes from the extracellular to transmembrane and/or intracellular domains that regulate receptor activity (181). For example, the WNT inhibitor DKK1 simultaneously bound to LRP6's BP1 and BP3 domains and stabilized a more "closed" conformation of LRP6's extracellular domain (169, 172, 184), which presumably preclude ligand binding and receptor oligomerization, respectively, through steric hindrance. However, the precise mechanisms of DKK1-mediated inhibition of WNT signaling remain under debate. Conversely, it is widely thought that WNTs stabilize a more "open" conformation of LRP5/6's extracellular domain that facilitates receptor oligomerization and WNT signalosome formation, although structural information on WNT:LRP5/6 complexes remains limited (181).

As we observed greatest canonical WNT signaling activity with combinatorial WNT3A and SELENOP treatment, we hypothesize that simultaneous binding of WNT3A and SELENOP to LRP5/6 induces larger conformational changes in LRP5/6's extracellular domain than WNT3A alone. These larger conformational changes, in turn, may be more conducive to WNT signalosome formation and thus potentiate WNT signaling activity to a greater extent than those induced by WNT3A alone. Although the protein structure of SELENOP has not yet been determined empirically, we used ColabFold, an AlphaFold-based, artificial intelligence protein-protein complex prediction program (103, 185), to model SELENOP:LRP6 and WNT3A:LRP6 complexes (**Figure 38**). Unfortunately, ColabFold was unable to confidently predict large portions of SELENOP's protein structure. Future structural studies on WNT3A and SELENOP, individually and in complex with LRP6, will help elucidate differential conformational changes induced in LRP6 by these ligands.

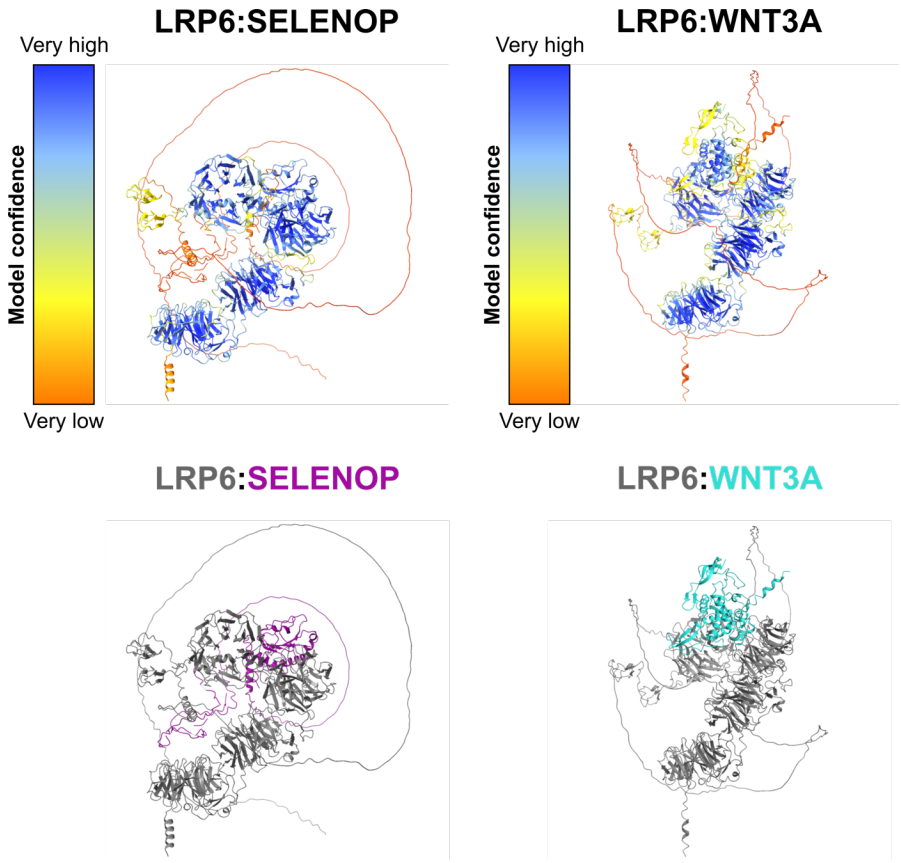

Figure 38. Predicted models of LRP6:SELENOP and LRP6:WNT3A complexes.

Additionally, our finding that SELENOP reduced cell surface LRP6 levels (**Figure 26D**) indicates that SELENOP may impact WNT signalosome internalization. Upon its formation at the plasma membrane, the WNT signalosome is endocytosed, which further subcellularly sequesters destruction complex components (182). To test the hypothesis that SELENOP promotes WNT signalosome internalization, we could transiently transfect cells with GFP-tagged LRP6, treat cells with WNT3A and without or with SELENOP, then perform confocal live-cell imaging. If SELENOP enhances WNT signalosome endocytosis, we would expect to observe more punctate, intracellular GFP-LRP6 localization within 1-2 hours of combinatorial WNT3A and SELENOP treatment, as compared to WNT3A treatment alone (186).

Both clathrin- and caveolin-mediated endocytosis have been implicated in WNT signalosome internalization (182), whereas only clathrin-mediated endocytosis has been implicated in SELENOP

internalization by LRP8 (54). To determine whether WNT3A:SELENOP:LRP6 endocytosis occurs by clathrin- and/or caveolin-dependent mechanisms, we could transiently transfect cells with GFP-tagged LRP6, treat cells with WNT3A and fluorophore-conjugated SELENOP, perform IF for GFP, clathrin, and caveolin, and image cells with confocal microscopy. Notably, we have already validated a GFP-LRP6 overexpression construct as well as anti-clathrin and anti-caveolin antibodies for IF, albeit with conventional fluorescence microscopy (**Figure 39**). Here, we observed punctate clathrin and caveolin staining patterns, consistent with those previously reported in the literature (94).

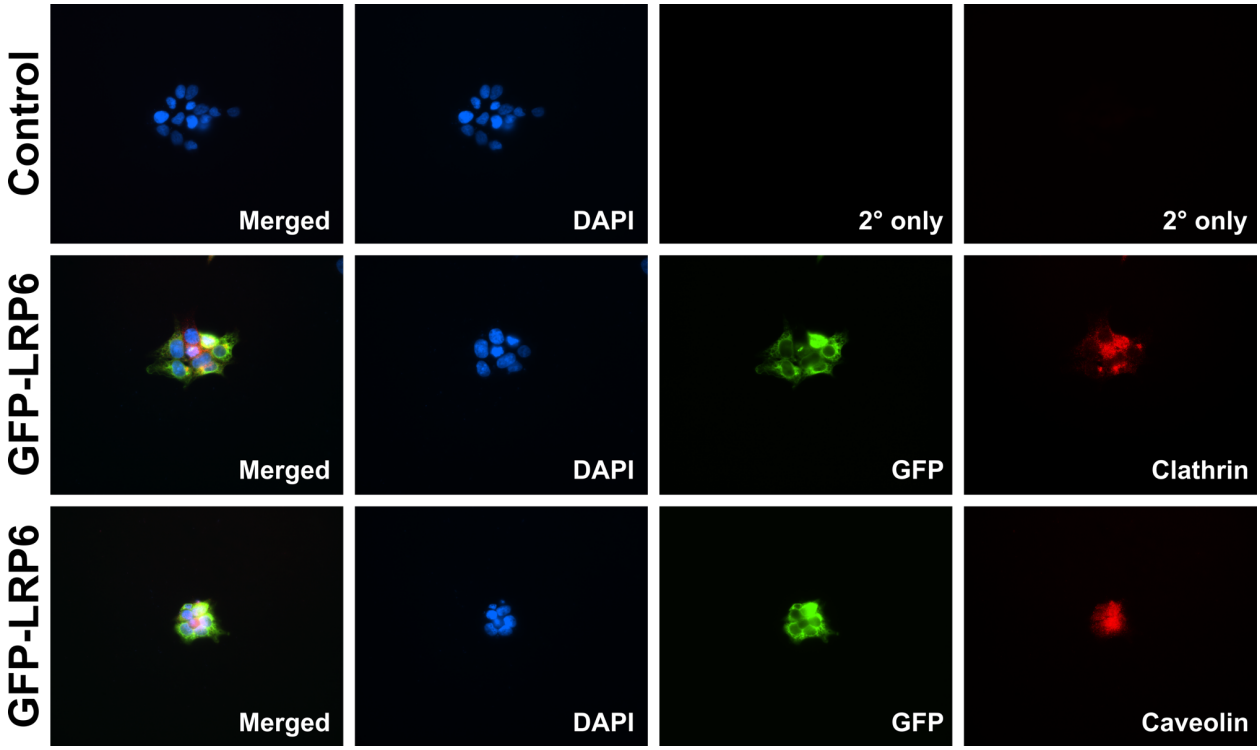

Figure 39. Validation of anti-clathrin and anti-caveolin antibodies for IF. Representative images of 293T cells transfected with GFP-LRP6 and stained for GFP and clathrin or caveolin.

If WNT3A:SELENOP:LRP6 endocytosis is predominantly clathrin-mediated, we would expect to observe greater SELENOP and LRP6 co-localization with clathrin than caveolin. Conversely, if WNT3A:SELENOP:LRP6 endocytosis is predominantly caveolin-mediated, we would expect to observe greater SELENOP and LRP6 co-localization with caveolin than clathrin. To further interrogate the clathrin and/or caveolin dependency of WNT3A:SELENOP:LRP6 endocytosis, we could pretreat the

cells with well-known inhibitors of these endocytic pathways, then perform similar experiments. In a previous study, treatment with the clathrin-dependent endocytosis inhibitor chlorpromazine, but not the caveolin-dependent endocytosis inhibitor nystatin, prevented LRP8-mediated SELENOP uptake in myoblasts (54). Additional endocytosis inhibitors for such experiments are listed in **Table 10**.

Inhibitor	Pathway	Reference(s)
Filipin	Caveolin-mediated	(187) Orlandi and Fishman. 1998. *J Cell Biol*.
Nystatin	Caveolin-mediated	(188) Bolard. 1986. *Biochim Biophys Acta*.
Chloroquine	Clathrin-mediated	(189) Wang et al. 1993. *J Cell Biol*.
Chlorpromazine	Clathrin-mediated	(189) Wang et al. 1993. *J Cell Biol*.
Dynasore	Clathrin-mediated	(190) Macia et al. 2006. *Dev Cell*.
Monesin	Clathrin-mediated	(191) Dickson et al. 1982. *Ann NY Acad Sci*.
Monodansylcadaverine	Clathrin-mediated	(192) Schlegel et al. 1982. *Proc Natl Acad Sci USA*.
Pitstop-1/2	Clathrin-mediated	(193) Dutta et al. 2012. *PLoS One*.

Table 10. Caveolin- and clathrin-mediated endocytosis inhibitors.

In addition to the studies described above, we conducted preliminary investigations into the effects of partial SELENOP deficiency on WNT signaling activity. As *Selenop* KO decreased WNT signaling activity, and this phenotype could be rescued by SELENOP overexpression, we expected to observe a dose-dependent relationship between SELENOP levels and WNT activity. Surprisingly, siRNA-mediated *SELENOP* KD (**Figure 40A**, **Figure 40C**) increased canonical WNT signaling activity in either 293 STF or RKO STF cells (**Figure 40B**, **Figure 40D**).

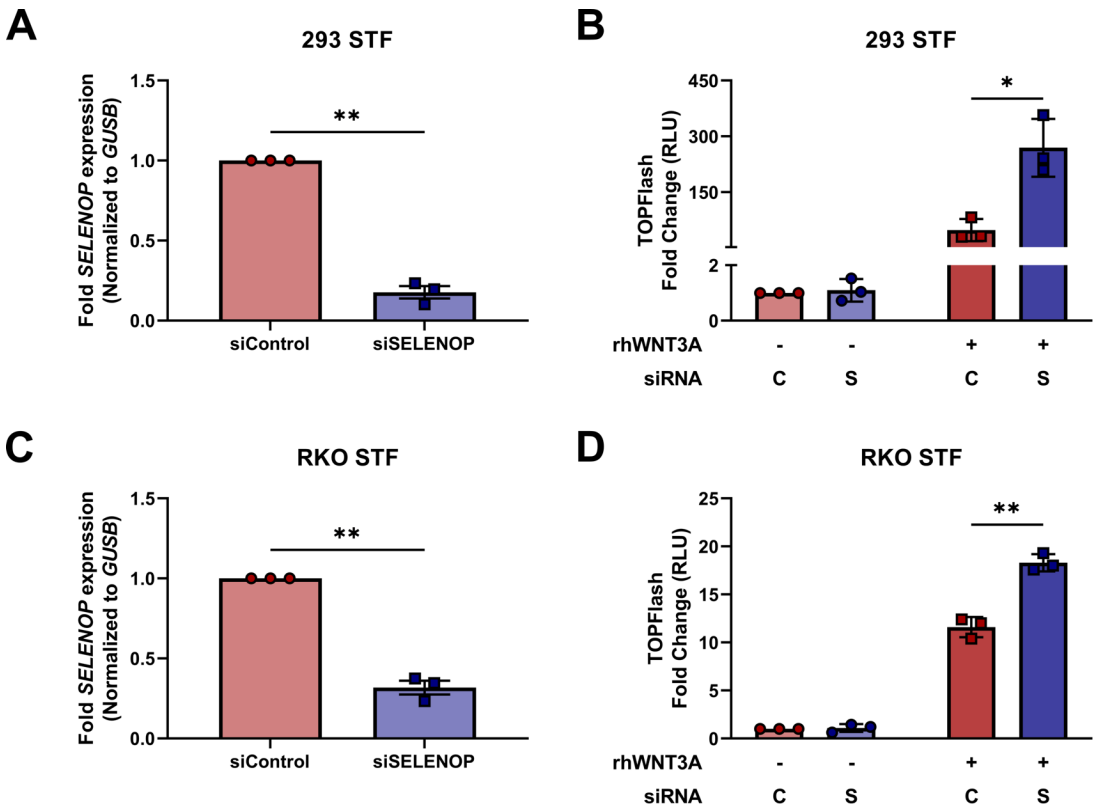

Figure 40. *SELENOP* KD increases canonical WNT signaling activity in noncancer and CRC cells. (A, C) RT-qPCR for SELENOP of (A) 293 STF and (C) RKO STF cells transfected with siControl or siSELENOP. (B, D) TOPFlash activity of (B) 293 STF and (D) RKO STF cells transfected with siControl or siSELENOP and treated without or with rhWNT3A. C: control, S: SELENOP. Pooled data from n=3 independent experiments. 2-sided paired t tests (A, C), 2-way repeated measures ANOVAs with 2-sided Sidak's multiple comparisons tests (B, D). *p<0.05, **p<0.01. Data are displayed as mean ± SEM.

One potential explanation for these unanticipated results involves SELENOP's broader role as a major Se source for SeP synthesis. We did not measure levels of other SePs in the experiments described above, and thus cannot exclude the possibility that *SELENOP* KD globally altered selenoproteome profiles in these cells. Moreover, additional SePs may function as WNT modulators, and thus alterations in their expression may impact WNT signaling activity. For instance, there is weak evidence that SELENOF and TXNRD1 modify WNT signaling. Namely, combinatorial *SELENOF* and *TXNRD1* KD in CT26 mouse colon carcinoma cells decreased *Apc* and *Axin1* levels in microarray, but not RT-qPCR analyses. Moreover, no changes in phospho-β-catenin protein levels were observed with *TXNRD1* and/or *SELENOF* KD (194). Clearly, the relationship between SELENOP levels and WNT activity is much more complex than presumed, and future research should strive to illuminate this nuance.

SELENOP in intestinal epithelial differentiation

As we and others have previously demonstrated that SELENOP secretion occurs in a Se-dependent, basolateral manner in Caco-2 monolayers (51, 118), we investigated the effects of Se localization on basolateral SELENOP secretion. To accomplish this, we polarized Caco-2 BBE cells on permeable supports (**Figure 41A**), added Se-containing media to either the basolateral or apical compartment, then measured SELENOP protein levels by ELISA. Consistent with prior reports, we predominantly observed basolateral SELENOP secretion (**Figure 41B**). Moreover, we detected no differences in the magnitude of basolateral SELENOP secretion after apical or basolateral Se supplementation (**Figure 41B**). These preliminary results suggest that the colonic epithelium may take up Se from both the apical and basolateral surfaces for SELENOP production and secretion.

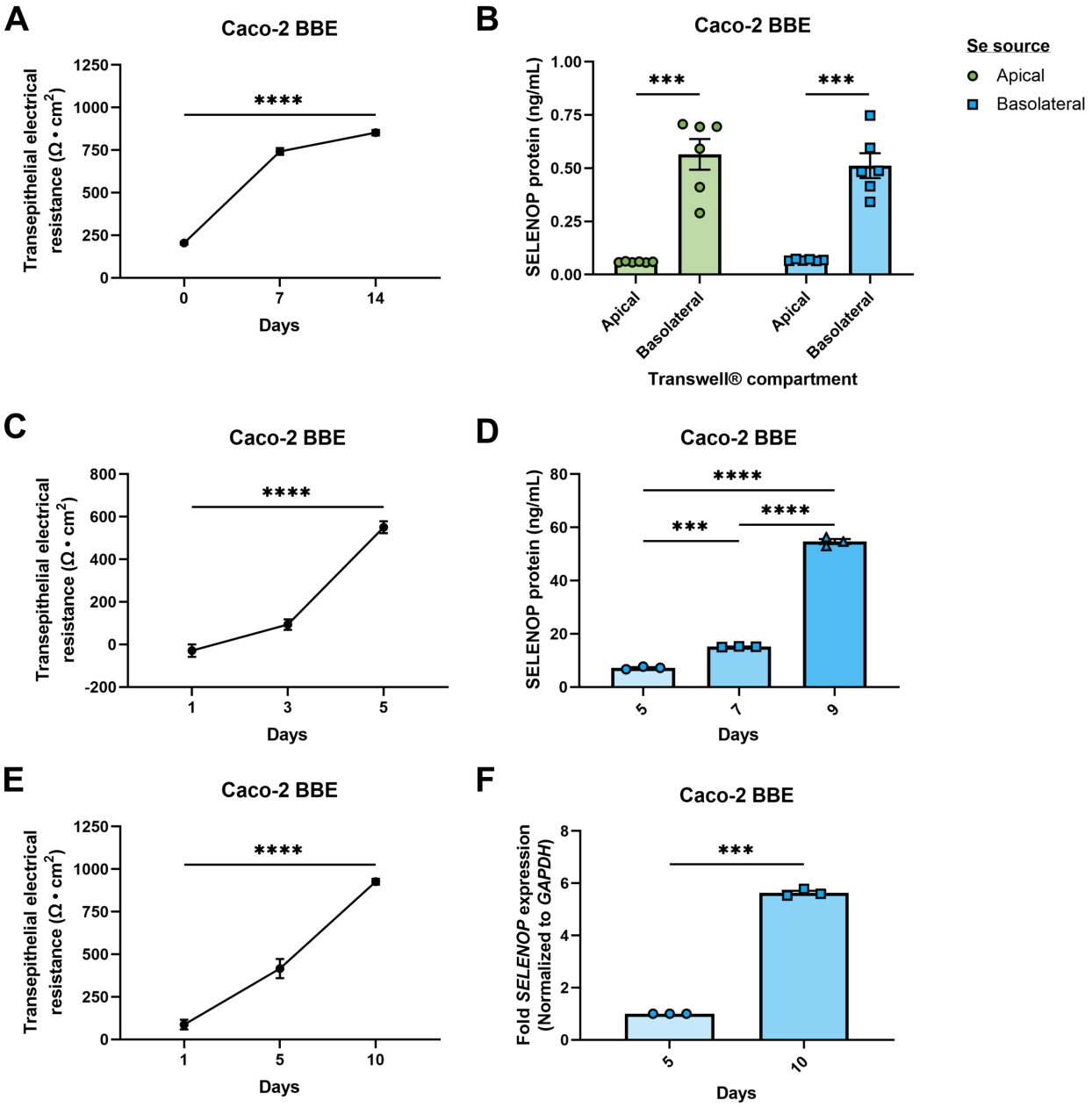

Figure 41. SELENOP secretion and expression dynamics. (A, B) (A) Transepithelial electrical resistance (TEER) measurements and (B) SELENOP ELISA on basolateral or apical media from Caco-2 BBE cells plated on Transwell® inserts with selenium (Se)-containing media in the indicated compartments. (C, D) (C) TEER measurements and (D) SELENOP ELISA on basolateral media from Caco-2 BBE cells plated on Transwell® inserts. (E, F) (E) TEER measurements and (F) *SELENOP* RT-qPCR of Caco-2 BBE cells plated on Transwell® inserts. Pooled data from n=6 (A, B) or n=3 (C-F) independent experiments. 1-way repeated measures ANOVAs with 2-sided Sidak's multiple comparisons tests (A, C, E), 2-way repeated measures ANOVA with 2-sided Sidak's multiple comparisons test (B), 1-way repeated measures ANOVA with 2-sided Tukey's multiple comparisons tests (D), 2-sided paired t test (F). ***p<0.001, ****p<0.0001. Data are displayed as mean ± SEM.

Since we observed greater SELENOP secretion by more differentiated cell types (**Figure 8E**), we hypothesized that SELENOP secretion rises as polarized monolayers continue to differentiate. Here, SELENOP secretion increased over time in polarized Caco-2 BBE cells (**Figure 41C**, **Figure 41D**). As we also routinely observe greater *SELENOP* expression in more differentiated cells (**Figure 8B**, **Figure 8C**, **Figure 8D**, **Figure 11**, **Figure 12**, **Figure 13A, Figure 16B**, **Figure 16C**), we predicted that these increases in SELENOP secretion were underlaid by increases in *SELENOP* expression. Indeed, *SELENOP* expression also increased over time in polarized Caco-2 BBE cells (**Figure 41E**, **Figure 41F**). These increases in SELENOP protein and mRNA expression throughout polarization concur with another study performed in Caco-2 cells (195). Conversely, we hypothesize that *SELENOP* KD would inhibit Caco-2 polarization, although this has not been reported by us or others. Taken together, these results suggest that SELENOP expression, production, and secretion may correlate with cellular differentiation status in the intestine.

To the best of our knowledge, a direct role for SELENOP in differentiation has previously only been studied in the context of adipogenesis. Namely, *Selenop* expression increased throughout differentiation of 3T3-L1 fibroblasts into adipocytes. Conversely, *Selenop* KD inhibited 3T3-L1 differentiation. Specifically, *Selenop* KD prevented lipid droplet formation, decreased lipogenic gene expression, and abolished insulin-induced glucose uptake in 3T3-L1 cells subjected to the adipocyte differentiation protocol (196). Given these findings, as well as the striking differences in *SELENOP* expression between undifferentiated and differentiated intestinal epithelial cells, we hypothesize that SELENOP contributes to intestinal differentiation.

Although no overt architectural phenotypes have been reported at baseline in the $Selenop^{-/-}$ or $Selenop^{\Delta IE/\Delta IE}$ intestine (50, 51), the effects of global and/or intestinal epithelial-specific *Selenop* KO on lineage allocation have not yet been investigated. This could be addressed with multiplex immunofluorescence (MxIF) of $Selenop^{+/+}$, $Selenop^{-/-}$ and $Selenop^{\Delta IE/\Delta IE}$ intestinal tissues for absorptive and secretory cell markers (**Table 11**). Unlike conventional IF, MxIF can detect dozens of antigens within

one section of tissue, and thus better resolve subtle differences in cell type distribution (197). Alternatively, flow cytometry on *Selenop*$^{+/+}$, *Selenop*$^{-/-}$ and *Selenop*$^{\Delta IE/\Delta IE}$ intestinal epithelia for validated cell surface markers constitutes another method to define relative cell type abundance (198–200) (**Table 12**). Notably, this protocol was previously optimized in our lab (201). Lastly, scRNA-seq on *Selenop*$^{+/+}$, *Selenop*$^{-/-}$ and *Selenop*$^{\Delta IE/\Delta IE}$ intestinal epithelia represents a third approach to interrogate the effects of *Selenop* knockout on lineage allocation (202) (**Table 13**).

Cell Type	Marker(s)	Reference(s)
Enterocyte	CD10 IAP	(203) Rodriguez-Juean et al. 2001. *Tissue Cell*. (204) Hinnebusch et al. 2004. *Am J Physiol Gastro Liver Physiol*.
Enteroendocrine	CHGA REG4	(205) Cetin et al. 1989. *Histochemistry*. (206) Grün et al. 2015. *Nature*.
Goblet	MUC2	(207) Reis et al. 1999. *Cancer Res*.
Paneth	LYZ1 LYZ2	(208) Ho et al. 1989. *Gastroenterology*.
Stem	LGR5 OLFM4 SOX9	(209) Barker et al. 2007. *Nature.* (210) van der Flier et al. 2009. *Gastroenterology*. (211) Formeister et al. 2009. *Am J Physiol Gastro Liver Physiol*.
Tuft	DCLK1	(212) Gerbe et al. 2009. *Gastroenterology*.

Table 11. Intestinal epithelial cell type-specific markers for MxIF. CHGA: chromogranin A, DCLK1: doublecortin-like kinase 1, IAP: intestinal alkaline phosphatase, LGR5: leucine-rich repeat-containing G-protein coupled receptor 5, LYZ1: lysozyme 1, LYZ2: lysozyme 2, MUC2: mucin 2, OLFM4: olfactomedin 4, REG4: regenerating islet-derived protein 4, SOX9: sex-determining region Y-box 9.

Cell Type	CD45	CD31	CD326	CD44	CD24	CD117	CD69	CD274
Stem	-	-	+	High	-	-	-	-
Absorptive Progenitor	-	-	+	Med	-	-	-	-
Enterocyte	-	-	+	Low/-	-	-	-	-
Secretory Progenitor	-	-	+	High	Med	Med	-	-
Enteroendocrine	-	-	+	Low/-	+	+	-	-
Goblet	-	-	+	Low/-	+	+	+	+
Tuft	-	-	+	Low/-	+	+	-	-

Table 12. Intestinal epithelial cell type-specific markers for flow cytometry.

Cell Type	Markers
Enterocyte	*Alpi*, *Apoa1*, *Apoa4*, *Fabp1*
Enteroendocrine	*Chga*, *Chgb*, *Neurog3*, *Tac1*, *Tph1*
Goblet	*Agr2*, *Clca3*, *Muc2*, *Tff3*
Paneth	*Ang4*, *Defa17*, *Defa22*, *Defa24*, *Lyz1*
Stem	*Ascl2*, *Axin2*, *Gkn3*, *Lgr5*, *Olfm4*, *Slc12a2*
Tuft	*Dclk1*, *Gfi1b*, *Il25*, *Trpm5*

Table 13. Intestinal epithelial cell type-specific markers for scRNA-seq. *Agr2*: anterior gradient 2, *Alpi*: alkaline phosphatase, intestinal; *Ang4*: angiogenin 4, *Apoa1*: apolipoprotein A1, *Apoa4*: apolipoprotein A4, *Ascl2*: achaete-scute family bHLH transcription factor 2, *Chga*: chromogranin A, *Chgb*: chromogranin B, *Clca3*: chloride channel accessory 3, *Dclk1*: doublecortin-like kinase 1, *Defa17*: defensin alpha 17, *Defa22*: defensin alpha 22, *Defa24*: defensin alpha 24, *Fabp1*: fatty acid binding protein 1, *Gfi1b*: growth factor independent 1B transcriptional repressor, *Gkn3*: gastrokine 3, *Il25*: interleukin 25, *Lgr5*: leucine-rich repeat-containing G protein-coupled receptor 5, *Lyz1*: lysozyme 1, *Muc2*: mucin 2, *Neurog3:* neurogenin 3, *Olfm4*: olfactomedin 4, *Slc12a2*: solute carrier family 12 member 2, *Tac1*: tachykinin precursor 1, *Tff3*: trefoil factor 3, *Tph1*: tryptophan hydroxylase 1.

Transcriptional regulation of *SELENOP* in the intestine

As SELENOP is widely considered a hepatokine that exacerbates metabolic dysfunction, the liver has served as the tissue of interest for most investigations into *SELENOP*'s mechanisms of transcriptional regulation (**Figure 42**). For example, two members of the forkhead box, class O (FOXO) family of transcription factors, FOXO1a and FOXO3a, have repeatedly been identified as transcriptional activators of hepatic *SELENOP* expression. FOXO1a overexpression promoted *SELENOP* transcription in both rat H4-II-EC-3 and human HepG2 hepatoma cells (213, 214). The metabolic hormone insulin activates protein kinase B (PKB), which in turn phosphorylates and inactivates FOXO1a. As expected, insulin treatment attenuated FOXO1a-induced *SELENOP* transcription in H4-II-E-C3 and HepG2 cells (213, 214). In addition to PKB, 5′-adenosine monophosphate (AMP)-activated protein kinase (AMPK) phosphorylates and inactivates FOXO1a and FOXO3a. Accordingly, the AMPK inhibitor palmitate increased *SELENOP* expression in HepG2 cells, and this effect was reversed through AMPK activation by salsalate, salicylate, or adiponectin. Moreover, salsalate or salicylate decreased hepatic *Selenop* expression and increased glucose tolerance in mice with either high fat diet-induced or spontaneous insulin resistance (215). Similarly, metformin, a known AMPK agonist and popular antihyperglycemic medication, decreased *Selenop* expression in H4-II-E-C3 cells and mouse liver tissue. Although AMPK can inactivate both FOXO1a and FOXO3a, this effect was primarily attributed to the action of FOXO3a, as metformin simultaneously decreased FOXO3a and increased FOXO1a binding to the *Selenop* promoter in H4-II-E-C3 cells (216).

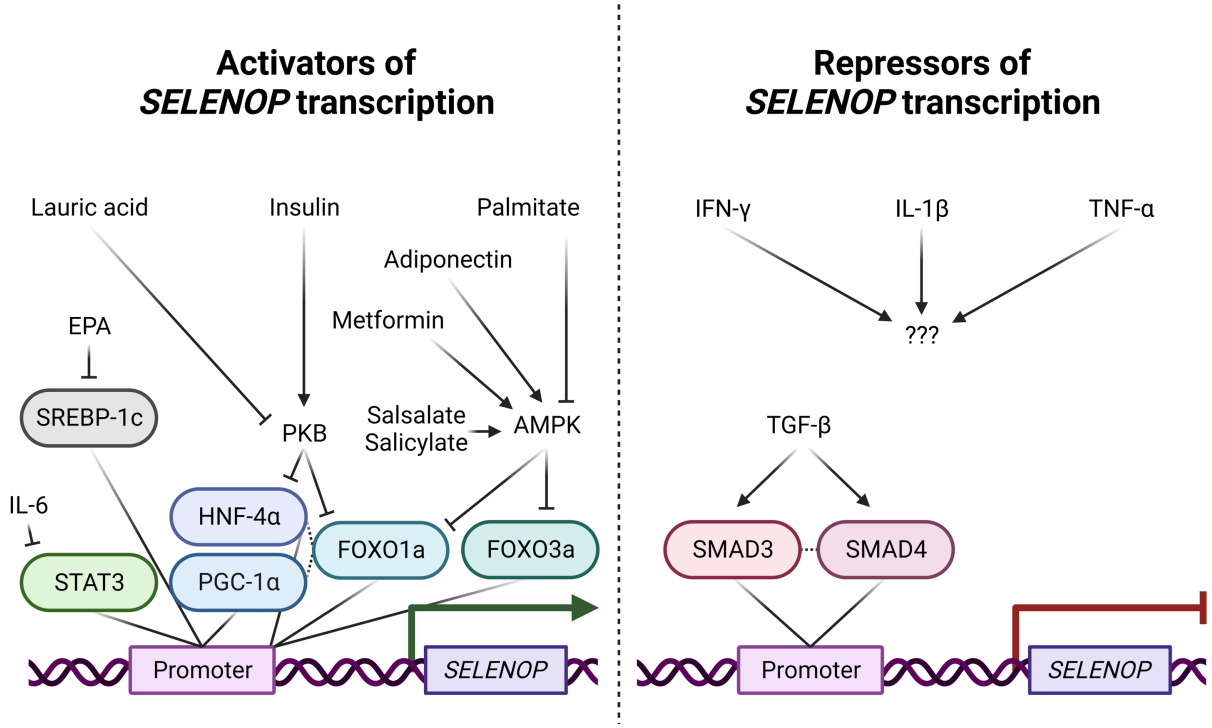

Figure 42. Known regulatory mechanisms of *SELENOP* transcription.

FOXO1a has also been demonstrated to act in concert with the transcription factors hepatic nuclear factor 4α (HNF-4α) and peroxisome proliferator-activated receptor gamma coactivator 1α (PGC-1α) to robustly upregulate *SELENOP* transcription. Simultaneous overexpression of PGC-1α, HNF-4α, and FOXO1a in HepG2 cells increased *SELENOP* expression to a much greater extent than overexpression of PGC-1α, HNF-4α, or FOXO1a alone. Moreover, HNF-4α was required for basal *SELENOP* expression in HepG2 cells, as inactivation of *SELENOP*'s HNF-4α binding site abolished promoter activity (214). Additionally, the medium-chain saturated fatty acid lauric acid, through PKB inhibition and resultant HNF-4α stabilization, increased *Selenop* expression in Hepa1-6 mouse hepatoma cells as well as in mouse liver tissue (217).

Two other activators of hepatic *SELENOP* transcription have been identified: sterol regulatory element-binding protein 1c (SREBP-1c) and signal transducer and activator of transcription 3 (STAT3), although their detailed mechanisms of action await further definition. SREBP-1c binding to the *Selenop*

promoter and thus *Selenop* expression was reduced by the polyunsaturated fatty acid eicosapentaenoic acid (EPA) in an AMPK-independent fashion in H4-II-EC-3 cells (218). Similarly, STAT3 binding to the *SELENOP* promoter and thus *SELENOP* expression was decreased by the pro-inflammatory cytokine IL-6 in HepG2 and Hep3B human hepatoma cells (141).

In addition to positive regulators of *SELENOP* transcription, previous studies have identified two negative regulators of *SELENOP* transcription, namely SMAD3 and SMAD4. Individual or combinatorial overexpression of SMAD3 and/or SMAD4 repressed *SELENOP* transcription in Hep G2 cells, as did treatment with the SMAD activator and pro-inflammatory cytokine TGF-β (219, 220). Additionally, the cytokines IFN-γ, IL-1β, and TNF-α repressed *SELENOP* promoter activity in Hep G2 cells, although the downstream transcription factors responsible for these effects remain unknown (140).

As previously mentioned, the current body of literature on *SELENOP*'s transcriptional regulation mechanisms predominantly focuses on hepatic *SELENOP* expression. In contrast, the transcriptional activators and/or repressors that govern intestinal *SELENOP* expression remain largely undefined. In Caco-2 cells, *FOXO1a*, *HNF-4α*, and *PGC-1α* expression increased in proportion to *SELENOP* expression as cells differentiated over the course of seven days. Moreover, mutation of *SELENOP*'s HNF-4α binding site abolished *SELENOP* promoter activity, suggesting that, as in the liver, HNF-4α is required for basal *SELENOP* expression in the intestine (195). In human colonoids, IL-6, but not IL-10 or TNF-α treatment decreased *SELENOP* expression (51). However, the relative contributions of STAT3/4, PGC-1α, HNF-4α, and FOXO1a to intestinal *SELENOP* expression, as well as the potential involvement of other transcription factors, requires further examination.

This sizeable knowledge gap could be addressed with reverse chromatin immunoprecipitation (R-ChIP). In contrast to ChIP, which reveals DNA sequences associated with a specific protein, R-ChIP identifies proteins associated with a specific DNA sequence. Like ChIP, R-ChIP first entails cross-linking protein:DNA complexes, isolating nuclei, and shearing chromatin. Next, the chromatin is denatured and hybridized to a biotin-labeled DNA probe complementary to your genomic region of interest.

Chromatin:probe hybrids are then isolated by streptavidin pulldown and subjected to mass spectrometry to identify DNA-associated proteins (221). To define transcription factors that potentially modulate *Selenop* expression in intestinal epithelial cells, we would perform R-ChIP on mouse colon and small intestine epithelium with a DNA probe that encompasses the *Selenop* promoter region. We would screen these transcription factor candidates for *Selenop* promoter activity in normal mouse colon epithelial cells. Specifically, we would genetically engineer YAMC cells to stably express the firefly luciferase gene under control of the *Selenop* promoter, transiently overexpress each transcription factor candidate, then measure bioluminescence (as a readout of *Selenop* promoter activity) as well as *Selenop* mRNA levels. We would then validate those that modify *Selenop* expression by mutating their respective DNA binding sequences in the *Selenop* promoter luciferase reporter, transiently overexpressing each transcription factor, and measuring bioluminescence as above.

SELENOP receptor(s) and isoforms in the intestine

As mentioned previously, LRP1 and LRP2 mediate SELENOP uptake in the muscle and kidney, respectively, while LRP8 mediates SELENOP uptake in the brain and testes (55, 56, 58, 59). However, the SELENOP receptor(s) in the intestine are unknown. As SELENOP has proven difficult, if not impossible, to detect with commercially available antibodies, it would be invaluable to genetically engineer (via CRISPR/Cas9 technology) a mouse with epitope-tagged, endogenous SELENOP (e.g. $Selenop^{FLAG}$). To determine whether LRP1, LRP2, and/or LRP8 function as SELENOP receptors in the intestine, we could interbreed $Selenop^{FLAG}$ with *Lrp1*, *Lrp2*, or *Lrp8* KO mice (222–224), harvest small intestine and colon tissue, then perform IHC for FLAG to detect SELENOP. Lower intestinal SELENOP protein levels in $Selenop^{FLAG}$*; Lrp1*, *Lrp2*, and/or *Lrp8* KO mice, as compared to WT mice, would suggest roles for LRP1, LRP2, and/or LRP8, respectively, as SELENOP receptors in the intestine.

LRP5 and LRP6 play pivotal, compensatory roles in embryonic development. Accordingly, global *Lrp6* KO is embryonic lethal, whereas global *Lrp5* KO leads to limb deformities (225, 226). Similarly, mice with combined, intestinal epithelial-specific *Lrp5* and *Lrp6* KO die within one day of

birth, yet mice with either intestinal epithelial-specific *Lrp5* or *Lrp6* KO are phenotypically normal (227). Thus, to determine if LRP5 and/or LRP6 mediate intestinal SELENOP uptake, we could interbreed $Selenop^{FLAG}$ with $Lrp5^{\Delta IE}$ or $Lrp6^{\Delta IE}$ mice, harvest small intestine and colon tissue, then perform IHC for FLAG to detect SELENOP.

In addition to identification of intestinal SELENOP receptors, a $Selenop^{FLAG}$ mouse would enable definition of intestinal SELENOP isoforms. By way of reminder, failure to recode *SELENOP*'s UGA codons as Sec yields truncated SELENOP isoforms. Four SELENOP isoforms have been observed in rat plasma, and two SELENOP isoforms have been observed in mouse and human plasma (41–46). However, the SELENOP isoforms present in the intestine remain unknown. To identify intestinal isoforms of SELENOP, we could immunoprecipitate FLAG-tagged, endogenous SELENOP from $Selenop^{FLAG}$ intestinal epithelial isolates, then perform SDS-PAGE followed by mass spectrometry. This approach may also identify novel SELENOP binding partners to further investigate.

Summary

Although this study describes a novel, WNT modulatory role for SELENOP through LRP5/6 interactions, SELENOP's detailed mechanism of action on WNT signaling, and particularly its potential involvement in WNT signalosome formation and/or internalization, has not yet been elucidated. In addition to these unanswered questions regarding SELENOP and WNT signaling, there also exist many outstanding questions about the broader functions of SELENOP in intestinal biology. Namely, SELENOP's roles in lineage allocation, as well as its transcriptional regulation mechanisms in the intestinal epithelium, remain uncharacterized. Moreover, the SELENOP isoforms and uptake receptors expressed by intestinal epithelial cells are unknown. Future studies should aim to address these questions to provide a more comprehensive understanding of SELENOP's roles in the intestine.

APPENDIX A: PROTEIN HOMOLOGY BETWEEN MOUSE LRP5 AND LRP6

```
mLRP5     1 METAPTRAPPPPPPPLLLLVLYCSL-VPAAASPLLLFANRRDVRLVDAGG 49
mLRP6     1 ------------MGAVLRSLLACSFCVLLRAAPLLLYANRRDLRLVDATN 38

mLRP5    50 VKLESTIVASGLEDAAAVDFQFSKGAVYWTDVSEEAIKQTYLNQTGAAAQ 99
mLRP6    39 GKENATIVVGGLEDAAAVDFVFGHGLIYWSDVSEEAIKRTEFNKT-ESVQ 87

mLRP5   100 NIVISGLVSPDGLACDWVGKKLYWTDSETNRIEVANLNGTSRKVLFWQDL 149
mLRP6    88 NVVVSGLLSPDGLACDWLGEKLYWTDSETNRIEVSNLDGSLRKVLFWQEL 137

mLRP5   150 DQPRAIALDPAHGYMYWTDWGEAPRIERAGMDGSTRKIIVDSDIYWPNGL 199
mLRP6   138 DQPRAIALDPSSGFMYWTDWGEVPKIERAGMDGSSRFVIINTEIYWPNGL 187

mLRP5   200 TIDLEEQKLYWADAKLSFIHRANLDGSFRQKVVEGSLTHPFALTLSGDTL 249
mLRP6   188 TLDYQERKLYWADAKLNFIHKSNLDGTNRQAVVKGSLPHPFALTLFEDTL 237

mLRP5   250 YWTDWQTRSIHACNKWTGEQRKEILSALYSPMDIQVLSQERQPPFHTPCE 299
mLRP6   238 YWTDWNTHSILACNKYTGEGLREIHSNIFSPMDIHAFSQQRQPNATNPCG 287

mLRP5   300 EDNGGCSHLCLLSPREPFYSCACPTGVQLQDNGKTCKTGAEEVLLLARRT 349
mLRP6   288 IDNGGCSHLCLMSPVKPFYQCACPTGVKLLENGKTCKDGATELLLLARRT 337

mLRP5   350 DLRRISLDTPDFTDIVLQVGDIRHAIAIDYDPLEGYVYWTDDEVRAIRRA 399
mLRP6   338 DLRRISLDTPDFTDIVLQLEDIRHAIAIDYDPVEGYIYWTDDEVRAIRRS 387

mLRP5   400 YLDGSGAQTLVNTEINDPDGIAVDWVARNLYWTDTGTDRIEVTRLNGTSR 449
mLRP6   388 FIDGSGSQFVVTAQIAHPDGIAVDWVARNLYWTDTGTDRIEVTRLNGTMR 437

mLRP5   450 KILVSEDLDEPRAIVLHPVMGLMYWTDWGENPKIECANLDGRDRHVLVNT 499
mLRP6   438 KILISEDLEEPRAIVLDPMVGYMYWTDWGEIPKIERAALDGSDRVVLVNT 487

mLRP5   500 SLGWPNGLALDLQEGKLYWGDAKTDKIEVINIDGTKRKTLLEDKLPHIFG 549
mLRP6   488 SLGWPNGLALDYDEGTIYWGDAKTDKIEVMNTDGTGRRVLVEDKIPHIFG 537

mLRP5   550 FTLLGDFIYWTDWQRRSIERVHKVKASRDVIIDQLPDLMGLKAVNVAKVV 599
mLRP6   538 FTLLGDYVYWTDWQRRSIERVHKRSAEREVIIDQLPDLMGLKATSVHRII 587

mLRP5   600 GTNPCADGNGGCSHLCFFTPRATKCGCPIGLELLSDMKTCIIPEAFLVFT 649
mLRP6   588 GSNPCAEDNGGCSHLCLYRPQGLRCACPIGFELISDMKTCIVPEAFLLFS 637

mLRP5   650 SRATIHRISLETNNNDVAIPLTGVKEASALDFDVSNNHIYWTDVSLKTIS 699
mLRP6   638 RRADIRRISLETNNNNVAIPLTGVKEASALDFDVTDNRIYWTDISLKTIS 687

mLRP5   700 RAFMNGSSVEHVIEFGLDYPEGMAVDWMGKNLYWADTGTNRIEVARLDGQ 749
mLRP6   688 RAFMNGSALEHVVEFGLDYPEGMAVDWLGKNLYWADTGTNRIEVSKLDGQ 737

mLRP5   750 FRQVLVWRDLDNPRSLALDPTKGYIYWTEWGGKPRIVRAFMDGTNCMTLV 799
mLRP6   738 HRQVLVWKDLDSPRALALDPAEGFMYWTEWGGKPKIDRAAMDGSERTTLV 787

mLRP5   800 DKVGRANDLTIDYADQRLYWTDLDTNMIESSNMLGQERMVIADDLPYPFG 849
mLRP6   788 PNVGRANGLTIDYAKRRLYWTDLDTNLIESSDMLGLNREVIADDLPHPFG 837

mLRP5   850 LTQYSDYIYWTDWNLHSIERADKTSGRNRTLIQGHLDFVMDILVFHSSRQ 899
mLRP6   838 LTQYQDYIYWTDWSRRSIERANKTSGQNRTIIQGHLDYVMDILVFHSSRQ 887
```

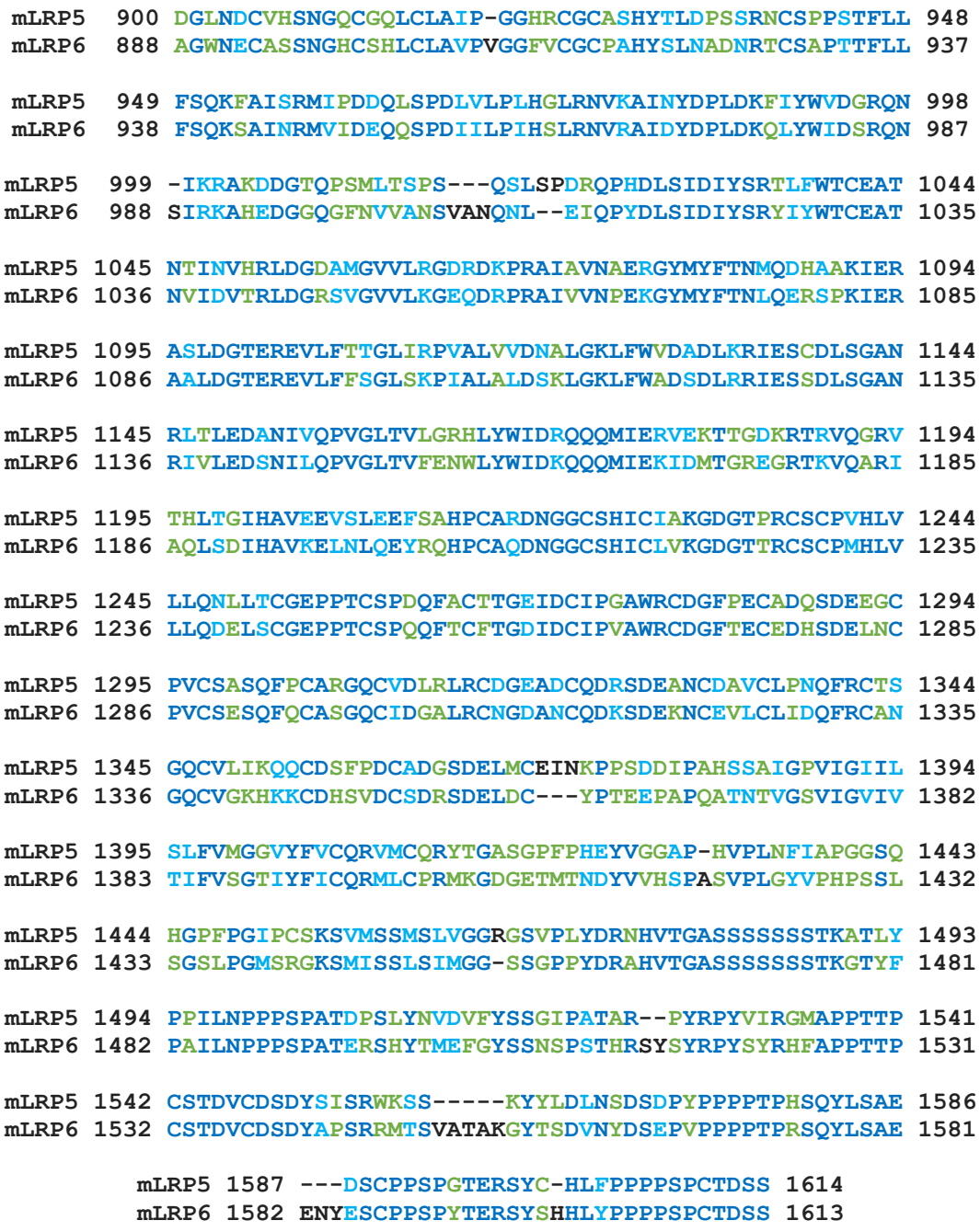

Figure 43. Pairwise sequence alignment of mouse LRP5 and LRP6 protein sequences.

APPENDIX B: *SELENOP* EXPRESSION IN COLORECTAL ADENOCARCINOMAS STRATIFIED BY WNT MUTATION STATUS

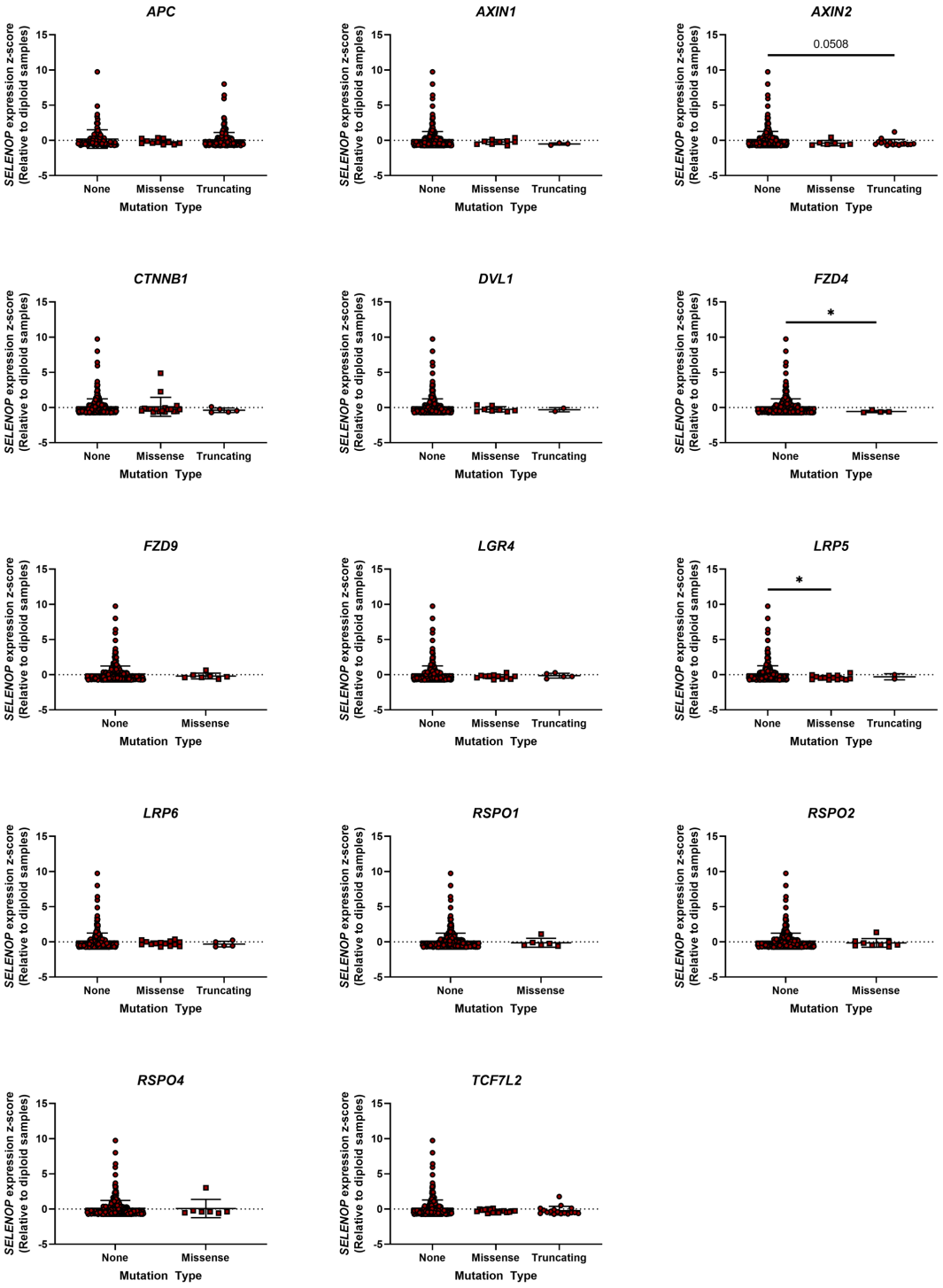

Figure 44. *SELENOP* expression in colon adenocarcinomas stratified by WNT mutation status. RNA-seq data from The Cancer Genome Atlas (TCGA). n=391 tumors. 2-tailed Mann-Whitney tests (two groups) or Kruskal-Wallis tests with 2-tailed Dunn's multiple comparisons tests (three groups). *p<0.05. Data are displayed as mean ± SD.

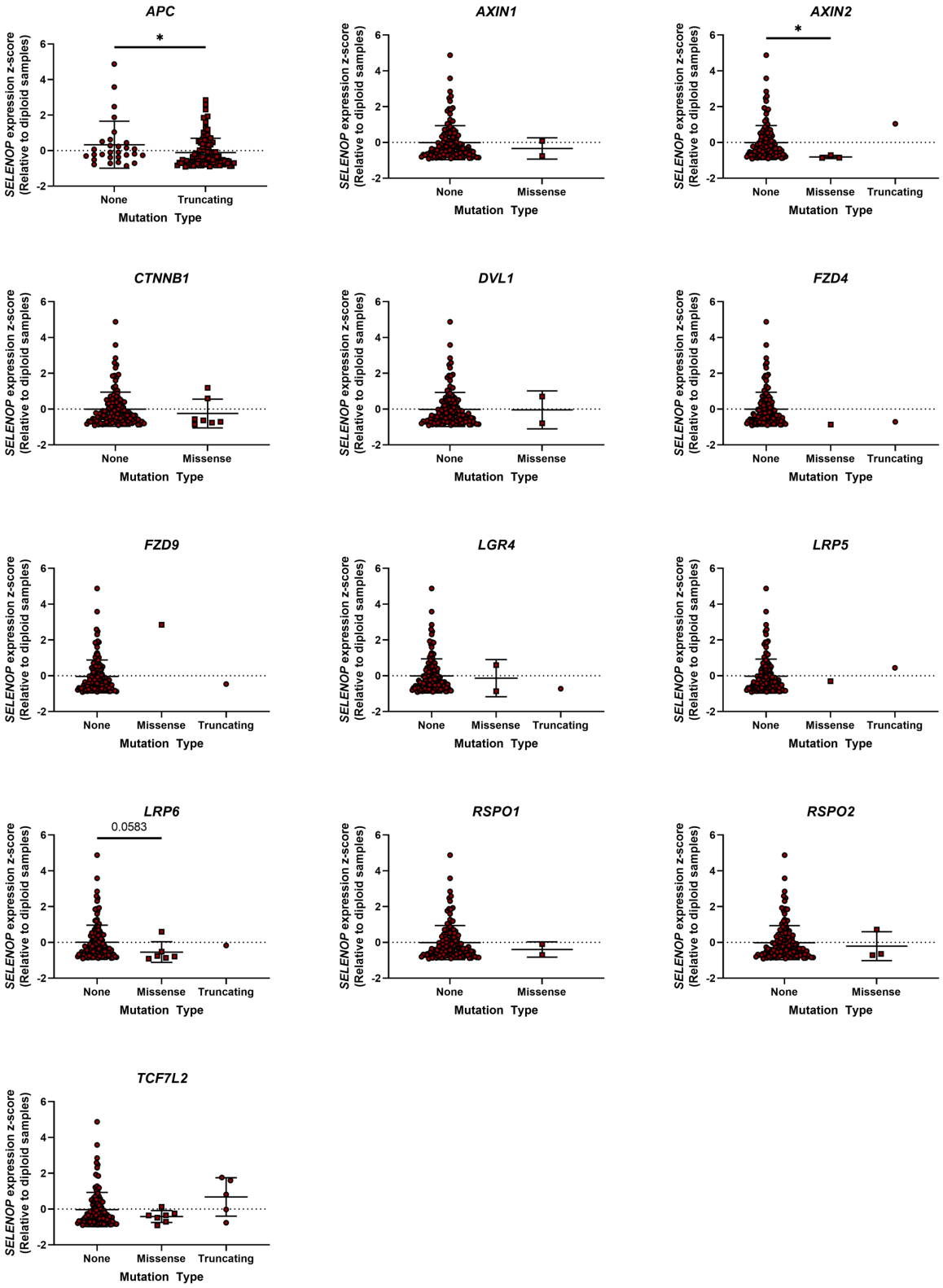

Figure 45. *SELENOP* expression in rectal adenocarcinomas stratified by WNT mutation status. RNA-seq data from The Cancer Genome Atlas (TCGA). n=226 tumors. 2-tailed Mann-Whitney tests (two groups) or Kruskal-Wallis tests with 2-tailed Dunn's multiple comparisons tests (three groups). *p<0.05. Data are displayed as mean ± SD.

APPENDIX C: PROTEIN HOMOLOGY BETWEEN MOUSE AND HUMAN SELENOP

Figure 46. Pairwise sequence alignment of human and mouse SELENOP protein sequences.

APPENDIX D: PROTEIN HOMOLOGY BETWEEN MOUSE AND HUMAN LRP6

```
hLRP6     1 MGAVLRSLLACSFCVLLRAAPLLLYANRRDLRLVDATNGKENATIVVGGL 50
mLRP6     1 MGAVLRSLLACSFCVLLRAAPLLLYANRRDLRLVDATNGKENATIVVGGL 50

hLRP6    51 EDAAAVDFVFSHGLIYWSDVSEEAIKRTEFNKTESVQNVVVSGLLSPDGL 100
mLRP6    51 EDAAAVDFVFGHGLIYWSDVSEEAIKRTEFNKTESVQNVVVSGLLSPDGL 100

hLRP6   101 ACDWLGEKLYWTDSETNRIEVSNLDGSLRKVLFWQELDQPRAIALDPSSG 150
mLRP6   101 ACDWLGEKLYWTDSETNRIEVSNLDGSLRKVLFWQELDQPRAIALDPSSG 150

hLRP6   151 FMYWTDWGEVPKIERAGMDGSSRFIIINSEIYWPNGLTLDYEEQKLYWAD 200
mLRP6   151 FMYWTDWGEVPKIERAGMDGSSRFVIINTEIYWPNGLTLDYQERKLYWAD 200

hLRP6   201 AKLNFIHKSNLDGTNRQAVVKGSLPHPFALTLFEDILYWTDWSTHSILAC 250
mLRP6   201 AKLNFIHKSNLDGTNRQAVVKGSLPHPFALTLFEDTLYWTDWNTHSILAC 250

hLRP6   251 NKYTGEGLREIHSDIFSPMDIHAFSQQRQPNATNPCGIDNGGCSHLCLMS 300
mLRP6   251 NKYTGEGLREIHSNIFSPMDIHAFSQQRQPNATNPCGIDNGGCSHLCLMS 300

hLRP6   301 PVKPFYQCACPTGVKLLENGKTCKDGATELLLLARRTDLRRISLDTPDFT 350
mLRP6   301 PVKPFYQCACPTGVKLLENGKTCKDGATELLLLARRTDLRRISLDTPDFT 350

hLRP6   351 DIVLQLEDIRHAIAIDYDPVEGYIYWTDDEVRAIRRSFIDGSGSQFVVTA 400
mLRP6   351 DIVLQLEDIRHAIAIDYDPVEGYIYWTDDEVRAIRRSFIDGSGSQFVVTA 400

hLRP6   401 QIAHPDGIAVDWVARNLYWTDTGTDRIEVTRLNGTMRKILISEDLEEPRA 450
mLRP6   401 QIAHPDGIAVDWVARNLYWTDTGTDRIEVTRLNGTMRKILISEDLEEPRA 450

hLRP6   451 IVLDPMVGYMYWTDWGEIPKIERAALDGSDRVVLVNTSLGWPNGLALDYD 500
mLRP6   451 IVLDPMVGYMYWTDWGEIPKIERAALDGSDRVVLVNTSLGWPNGLALDYD 500

hLRP6   501 EGKIYWGDAKTDKIEVMNTDGTGRRVLVEDKIPHIFGFTLLGDYVYWTDW 550
mLRP6   501 EGTIYWGDAKTDKIEVMNTDGTGRRVLVEDKIPHIFGFTLLGDYVYWTDW 550

hLRP6   551 QRRSIERVHKRSAEREVIIDQLPDLMGLKATNVHRVIGSNPCAEENGGCS 600
mLRP6   551 QRRSIERVHKRSAEREVIIDQLPDLMGLKATSVHRIIGSNPCAEDNGGCS 600

hLRP6   601 HLCLYRPQGLRCACPIGFELISDMKTCIVPEAFLLFSRRADIRRISLETN 650
mLRP6   601 HLCLYRPQGLRCACPIGFELISDMKTCIVPEAFLLFSRRADIRRISLETN 650

hLRP6   651 NNNVAIPLTGVKEASALDFDVTDNRIYWTDISLKTISRAFMNGSALEHVV 700
mLRP6   651 NNNVAIPLTGVKEASALDFDVTDNRIYWTDISLKTISRAFMNGSALEHVV 700

hLRP6   701 EFGLDYPEGMAVDWLGKNLYWADTGTNRIEVSKLDGQHRQVLVWKDLDSP 750
mLRP6   701 EFGLDYPEGMAVDWLGKNLYWADTGTNRIEVSKLDGQHRQVLVWKDLDSP 750

hLRP6   751 RALALDPAEGFMYWTEWGGKPKIDRAAMDGSERTTLVPNVGRANGLTIDY 800
mLRP6   751 RALALDPAEGFMYWTEWGGKPKIDRAAMDGSERTTLVPNVGRANGLTIDY 800

hLRP6   801 AKRRLYWTDLDTNLIESSNMLGLNREVIADDLPHPFGLTQYQDYIYWTDW 850
mLRP6   801 AKRRLYWTDLDTNLIESSDMLGLNREVIADDLPHPFGLTQYQDYIYWTDW 850

hLRP6   851 SRRSIERANKTSGQNRTIIQGHLDYVMDILVFHSSRQSGWNECASSNGHC 900
mLRP6   851 SRRSIERANKTSGQNRTIIQGHLDYVMDILVFHSSRQAGWNECASSNGHC 900
```

```
hLRP6   901 SHLCLAVPVGGFVCGCPAHYSLNADNRTCSAPTTFLLFSQKSAINRMVID 950
mLRP6   901 SHLCLAVPVGGFVCGCPAHYSLNADNRTCSAPTTFLLFSQKSAINRMVID 950

hLRP6   951 EQQSPDIILPIHSLRNVRAIDYDPLDKQLYWIDSRQNMIRKAQEDGSQGF 1000
mLRP6   951 EQQSPDIILPIHSLRNVRAIDYDPLDKQLYWIDSRQNSIRKAHEDGGQGF 1000

hLRP6  1001 TVVVSSVPSQNLEIQPYDLSIDIYSRYIYWTCEATNVINVTRLDGRSVGV 1050
mLRP6  1001 NVVANSVANQNLEIQPYDLSIDIYSRYIYWTCEATNVIDVTRLDGRSVGV 1050

hLRP6  1051 VLKGEQDRPRAIVVNPEKGYMYFTNLQERSPKIERAALDGTEREVLFFSG 1100
mLRP6  1051 VLKGEQDRPRAIVVNPEKGYMYFTNLQERSPKIERAALDGTEREVLFFSG 1100

hLRP6  1101 LSKPIALALDSRLGKLFWADSDLRRIESSDLSGANRIVLEDSNILQPVGL 1150
mLRP6  1101 LSKPIALALDSKLGKLFWADSDLRRIESSDLSGANRIVLEDSNILQPVGL 1150

hLRP6  1151 TVFENWLYWIDKQQQMIEKIDMTGREGRTKVQARIAQLSDIHAVKELNLQ 1200
mLRP6  1151 TVFENWLYWIDKQQQMIEKIDMTGREGRTKVQARIAQLSDIHAVKELNLQ 1200

hLRP6  1201 EYRQHPCAQDNGGCSHICLVKGDGTTRCSCPMHLVLLQDELSCG------ 1244
mLRP6  1201 EYRQHPCAQDNGGCSHICLVKGDGTTRCSCPMHLVLLQDELSCGEPPTCS 1250

hLRP6  1245 ------------------------------------ESQFQCASGQC 1255
mLRP6  1251 PQQFTCFTGDIDCIPVAWRCDGFTECEDHSDELNCPVCSESQFQCASGQC 1300

hLRP6  1256 IDGALRCNGDANCQDKSDEKNCEVLCLIDQFRCANGQCIGKHKKCDHNVD 1305
mLRP6  1301 IDGALRCNGDANCQDKSDEKNCEVLCLIDQFRCANGQCVGKHKKCDHSVD 1350

hLRP6  1306 CSDKSDELDCYPTEEPAPQATNTVGSVIGVIVTIFVSGTVYFICQRMLCP 1355
mLRP6  1351 CSDRSDELDCYPTEEPAPQATNTVGSVIGVIVTIFVSGTIYFICQRMLCP 1400

hLRP6  1356 RMKGDGETMTNDYVVHGPASVPLGYVPHPSSLSGSLPGMSRGKSMISSLS 1405
mLRP6  1401 RMKGDGETMTNDYVVHSPASVPLGYVPHPSSLSGSLPGMSRGKSMISSLS 1450

hLRP6  1406 IMGGSSGPPYDRAHVTGASSSSSSSTKGTYFPAILNPPPSPATERSHYTM 1455
mLRP6  1451 IMGGSSGPPYDRAHVTGASSSSSSSTKGTYFPAILNPPPSPATERSHYTM 1500

hLRP6  1456 EFGYSSNSPSTHRSYSYRPYSYRHFAPPTTPCSTDVCDSDYAPSRRMTSV 1505
mLRP6  1501 EFGYSSNSPSTHRSYSYRPYSYRHFAPPTTPCSTDVCDSDYAPSRRMTSV 1550

hLRP6  1506 ATAKGYTSDLNYDSEPVPPPPTPRSQYLSAEENYESCPPSPYTERSYSHH 1555
mLRP6  1551 ATAKGYTSDVNYDSEPVPPPPTPRSQYLSAEENYESCPPSPYTERSYSHH 1600

                hLRP6 1556 LYPPPPSPCTDSS   1568
                mLRP6 1601 LYPPPPSPCTDSS   1613

  Fully conserved/Highly conserved/Poorly conserved/Not conserved

                95.4% identity/96.6% similarity
```

Figure 47. Pairwise sequence alignment of human and mouse LRP6 protein sequences.

APPENDIX E: ATTEMPTS TO VALIDATE ANTI-SELENOP ANTIBODIES FOR IF

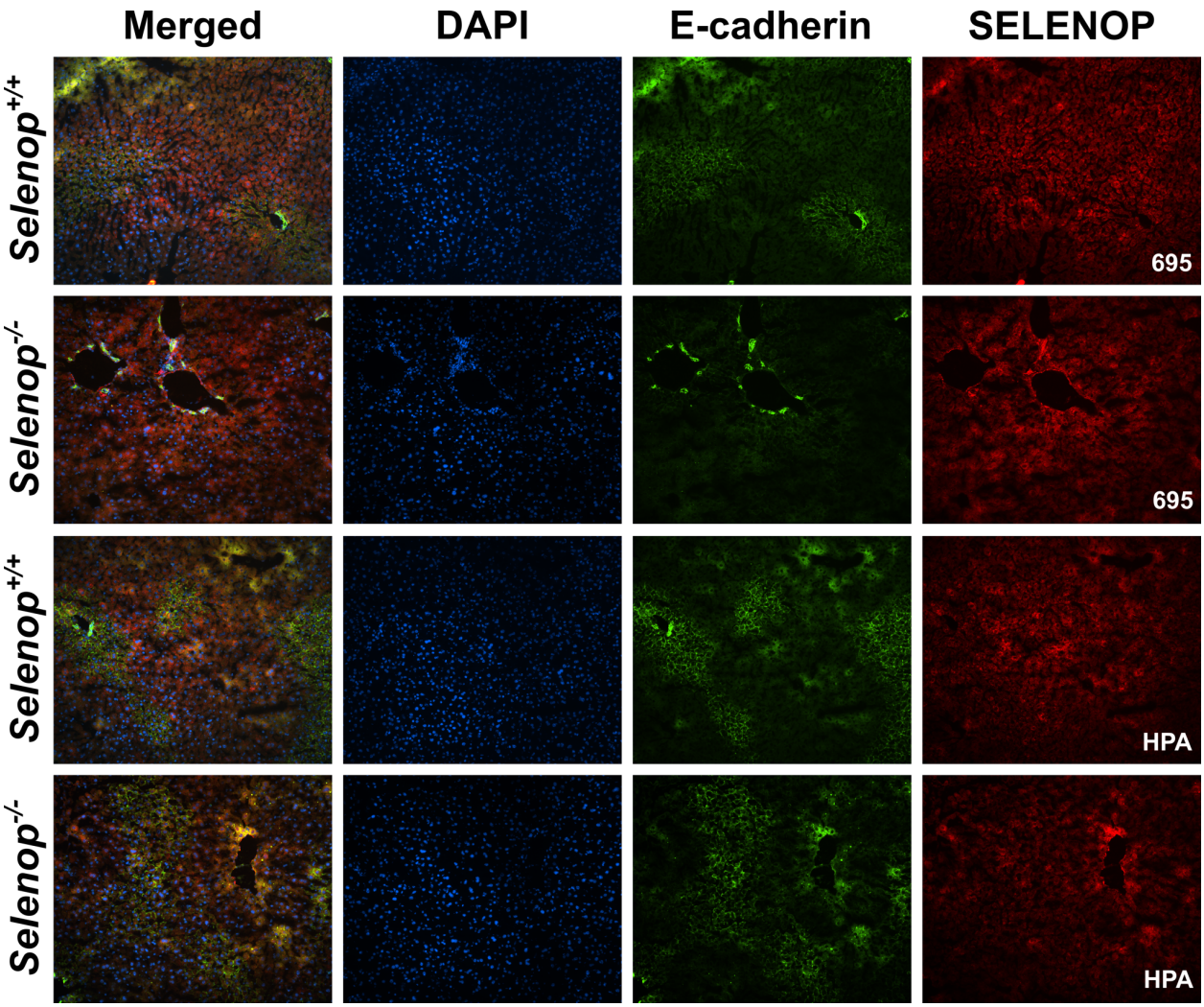

Figure 48. Attempts to validate anti-SELENOP antibodies for IF in the liver. Representative images of *Selenop*$^{+/+}$ and *Selenop*$^{-/-}$ liver stained for E-cadherin and SELENOP (with 695 or HPA antibodies).

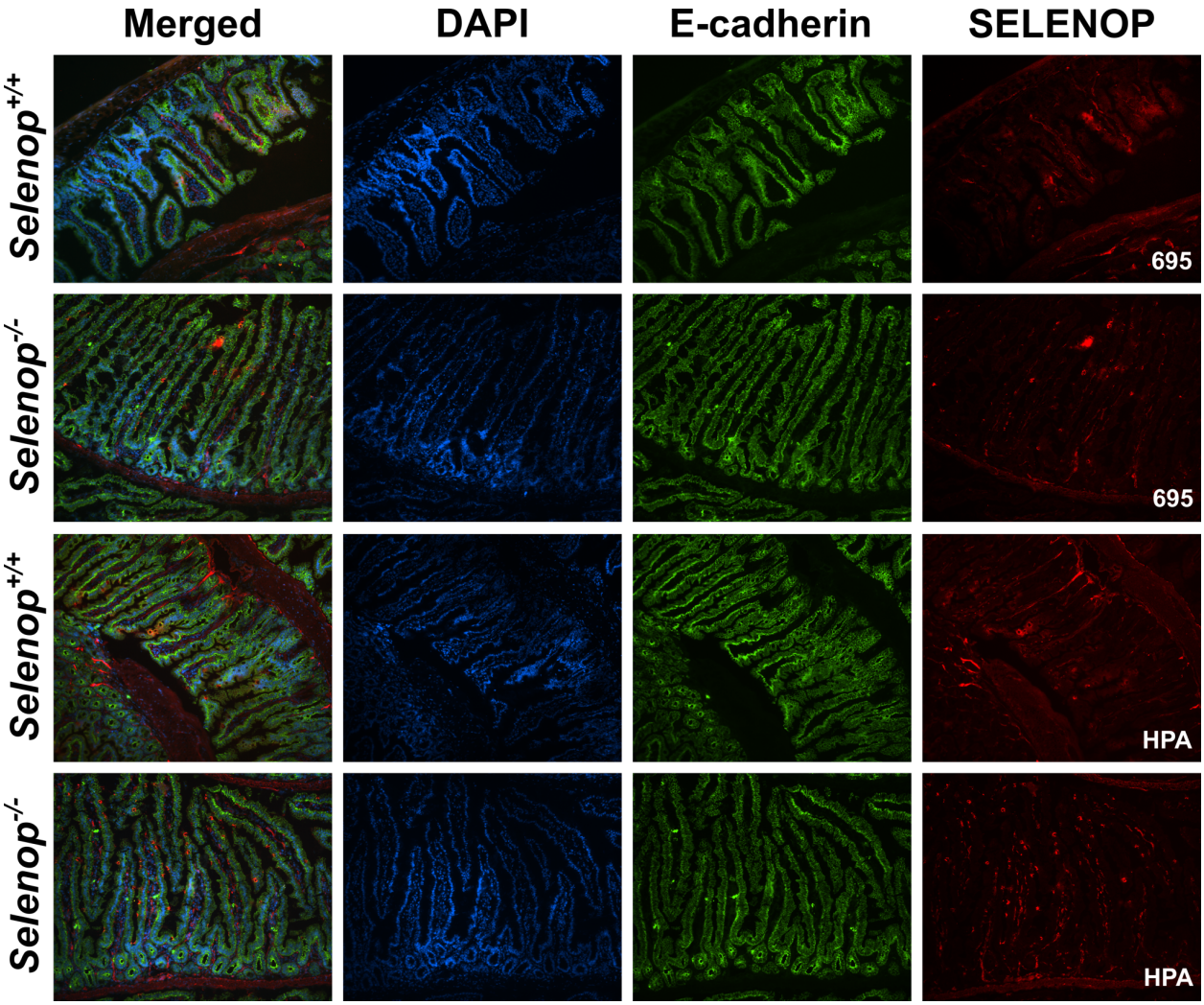

Figure 49. Attempts to validate anti-SELENOP antibodies for IF in the small intestine. Representative images of *Selenop*$^{+/+}$ and *Selenop*$^{-/-}$ small intestine stained for E-cadherin and SELENOP (with 695 or HPA antibodies).

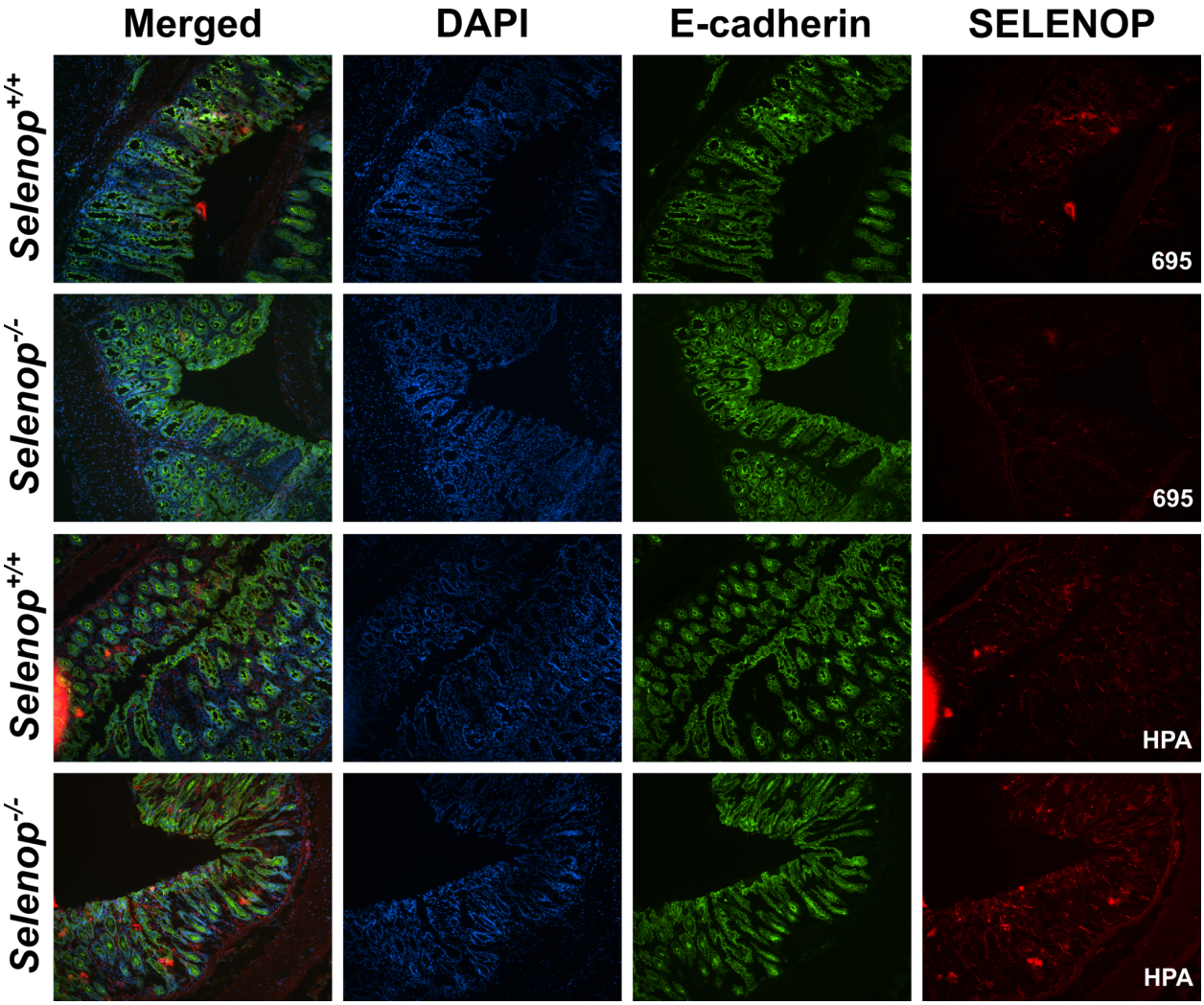

Figure 50. Attempts to validate anti-SELENOP antibodies for IF in the colon. Representative images of *Selenop*$^{+/+}$ and *Selenop*$^{-/-}$ colon stained for E-cadherin and SELENOP (with 695 or HPA antibodies).

REFERENCES

1. Beumer J, Clevers H. Cell fate specification and differentiation in the adult mammalian intestine. *Nat Rev Mol Cell Bio* 2021;22(1):39–53.

2. Morris AL, Mohiuddin SS. *Biochemistry, Nutrients [Internet]*. Treasure Island, FL: StatPearls Publishing; 2023:

3. Nusse R, Clevers H. Wnt/β-Catenin Signaling, Disease, and Emerging Therapeutic Modalities. *Cell* 2017;169(6):985–999.

4. Daulat AM, Borg J-P. Wnt/Planar Cell Polarity Signaling: New Opportunities for Cancer Treatment. *Trends Cancer* 2017;3(2):113–125.

5. De A. Wnt/Ca2+ signaling pathway: a brief overview.. *Acta Bioch Bioph Sin* 2011;43(10):745–56.

6. Sonavane PR, Willert K. Controlling Wnt Signaling Specificity and Implications for Targeting WNTs Pharmacologically.. *Handb Exp Pharmacol* 2021;269:3–28.

7. May P, Woldt E, Matz RL, Boucher P. The LDL receptor-related protein (LRP) family: An old family of proteins with new physiological functions. *Ann Med* 2007;39(3):219–228.

8. Fernandez-Castaneda A et al. Identification of the Low Density Lipoprotein (LDL) Receptor-related Protein-1 Interactome in Central Nervous System Myelin Suggests a Role in the Clearance of Necrotic Cell Debris*. *J Biol Chem* 2013;288(7):4538–4548.

9. Marzolo M-P, Farfn P. New Insights into the Roles of Megalin/LRP2 and the Regulation of its Functional Expression. *Biol Res* 2011;44(1):89–105.

10. Shen C, Xiong W-C, Mei L. LRP4 in neuromuscular junction and bone development and diseases. *Bone* 2015;80:101–108.

11. Lane-Donovan C, Herz J. The ApoE receptors Vldlr and Apoer2 in central nervous system function and disease. *J Lipid Res* 2017;58(6):1036–1043.

12. Zhang J et al. LRP8 mediates Wnt/β-catenin signaling and controls osteoblast differentiation. *J Bone Miner Res* 2012;27(10):2065–2074.

13. Fang Z et al. Low-density lipoprotein receptor-related protein 8 facilitates the proliferation and invasion of non-small cell lung cancer cells by regulating the Wnt/β-catenin signaling pathway. *Bioengineered* 2022;13(3):6807–6818.

14. Joiner DM, Ke J, Zhong Z, Xu HE, Williams BO. LRP5 and LRP6 in development and disease. *Trends Endocrinol Metabolism* 2013;24(1):31–39.

15. Chen S et al. Structural and Functional Studies of LRP6 Ectodomain Reveal a Platform for Wnt Signaling. *Dev Cell* 2011;21(5):848–861.

16. Liu C-C, Pearson C, Bu G. Cooperative Folding and Ligand-binding Properties of LRP6 β-Propeller Domains*. *J Biol Chem* 2009;284(22):15299–15307.

17. Brown K, Arthur J. Selenium, selenoproteins and human health: a review. *Public Health Nutr* 2001;4(2b):593–599.

18. Stadtman TC. Selenocysteine.. *Annu Rev Biochem* 1996;65(1):83–100.

19. Berry MJ et al. Selenocysteine incorporation directed from the 3′UTR: Characterization of eukaryotic EFsec and mechanistic implications. *Biofactors* 2001;14(1-4):17–24.

20. Copeland PR, Fletcher JE, Carlson BA, Hatfield DL, Driscoll DM. A novel RNA binding protein, SBP2, is required for the translation of mammalian selenoprotein mRNAs. *Embo J* 2000;19(2):306–314.

21. Tujebajeva RM et al. Decoding apparatus for eukaryotic selenocysteine insertion. *Embo Rep* 2000;1(2):158–163.

22. Hatfield D, Lee BJ, Hampton L, Diamond AM. Selenium induces changes in the selenocysteine tRNA[Ser]Sec population in mammalian cells. *Nucleic Acids Res* 1991;19(4):939–943.

23. Seyedali A, Berry MJ. Nonsense-mediated decay factors are involved in the regulation of selenoprotein mRNA levels during selenium deficiency. *Rna* 2014;20(8):1248–1256.

24. Steinbrenner H, Speckmann B, Klotz L-O. Selenoproteins: Antioxidant selenoenzymes and beyond. *Arch Biochem Biophys* 2016;595:113–119.

25. Brigelius-Flohé R, Maiorino M. Glutathione peroxidases. *Biochimica Et Biophysica Acta Bba - Gen Subj* 2013;1830(5):3289–3303.

26. Arnér ESJ, Holmgren A. Physiological functions of thioredoxin and thioredoxin reductase: Thioredoxin and thioredoxin reductase. *Eur J Biochem* 2000;267(20):6102–6109.

27. Luongo C, Dentice M, Salvatore D. Deiodinases and their intricate role in thyroid hormone homeostasis. *Nat Rev Endocrinol* 2019;15(8):479–488.

28. Kaya A, Lee BC, Gladyshev VN. Regulation of Protein Function by Reversible Methionine Oxidation and the Role of Selenoprotein MsrB1. *Antioxid Redox Sign* 2015;23(10):814–822.

29. Xu X et al. Selenophosphate synthetase 2 is essential for selenoprotein biosynthesis. *Faseb J* 2006;20(4):A428–A428.

30. Pitts MW, Hoffmann PR. Endoplasmic reticulum-resident selenoproteins as regulators of calcium signaling and homeostasis. *Cell Calcium* 2018;70:76–86.

31. Cox AG et al. Selenoprotein H is an essential regulator of redox homeostasis that cooperates with p53 in development and tumorigenesis. *Proc National Acad Sci* 2016;113(38):E5562–E5571.

32. Han S-J, Lee BC, Yim SH, Gladyshev VN, Lee S-R. Characterization of Mammalian Selenoprotein O: A Redox-Active Mitochondrial Protein. *Plos One* 2014;9(4):e95518.

33. Moustafa ME, El-Srouji R. CHARACTERIZATION OF SELENOPROTEIN V. *Faseb J* 2010;24(S1):916.12-916.12.

34. Whanger PD. Selenoprotein expression and function—Selenoprotein W. *Biochimica Et Biophysica Acta Bba - Gen Subj* 2009;1790(11):1448–1452.

35. Stoytcheva ZR, Berry MJ. Transcriptional regulation of mammalian selenoprotein expression. *Biochimica Et Biophysica Acta Bba - Gen Subj* 2009;1790(11):1429–1440.

36. Burk RF, Hill KE. Selenoprotein P-expression, functions, and roles in mammals.. *Biochim Biophys Acta* 2009;1790(11):1441–7.

37. Hondal RJ, Ma S, Caprioli RM, Hill KE, Burk RF. Heparin-binding Histidine and Lysine Residues of Rat Selenoprotein P*. *J Biol Chem* 2001;276(19):15823–15831.

38. Arteel GE, Franken S, Kappler J, Sies H. Binding of Selenoprotein P to Heparin: Characterization with Surface Plasmon Resonance. *Biol Chem* 2000;381(3):265–268.

39. Ma S, Hill KE, Burk RF, Caprioli RM. Mass Spectrometric Identification of N- and O- Glycosylation Sites of Full-Length Rat Selenoprotein P and Determination of Selenide−Sulfide and Disulfide Linkages in the Shortest Isoform †. *Biochemistry-us* 2003;42(32):9703–9711.

40. Stoytcheva Z, Tujebajeva RM, Harney JW, Berry MJ. Efficient incorporation of multiple selenocysteines involves an inefficient decoding step serving as a potential translational checkpoint and ribosome bottleneck.. *Mol Cell Biol* 2006;26(24):9177–84.

41. Himeno S, Chittum HS, Burk RF. Isoforms of Selenoprotein P in Rat Plasma EVIDENCE FOR A FULL-LENGTH FORM AND ANOTHER FORM THAT TERMINATES AT THE SECOND UGA IN THE OPEN READING FRAME*. *J Biol Chem* 1996;271(26):15769–15775.

42. Ma S, Hill KE, Caprioli RM, Burk RF. Mass Spectrometric Characterization of Full-length Rat Selenoprotein P and Three Isoforms Shortened at the C Terminus EVIDENCE THAT THREE UGA CODONS IN THE mRNA OPEN READING FRAME HAVE ALTERNATIVE FUNCTIONS OF SPECIFYING SELENOCYSTEINE INSERTION OR TRANSLATION TERMINATION∗ 210. *J Biol Chem* 2002;277(15):12749–12754.

43. Hill KE et al. The selenium-rich C-terminal domain of mouse selenoprotein P is necessary for the supply of selenium to brain and testis but not for the maintenance of whole body selenium.. *J Biological Chem* 2007;282(15):10972–80.

44. Åkesson B, Bellew T, Burk RF. Purification of selenoprotein P from human plasma. *Biochimica Et Biophysica Acta Bba - Protein Struct Mol Enzym* 1994;1204(2):243–249.

45. Méplan C et al. Relative Abundance of Selenoprotein P Isoforms in Human Plasma Depends on Genotype, Se Intake, and Cancer Status. *Antioxid Redox Sign* 2009;11(11):2631–2640.

46. Ballihaut G, Kilpatrick LE, Kilpatrick EL, Davis WC. Multiple forms of selenoprotein P in a candidate human plasma standard reference material. *Metallomics* 2012;4(6):533–538.

47. Kurokawa S et al. Sepp1UF forms are N-terminal selenoprotein P truncations that have peroxidase activity when coupled with thioredoxin reductase-1. *Free Radical Bio Med* 2014;69:67–76.

48. Arteel GE, Sies H. The biochemistry of selenium and the glutathione system. *Environ Toxicol Phar* 2001;10(4):153–158.

49. Takebe G et al. A Comparative Study on the Hydroperoxide and Thiol Specificity of the Glutathione Peroxidase Family and Selenoprotein P*. *J Biol Chem* 2002;277(43):41254–41258.

50. Barrett CW et al. Selenoprotein P influences colitis-induced tumorigenesis by mediating stemness and oxidative damage. *J Clin Invest* 2015;125(7):2646–2660.

51. Short SP et al. Colonic epithelial-derived Selenoprotein P is the source for antioxidant-mediated protection in colitis-associated cancer. *Gastroenterology* [published online ahead of print: 2021]; doi:10.1053/j.gastro.2020.12.059

52. Read R et al. Selenium and amino acid composition of selenoprotein P, the major selenoprotein in rat serum.. *J Biol Chem* 1990;265(29):17899–17905.

53. Hill KE et al. Production of Selenoprotein P (Sepp1) by Hepatocytes Is Central to Selenium Homeostasis. *J Biol Chem* 2012;287(48):40414–40424.

54. Kurokawa S, Hill KE, McDonald WH, Burk RF. Long Isoform Mouse Selenoprotein P (Sepp1) Supplies Rat Myoblast L8 Cells with Selenium via Endocytosis Mediated by Heparin Binding Properties and Apolipoprotein E Receptor-2 (ApoER2)*. *J Biol Chem* 2012;287(34):28717–28726.

55. Misu H et al. Deficiency of the hepatokine selenoprotein P increases responsiveness to exercise in mice through upregulation of reactive oxygen species and AMP-activated protein kinase in muscle. *Nat Med* 2017;23(4):508–516.

56. Olson GE, Winfrey VP, Hill KE, Burk RF. Megalin Mediates Selenoprotein P Uptake by Kidney Proximal Tubule Epithelial Cells. *J Biol Chem* 2008;283(11):6854–6860.

57. Burk RF et al. Deletion of Apolipoprotein E Receptor-2 in Mice Lowers Brain Selenium and Causes Severe Neurological Dysfunction and Death When a Low-Selenium Diet Is Fed. *J Neurosci* 2007;27(23):6207–6211.

58. Olson GE, Winfrey VP, NagDas SK, Hill KE, Burk RF. Apolipoprotein E Receptor-2 (ApoER2) Mediates Selenium Uptake from Selenoprotein P by the Mouse Testis. *J Biol Chem* 2007;282(16):12290–12297.

59. Burk RF et al. Selenoprotein P and apolipoprotein E receptor-2 interact at the blood-brain barrier and also within the brain to maintain an essential selenium pool that protects against neurodegeneration.. *Faseb J Official Publ Fed Am Soc Exp Biology* 2014;28(8):3579–88.

60. Hill KE, Zhou J, McMahan WJ, Motley AK, Burk RF. Neurological Dysfunction Occurs in Mice with Targeted Deletion of the Selenoprotein P Gene. *J Nutrition* 2004;134(1):157–161.

61. Olson GE, Winfrey VP, Nagdas SK, Hill KE, Burk RF. Selenoprotein P is required for mouse sperm development.. *Biol Reprod* 2005;73(1):201–11.

62. Kurokawa S, Bellinger FP, Hill KE, Burk RF, Berry MJ. Isoform-specific Binding of Selenoprotein P to the β-Propeller Domain of Apolipoprotein E Receptor 2 Mediates Selenium Supply. *J Biol Chem* 2014;289(13):9195–9207.

63. Short SP, Pilat JM, Williams CS. Roles for selenium and selenoprotein P in the development, progression, and prevention of intestinal disease.. *Free Radic Biology Medicine* 2018;127:26–35.

64. Pegg AE. Methylation of the O6 Position of Guanine in DNA is the Most Likely Initiating Event in Carcinogenesis by Methylating Agents. *Cancer Invest* 2009;2(3):223–231.

65. Okayasu I, Ohkusa T, Kajiura K, Kanno J, Sakamoto S. Promotion of colorectal neoplasia in experimental murine ulcerative colitis.. *Gut* 1996;39(1):87.

66. Murawaki Y et al. Aberrant expression of selenoproteins in the progression of colorectal cancer. *Cancer Lett* 2008;259(2):218–230.

67. Al-Taie OH et al. Expression Profiling and Genetic Alterations of the Selenoproteins GI-GPx and SePP in Colorectal Carcinogenesis. *Nutrition Cancer* 2004;48(1):6–14.

68. Mork H et al. Inverse mRNA Expression of the Selenocysteine-Containing Proteins GI-GPx and SeP in Colorectal Adenomas Compared With Adjacent Normal Mucosa. *Nutrition Cancer* 2000;37(1):108–116.

69. Early DS, Hill K, Burk R, Palmer I. Selenoprotein levels in patients with colorectal adenomas and cancer. *Am J Gastroenterology* 2002;97(3):745–748.

70. Méplan C et al. Genetic variants in selenoprotein genes increase risk of colorectal cancer. *Carcinogenesis* 2010;31(6):1074–1079.

71. Peters U et al. Variation in the Selenoenzyme Genes and Risk of Advanced Distal Colorectal Adenoma. *Cancer Epidem Biomar* 2008;17(5):1144–1154.

72. Brown RE et al. MTG16 (CBFA2T3) regulates colonic epithelial differentiation, colitis, and tumorigenesis by repressing E protein transcription factors. *Jci Insight* [published online ahead of print: 2022]; doi:10.1172/jci.insight.153045

73. Elmentaite R et al. Cells of the human intestinal tract mapped across space and time. *Nature* 2021;597(7875):250–255.

74. Becker WR et al. Single-cell analyses define a continuum of cell state and composition changes in the malignant transformation of polyps to colorectal cancer. *Nat Genet* 2022;54(7):985–995.

75. Chen B et al. Differential pre-malignant programs and microenvironment chart distinct paths to malignancy in human colorectal polyps. *Cell* 2021;184(26):6262-6280.e26.

76. Pelka K et al. Spatially organized multicellular immune hubs in human colorectal cancer. *Cell* 2021;184(18):4734-4752.e20.

77. Gulati GS et al. Single-cell transcriptional diversity is a hallmark of developmental potential. *Science* 2020;367(6476):405–411.

78. Sande BV de et al. A scalable SCENIC workflow for single-cell gene regulatory network analysis. *Nat Protoc* 2020;15(7):2247–2276.

79. Aibar S et al. SCENIC: single-cell regulatory network inference and clustering. *Nat Methods* 2017;14(11):1083–1086.

80. Burk RF, Norsworthy BK, Hill KE, Motley AK, Byrne DW. Effects of Chemical Form of Selenium on Plasma Biomarkers in a High-Dose Human Supplementation Trial. *Cancer Epidem Biomar* 2006;15(4):804–810.

81. Hoadley KA et al. Cell-of-Origin Patterns Dominate the Molecular Classification of 10,000 Tumors from 33 Types of Cancer. *Cell* 2018;173(2):291-304.e6.

82. Cerami E et al. The cBio Cancer Genomics Portal: An Open Platform for Exploring Multidimensional Cancer Genomics Data. *Cancer Discov* 2012;2(5):401–404.

83. Gao J et al. Integrative Analysis of Complex Cancer Genomics and Clinical Profiles Using the cBioPortal. *Sci Signal* 2013;6(269):pl1.

84. Villanueva JW et al. Comprehensive microRNA analysis across genome-edited colorectal cancer organoid models reveals miR-24 as a candidate regulator of cell survival. *Bmc Genomics* 2022;23(1):792.

85. Powell AE et al. The Pan-ErbB Negative Regulator Lrig1 Is an Intestinal Stem Cell Marker that Functions as a Tumor Suppressor. *Cell* 2012;149(1):146–158.

86. Cheung AF et al. Complete deletion of Apc results in severe polyposis in mice. *Oncogene* 2010;29(12):1857–1864.

87. Hill KE et al. Deletion of Selenoprotein P Alters Distribution of Selenium in the Mouse*. *J Biol Chem* 2003;278(16):13640–13646.

88. Powell AE et al. Inducible loss of one Apc allele in Lrig1-expressing progenitor cells results in multiple distal colonic tumors with features of familial adenomatous polyposis. *Am J Physiol-gastr L* 2014;307(1):G16–G23.

89. Faustino-Rocha A et al. Estimation of rat mammary tumor volume using caliper and ultrasonography measurements. *Lab Animal* 2013;42(6):217–224.

90. Thompson JJ et al. Blood vessel epicardial substance (BVES) reduces LRP6 receptor and cytoplasmic -catenin levels to modulate Wnt signaling and intestinal homeostasis.. *Carcinogenesis* [published online ahead of print: 2018]; doi:10.1093/carcin/bgz007

91. Schneider CA, Rasband WS, Eliceiri KW. NIH Image to ImageJ: 25 years of image analysis. *Nat Methods* 2012;9(7):671–675.

92. Barrett C, Short S, Choksi Y, Williams C. Whole-mount Enteroid Proliferation Staining. *Bio-protocol* 2016;6(12). doi:10.21769/bioprotoc.1837

93. Short SP et al. Serine Threonine Kinase 17A maintains the epithelial state in colorectal cancer cells. *Mol Cancer Res* 2019;17(4):molcanres.0990.2018.

94. Saito-Diaz K et al. APC Inhibits Ligand-Independent Wnt Signaling by the Clathrin Endocytic Pathway. *Dev Cell* 2018;44(5):566-581.e8.

95. Xu Q et al. Vascular Development in the Retina and Inner Ear. *Cell* 2004;116(6):883–895.

96. Whitehead RH, Robinson PS. Establishment of conditionally immortalized epithelial cell lines from the intestinal tissue of adult normal and transgenic mice. *Am J Physiol-gastr L* 2009;296(3):G455–G460.

97. Pilat JM et al. SELENOP modifies sporadic colorectal carcinogenesis and WNT signaling activity through LRP5/6 interactions. *J Clin Invest* [published online ahead of print: 2023]; doi:10.1172/jci165988

98. Doherty JE et al. Hyperactive piggyBac Gene Transfer in Human Cells and In Vivo. *Hum Gene Ther* 2012;23(3):311–320.

99. Sanjana NE, Shalem O, Zhang F. Improved vectors and genome-wide libraries for CRISPR screening. *Nat Methods* 2014;11(8):783–784.

100. Graepel KW, Agostini ML, Lu X, Sexton NR, Denison MR. Fitness Barriers Limit Reversion of a Proofreading-Deficient Coronavirus. *J Virol* 2019;93(20). doi:10.1128/jvi.00711-19

101. Katzen F. Gateway® recombinational cloning: a biological operating system. *Expert Opin Drug Dis* 2007;2(4):571–589.

102. Needleman SB, Wunsch CD. A general method applicable to the search for similarities in the amino acid sequence of two proteins. *J Mol Biol* 1970;48(3):443–453.

103. Mirdita M et al. ColabFold: making protein folding accessible to all. *Nat Methods* 2022;19(6):679–682.

104. Pettersen EF et al. UCSF ChimeraX : Structure visualization for researchers, educators, and developers. *Protein Sci* 2020;30(1):70–82.

105. Burt RW. Colon cancer screening. *Gastroenterology* 2000;119(3):837–853.

106. Grivennikov SI, Cominelli F. Colitis-Associated and Sporadic Colon Cancers: Different Diseases, Different Mutations?. *Gastroenterology* 2016;150(4):808–810.

107. Slattery ML. Diet, lifestyle, and colon cancer.. *Seminars Gastrointest Dis* 2000;11(3):142–6.

108. Palma FDED et al. The Molecular Hallmarks of the Serrated Pathway in Colorectal Cancer. *Cancers* 2019;11(7):1017.

109. Hoffmann PR et al. The selenoproteome exhibits widely varying, tissue-specific dependence on selenoprotein P for selenium supply. *Nucleic Acids Res* 2007;35(12):3963–3973.

110. Yin X et al. Niche-independent high-purity cultures of Lgr5+ intestinal stem cells and their progeny. *Nat Methods* 2014;11(1):106–112.

111. Augenlicht L. Hidden effects of mouse chow. *Science* 2014;346(6210):710–710.

112. Sato T et al. Single Lgr5 stem cells build crypt-villus structures in vitro without a mesenchymal niche. *Nature* 2009;459(7244):262–265.

113. Berg KCG et al. Multi-omics of 34 colorectal cancer cell lines - a resource for biomedical studies. *Mol Cancer* 2017;16(1):116.

114. Tamai K et al. LDL-receptor-related proteins in Wnt signal transduction. *Nature* 2000;407(6803):530–535.

115. Chiu-Ugalde J et al. Mutation of megalin leads to urinary loss of selenoprotein P and selenium deficiency in serum, liver, kidneys and brain. *Biochem J* 2010;431(1):103–111.

116. Pietschmann N et al. Selenoprotein P is the essential selenium transporter for bones. *Metallomics* 2014;6(5):1043–1049.

117. Malinauskas T, Jones EY. Extracellular modulators of Wnt signalling. *Curr Opin Struc Biol* 2014;29:77–84.

118. Speckmann B, Bidmon H-J, Borchardt A, Sies H, Steinbrenner H. Intestinal selenoprotein P in epithelial cells and in plasma cells. *Arch Biochem Biophys* 2014;541:30–36.

119. Schaum N et al. Single-cell transcriptomics of 20 mouse organs creates a Tabula Muris. *Nature* 2018;562(7727):367–372.

120. Bhattacharyya A, Chattopadhyay R, Mitra S, Crowe SE. Oxidative Stress: An Essential Factor in the Pathogenesis of Gastrointestinal Mucosal Diseases. *Physiol Rev* 2014;94(2):329–354.

121. Hughes DJ et al. Expression of Selenoprotein Genes and Association with Selenium Status in Colorectal Adenoma and Colorectal Cancer. *Nutrients* 2018;10(11):1812.

122. Nakanishi Y, Diaz-Meco MT, Moscat J. Serrated Colorectal Cancer: The Road Less Travelled?. *Trends Cancer* 2019;5(11):742–754.

123. Jass JR. Classification of colorectal cancer based on correlation of clinical, morphological and molecular features. *Histopathology* 2007;50(1):113–130.

124. M. P Timothy, P. R Chandrajit, A. R-B Miguel. Colorectal Carcinogenesis: MSI-H Versus MSI-L. *Dis Markers* 2004;20(4–5):199–206.

125. Sæterdal I et al. Frameshift-mutation-derived peptides as tumor-specific antigens in inherited and spontaneous colorectal cancer. *Proc National Acad Sci* 2001;98(23):13255–13260.

126. Kang S et al. The significance of microsatellite instability in colorectal cancer after controlling for clinicopathological factors. *Medicine* 2018;97(9):e0019.

127. Gryfe R et al. Tumor Microsatellite Instability and Clinical Outcome in Young Patients with Colorectal Cancer. *New Engl J Medicine* 2000;342(2):69–77.

128. Keshinro A et al. Tumor-Infiltrating Lymphocytes, Tumor Mutational Burden, and Genetic Alterations in Microsatellite Unstable, Microsatellite Stable, or Mutant POLE/POLD1 Colon Cancer.. *Jco Precis Oncol* 2020;5. doi:10.1200/po.20.00456

129. Bauer K et al. Dendritic cell and macrophage infiltration in microsatellite-unstable and microsatellite-stable colorectal cancer. *Fam Cancer* 2011;10(3):557.

130. Buckowitz A et al. Microsatellite instability in colorectal cancer is associated with local lymphocyte infiltration and low frequency of distant metastases. *Brit J Cancer* 2005;92(9):1746–1753.

131. Takemoto N et al. The Correlation of Microsatellite Instability and Tumor-infiltrating Lymphocytes in Hereditary Non-polyposis Colorectal Cancer (HNPCC) and Sporadic Colorectal Cancers: the Significance of Different Types of Lymphocyte Infiltration. *Jpn J Clin Oncol* 2004;34(2):90–98.

132. Narayanan S et al. Tumor Infiltrating Lymphocytes and Macrophages Improve Survival in Microsatellite Unstable Colorectal Cancer. *Sci Rep-uk* 2019;9(1):13455.

133. Michel S et al. High density of FOXP3-positive T cells infiltrating colorectal cancers with microsatellite instability. *Brit J Cancer* 2008;99(11):1867–1873.

134. Digiacomo N et al. Neuroendocrine Differentiation, Microsatellite Instability, and Tumor-infiltrating Lymphocytes in Advanced Colorectal Cancer With BRAF Mutation.. *Clin Colorectal Canc* 2018;18(2):e251–e260.

135. Lee S-Y et al. Microsatellite Instability, EMAST, and Morphology Associations with T Cell Infiltration in Colorectal Neoplasia. *Digest Dis Sci* 2011;57(1):72–78.

136. Phillips SM et al. Tumour-infiltrating lymphocytes in colorectal cancer with microsatellite instability are activated and cytotoxic. *Brit J Surg* 2004;91(4):469–475.

137. Toor SM, Nair VS, Murshed K, Nada MA, Elkord E. Tumor-Infiltrating Lymphoid Cells in Colorectal Cancer Patients with Varying Disease Stages and Microsatellite Instability-High/Stable Tumors. *Nato Adv Sci Inst Se* 2021;9(1):64.

138. Duque GA, Descoteaux A. Macrophage Cytokines: Involvement in Immunity and Infectious Diseases. *Front Immunol* 2014;5:491.

139. Dong C. Cytokine Regulation and Function in T Cells. *Annu Rev Immunol* 2021;39(1):1–26.

140. Dreher I, Jakobs TC, Köhrle J. Cloning and Characterization of the Human Selenoprotein P Promoter RESPONSE OF SELENOPROTEIN P EXPRESSION TO CYTOKINES IN LIVER CELLS*. *J Biol Chem* 1997;272(46):29364–29371.

141. Martitz J et al. Gene-specific regulation of hepatic selenoprotein expression by interleukin-6. *Metallomics* 2015;7(11):1515–1521.

142. Irons R, Carlson BA, Hatfield DL, Davis CD. Both selenoproteins and low molecular weight selenocompounds reduce colon cancer risk in mice with genetically impaired selenoprotein expression.. *J Nutrition* 2006;136(5):1311–7.

143. Müller MF et al. Deletion of Glutathione Peroxidase-2 Inhibits Azoxymethane-Induced Colon Cancer Development. *Plos One* 2013;8(8):e72055.

144. Tsuji PA et al. Knockout of the 15 kDa Selenoprotein Protects against Chemically-Induced Aberrant Crypt Formation in Mice. *Plos One* 2012;7(12):e50574.

145. Choi JW et al. Longitudinal Tracing of Spontaneous Regression and Anti-angiogenic Response of Individual Microadenomas during Colon Tumorigenesis. *Theranostics* 2015;5(7):724–732.

146. Yamada Y et al. Microadenomatous lesions involving loss of Apc heterozygosity in the colon of adult Apc(Min/+) mice.. *Cancer Res* 2002;62(22):6367–70.

147. Oyama T et al. Further upregulation of β-catenin/Tcf transcription is involved in the development of macroscopic tumors in the colon of ApcMin/+ mice. *Carcinogenesis* 2008;29(3):666–672.

148. Krehl S et al. Glutathione peroxidase-2 and selenium decreased inflammation and tumors in a mouse model of inflammation-associated carcinogenesis whereas sulforaphane effects differed with selenium supply. *Carcinogenesis* 2012;33(3):620–628.

149. Barrett CW et al. Tumor Suppressor Function of the Plasma Glutathione Peroxidase Gpx3 in Colitis-Associated Carcinoma. *Cancer Res* 2013;73(3):1245–1255.

150. Canter JA et al. Selenium and the 15kDa Selenoprotein Impact Colorectal Tumorigenesis by Modulating Intestinal Barrier Integrity. *Int J Mol Sci* 2021;22(19):10651.

151. Nagao-Kitamoto H, Kitamoto S, Kamada N. Inflammatory bowel disease and carcinogenesis. *Cancer Metast Rev* 2022;41(2):301–316.

152. Burk RF, Hill KE. SELENOPROTEIN P: An Extracellular Protein with Unique Physical Characteristics and a Role in Selenium Homeostasis. *Annu Rev Nutr* 2005;25(1):215–235.

153. Jin N et al. Sodium selenate activated Wnt/β-catenin signaling and repressed amyloid-β formation in a triple transgenic mouse model of Alzheimer's disease. *Exp Neurol* 2017;297:36–49.

154. Zheng R et al. Selenomethionine promoted hippocampal neurogenesis via the PI3K-Akt-GSK3β-Wnt pathway in a mouse model of Alzheimer's disease. *Biochem Bioph Res Co* 2017;485(1):6–15.

155. Korbut E, Ptak-Belowska A, Brzozowski T. Inhibitory effect of selenomethionine on carcinogenesis in the model of human colorectal cancer in vitro and its link to the Wnt/β-catenin pathway.. *Acta Biochim Pol* 2018;65(3):359–366.

156. Kipp A et al. Four selenoproteins, protein biosynthesis, and Wnt signalling are particularly sensitive to limited selenium intake in mouse colon. *Mol Nutr Food Res* 2009;53(12):1561–1572.

157. Rao CV et al. Chemoprevention of familial adenomatous polyposis development in the APCmin mouse model by 1,4-phenylene bis(methylene)selenocyanate. *Carcinogenesis* 2000;21(4):617–621.

158. Davis CD, Zeng H, Finley JW. Selenium-enriched broccoli decreases intestinal tumorigenesis in multiple intestinal neoplasia mice.. *J Nutrition* 2002;132(2):307–9.

159. Albuquerque C et al. The 'just-right' signaling model: APC somatic mutations are selected based on a specific level of activation of the β-catenin signaling cascade. *Hum Mol Genet* 2002;11(13):1549–1560.

160. Pollard P et al. The Apc1322T Mouse Develops Severe Polyposis Associated With Submaximal Nuclear β-Catenin Expression. *Gastroenterology* 2009;136(7):2204-2213.e13.

161. Anthony CC, Robbins DJ, Ahmed Y, Lee E. Nuclear Regulation of Wnt/β-Catenin Signaling: It's a Complex Situation. *Genes-basel* 2020;11(8):886.

162. Plisov S et al. Cited1 Is a Bifunctional Transcriptional Cofactor That Regulates Early Nephronic Patterning. *J Am Soc Nephrol* 2005;16(6):1632–1644.

163. Méniel V et al. Cited1 Deficiency Suppresses Intestinal Tumorigenesis. *Plos Genet* 2013;9(8):e1003638.

164. Romagnolo B et al. Intestinal dysplasia and adenoma in transgenic mice after overexpression of an activated beta-catenin.. *Cancer Res* 1999;59(16):3875–9.

165. Kim K, Pang KM, Evans M, Hay ED. Overexpression of β-Catenin Induces Apoptosis Independent of Its Transactivation Function with LEF-1 or the Involvement of Major G1 Cell Cycle Regulators. *Mol Biol Cell* 2000;11(10):3509–3523.

166. Damalas A et al. Excess β-catenin promotes accumulation of transcriptionally active p53. *Embo J* 1999;18(11):3054–3063.

167. Mii Y, Takada S. Heparan Sulfate Proteoglycan Clustering in Wnt Signaling and Dispersal. *Frontiers Cell Dev Biology* 2020;8:631.

168. Fuerer C, Habib SJ, Nusse R. A study on the interactions between heparan sulfate proteoglycans and Wnt proteins. *Dev. Dyn.* 2010;239(1):184–190.

169. Bourhis E et al. Reconstitution of a Frizzled8·Wnt3a·LRP6 Signaling Complex Reveals Multiple Wnt and Dkk1 Binding Sites on LRP6. *J Biol Chem* 2010;285(12):9172–9179.

170. Gong Y et al. Wnt Isoform-Specific Interactions with Coreceptor Specify Inhibition or Potentiation of Signaling by LRP6 Antibodies. *Plos One* 2010;5(9):e12682.

171. Bourhis E et al. Wnt Antagonists Bind through a Short Peptide to the First β-Propeller Domain of LRP5/6. *Structure* 2011;19(10):1433–1442.

172. Ahn VE et al. Structural Basis of Wnt Signaling Inhibition by Dickkopf Binding to LRP5/6. *Dev Cell* 2011;21(5):862–873.

173. Sakai E et al. Combined mutation of Apc, Kras and Tgfbr2 effectively drives metastasis of intestinal cancer. *Cancer Res* 2017;78(5):canres.3303.2017.

174. Oshima M et al. Loss of Apc heterozygosity and abnormal tissue building in nascent intestinal polyps in mice carrying a truncated Apc gene.. *Proc National Acad Sci* 1995;92(10):4482–4486.

175. Nayini JR et al. Effect of dietary benzylselenocyanate on azoxymethane-induced colon carcinogenesis in Male F344 rats. *Nutrition Cancer* 1991;15(2):129–139.

176. Reddy BS et al. Chemoprevention of Colon Cancer by Organoselenium Compounds and Impact of High- or Low-Fat Diets. *Jnci J National Cancer Inst* 1997;89(7):506–512.

177. Barrett CW et al. Dietary Selenium Deficiency Exacerbates DSS-Induced Epithelial Injury and AOM/DSS-Induced Tumorigenesis. *Plos One* 2013;8(7):e67845.

178. Masuda J et al. Dietary Supplementation of Selenoneine-Containing Tuna Dark Muscle Extract Effectively Reduces Pathology of Experimental Colorectal Cancers in Mice. *Nutrients* 2018;10(10):1380.

179. Saxena A et al. Dietary selenium protects adiponectin knockout mice against chronic inflammation induced colon cancer. *Cancer Biol Ther* 2017;18(4):257–267.

180. Kim J-H et al. Effects of Selenium on Colon Carcinogenesis Induced by Azoxymethane and Dextran Sodium Sulfate in Mouse Model with High-Iron Diet. *Laboratory Animal Res* 2010;27(1):9–18.

181. DeBruine ZJ, Xu HE, Melcher K. Assembly and architecture of the Wnt/β-catenin signalosome at the membrane: Wnt signalosome assembly. *Brit J Pharmacol* 2017;174(24):4564–4574.

182. Colozza G, Koo B. Wnt/β-catenin signaling: Structure, assembly and endocytosis of the signalosome. *Dev Growth Differ* 2021;63(3):199–218.

183. Bilić J et al. Wnt Induces LRP6 Signalosomes and Promotes Dishevelled-Dependent LRP6 Phosphorylation. *Science* 2007;316(5831):1619–1622.

184. Matoba K et al. Conformational Freedom of the LRP6 Ectodomain Is Regulated by N-glycosylation and the Binding of the Wnt Antagonist Dkk1. *Cell Reports* 2017;18(1):32–40.

185. Evans R et al. Protein complex prediction with AlphaFold-Multimer. *Biorxiv* 2022;2021.10.04.463034.

186. Yamamoto H, Komekado H, Kikuchi A. Caveolin Is Necessary for Wnt-3a-Dependent Internalization of LRP6 and Accumulation of β-Catenin. *Dev Cell* 2006;11(2):213–223.

187. Orlandi PA, Fishman PH. Filipin-dependent Inhibition of Cholera Toxin: Evidence for Toxin Internalization and Activation through Caveolae-like Domains. *J Cell Biology* 1998;141(4):905–915.

188. Bolard J. How do the polyene macrolide antibiotics affect the cellular membrane properties?. *Biochimica Et Biophysica Acta Bba - Rev Biomembr* 1986;864(3–4):257–304.

189. Wang LH, Rothberg KG, Anderson RG. Mis-assembly of clathrin lattices on endosomes reveals a regulatory switch for coated pit formation.. *J Cell Biology* 1993;123(5):1107–1117.

190. Macia E et al. Dynasore, a Cell-Permeable Inhibitor of Dynamin. *Dev Cell* 2006;10(6):839–850.

191. Dickson RB, Willingham MC, Pastan IH. Receptor-mediated endocytosis of alpha 2-macroglobulin: inhibition by ionophores and stimulation by Na+ and HCO3(-).. *Ann Ny Acad Sci* 1982;401:38–49.

192. Schlegel R, Dickson RB, Willingham MC, Pastan IH. Amantadine and dansylcadaverine inhibit vesicular stomatitis virus uptake and receptor-mediated endocytosis of alpha 2-macroglobulin.. *Proc National Acad Sci* 1982;79(7):2291–2295.

193. Dutta D, Williamson CD, Cole NB, Donaldson JG. Pitstop 2 Is a Potent Inhibitor of Clathrin-Independent Endocytosis. *Plos One* 2012;7(9):e45799.

194. Tsuji PA et al. The 15kDa Selenoprotein and Thioredoxin Reductase 1 Promote Colon Cancer by Different Pathways. *PLoS ONE* 2015;10(4):e0124487.

195. Speckmann B et al. Proinflammatory cytokines down-regulate intestinal selenoprotein P biosynthesis via NOS2 induction. *Free Radical Bio Med* 2010;49(5):777–785.

196. Zhang Y, Chen X. Reducing selenoprotein P expression suppresses adipocyte differentiation as a result of increased preadipocyte inflammation. *Am J Physiol-endoc M* 2011;300(1):E77–E85.

197. Gerdes MJ et al. Highly multiplexed single-cell analysis of formalin-fixed, paraffin-embedded cancer tissue. *Proc National Acad Sci* 2013;110(29):11982–11987.

198. Jadhav U et al. Dynamic Reorganization of Chromatin Accessibility Signatures during Dedifferentiation of Secretory Precursors into Lgr5+ Intestinal Stem Cells. *Cell Stem Cell* 2017;21(1):65-77.e5.

199. Habowski AN, Bates JM, Flesher JL, Edwards RA, Waterman ML. Isolation of murine large intestinal crypt cell populations with flow sorting[published online ahead of print: 2020]; doi:10.21203/rs.3.pex-994/v1

200. Habowski AN et al. Transcriptomic and proteomic signatures of stemness and differentiation in the colon crypt. *Commun Biology* 2020;3(1):453.

201. Brown R. Myeloid translocation genes in intestinal and colonic epithelial differentiation, regeneration, and tumorigenesis2022;

202. Haber AL et al. A single-cell survey of the small intestinal epithelium. *Nature* 2017;551(7680):333–339.

203. Rodriguez-Juan C et al. Cell surface phenotype and cytokine secretion in Caco-2 cell cultures: increased RANTES production and IL-2 transcription upon stimulation with IL-1beta.. *Tissue Cell* 2001;33(6):570–9.

204. Hinnebusch BF et al. Enterocyte differentiation marker intestinal alkaline phosphatase is a target gene of the gut-enriched Kruppel-like factor.. *Am J Physiology Gastrointest Liver Physiology* 2003;286(1):G23-30.

205. Cetin Y, Müller-Köppel L, Aunis D, Bader MF, Grube D. Chromogranin A (CgA) in the gastro-entero-pancreatic (GEP) endocrine system. II. CgA in mammalian entero-endocrine cells.. *Histochemistry* 1989;92(4):265–75.

206. Grün D et al. Single-cell messenger RNA sequencing reveals rare intestinal cell types. *Nature* 2015;525(7568):251–255.

207. Reis CA et al. Intestinal metaplasia of human stomach displays distinct patterns of mucin (MUC1, MUC2, MUC5AC, and MUC6) expression.. *Cancer Res* 1999;59(5):1003–7.

208. Ho SB, Itzkowitz SH, Friera AM, Jiang S-H, Kim YS. Cell lineage markers in premalignant and malignant colonic mucosa. *Gastroenterology* 1989;97(2):392–404.

209. Barker N et al. Identification of stem cells in small intestine and colon by marker gene Lgr5. *Nature* 2007;449(7165):1003–1007.

210. Flier LG van der, Haegebarth A, Stange DE, Wetering M van de, Clevers H. OLFM4 Is a Robust Marker for Stem Cells in Human Intestine and Marks a Subset of Colorectal Cancer Cells. *Gastroenterology* 2009;137(1):15–17.

211. Formeister EJ et al. Distinct SOX9 levels differentially mark stem/progenitor populations and enteroendocrine cells of the small intestine epithelium. *Am J Physiol-gastr L* 2009;296(5):G1108–G1118.

212. Gerbe F, Brulin B, Makrini L, Legraverend C, Jay P. DCAMKL-1 Expression Identifies Tuft Cells Rather Than Stem Cells in the Adult Mouse Intestinal Epithelium. *Gastroenterology* 2009;137(6):2179–2180.

213. Walter PL, Steinbrenner H, Barthel A, Klotz L-O. Stimulation of selenoprotein P promoter activity in hepatoma cells by FoxO1a transcription factor. *Biochem Bioph Res Co* 2008;365(2):316–321.

214. Speckmann B et al. Selenoprotein P expression is controlled through interaction of the coactivator PGC-1α with FoxO1a and hepatocyte nuclear factor 4α transcription factors. *Hepatology* 2008;48(6):1998–2006.

215. Jung TW et al. Salsalate and Adiponectin Improve Palmitate-Induced Insulin Resistance via Inhibition of Selenoprotein P through the AMPK-FOXO1α Pathway. *Plos One* 2013;8(6):e66529.

216. Takayama H et al. Metformin Suppresses Expression of the Selenoprotein P Gene via an AMP-activated Kinase (AMPK)/FoxO3a Pathway in H4IIEC3 Hepatocytes*. *J Biol Chem* 2014;289(1):335–345.

217. Kamoshita K et al. Lauric acid impairs insulin-induced Akt phosphorylation by upregulating SELENOP expression via HNF4α induction. *Am J Physiol-endoc M* 2022;322(6):E556–E568.

218. Tajima-Shirasaki N et al. Eicosapentaenoic acid down-regulates expression of the selenoprotein P gene by inhibiting SREBP-1c protein independently of the AMP-activated protein kinase pathway in H4IIEC3 hepatocytes. *J Biol Chem* 2017;292(26):10791–10800.

219. Mostert V, Dreher I, Köhrle J, Abel J. Transforming growth factor-β1 inhibits expression of selenoprotein P in cultured human liver cells. *Febs Lett* 1999;460(1):23–26.

220. Mostert V, Wolff S, Dreher I, Köhrle J, Abel J. Identification of an element within the promoter of human selenoprotein P responsive to transforming growth factor-β. *Eur J Biochem* 2011;268(23):6176–6181.

221. Wen X et al. Reverse Chromatin Immunoprecipitation (R-ChIP) enables investigation of the upstream regulators of plant genes. *Commun Biology* 2020;3(1):770.

222. Herz J, Clouthier DE, Hammer RE. LDL receptor-related protein internalizes and degrades uPA-PAI-1 complexes and is essential for embryo implantation. *Cell* 1992;71(3):411–421.

223. Willnow TE et al. Defective forebrain development in mice lacking gp330/megalin.. *Proc National Acad Sci* 1996;93(16):8460–8464.

224. Trommsdorff M et al. Reeler/Disabled-like Disruption of Neuronal Migration in Knockout Mice Lacking the VLDL Receptor and ApoE Receptor 2. *Cell* 1999;97(6):689–701.

225. Holmen SL et al. Decreased BMD and Limb Deformities in Mice Carrying Mutations in Both Lrp5 and Lrp6. *J Bone Miner Res* 2004;19(12):2033–2040.

226. Kelly OG, Pinson KI, Skarnes WC. The Wnt co-receptors Lrp5 and Lrp6 are essential for gastrulation in mice. *Development* 2004;131(12):2803–2815.

227. Zhong Z, Baker JJ, Zylstra-Diegel CR, Williams BO. Lrp5 and Lrp6 play compensatory roles in mouse intestinal development. *J. Cell. Biochem.* 2012;113(1):31–38.